

HYBRID BEAMFORMING AND ONE-BIT PRECODING
FOR LARGE-SCALE ANTENNA ARRAYS

by

Foad Sohrabi

A thesis submitted in conformity with the requirements
for the degree of Doctor of Philosophy
Graduate Department of Electrical and Computer Engineering
University of Toronto

Abstract

Hybrid Beamforming and One-Bit Precoding
for Large-Scale Antenna Arrays

Foad Sohrabi

Doctor of Philosophy

Graduate Department of Electrical and Computer Engineering
University of Toronto

2018

Employing large antenna arrays is a promising candidate for the next generation of wireless systems. However, the conventional fully digital beamforming methods which require one high resolution radio frequency (RF) chain per antenna element is not viable for large antenna arrays due to the high cost and high power consumption of RF chain components. To address this hardware limitation challenge, this thesis considers two architectures: (1) Hybrid beamforming architecture in which the overall beamformer consists of a low-dimensional digital beamformer followed by an analog beamformer; (2) One-bit beamforming architecture in which one RF chain is dedicated for each antenna element but with only 1-bit resolution per complex dimension.

There are three parts to this thesis. The first part considers hybrid beamforming design for narrowband flat-fading channels. It is shown that the hybrid beamforming architecture can realize any fully digital beamformer exactly if the number of RF chains is twice the total number of data streams. For cases with fewer number of RF chains, heuristic designs are proposed for both the transmission scenario of a single-user multiple-input multiple-output (SU-MIMO) system and a downlink multi-user multiple-input single-output (MU-MISO) system. For each scenario, the proposed design is numerically shown to achieve a performance close to the performance of the fully digital beamforming baseline.

The second part studies the hybrid beamforming design for broadband millimeter wave (mmWave) systems with orthogonal frequency division multiplexing (OFDM) modulation where it is desirable to design common analog beamformer for the entire band. First, for a SU-MIMO system, it is shown that hybrid beamforming with a small number of RF chains can asymptotically approach the performance of fully digital beamforming for a sufficiently large number of

transceiver antennas. For systems with a practical number of antennas, heuristic designs are then proposed to maximize the overall spectral efficiency for both SU-MIMO and MU-MISO scenarios. It is numerically shown that the proposed algorithms with practical number of RF chains can already approach the performance of fully digital beamforming baselines.

In the final part of this thesis, the 1-bit symbol-level precoding architecture for a downlink massive MIMO system with quadrature amplitude modulation (QAM) signalling is studied. First, a constellation range design as well as a non-linear one-bit precoding design is proposed in order to minimize the average symbol error rate (SER) for the single-user scenario. Those designs are further generalized for the multi-user scenario. Finally, the performance of the proposed scheme is analytically studied and it is shown that for large-scale antenna arrays there is a constant 2dB gap between the proposed design and the conventional zero-forcing (ZF) scheme with per-symbol power constraint. The simulation results verify that the proposed design can achieve a promising performance for large antenna arrays with low resolution RF chains.

To my lovely wife:

Mahsa

&

To my beloved parents:

Parvin and Mojtaba

Acknowledgements

First and foremost, I would like to express my deepest appreciation and gratitude to my supervisor, Prof. Wei Yu, for his insightful guidance and generous support at every stage of my Ph.D. study. Without his technical support and constant help, the completion of this thesis would have not been possible. I would also like to thank him for his endless patience and great effort in editing and improving my academic papers.

During the last year of my study, I was fortunate to meet Prof. Ya-Feng Liu in his visit of University of Toronto. I would like to thank him for his collaboration and guidance which help me to complete this thesis.

I would like to express my gratitude to my thesis committee members, Prof. Andreas F. Molisch, Prof. Raviraj Adve, and Prof. Ashish Khisti for their careful reading of this document and their invaluable comments. I would also like to thank Prof. Sean V. Hum for serving on my supervisory committee.

I would like to acknowledge my U of T colleagues, who made my PhD the most memorable experience of my life. In particular, I would like to thank Arvin Ayoughi, Zhilin Chen, Faouzi Bellili, Liang Liu, Saeed Khosravirad, Masoud Barekatein, Farhang Vedadi, Hamed Sadeghi, Ali Jokar, Moein Soltani, and Erfan Meskar.

I would like to deeply thank my parents, Parvin and Mojtaba, for their endless love and support through my life.

Last but not least, I owe my deepest thanks to my lovely wife, Mahsa, for her endless love, countless sacrifices and timely encouragements. I would also like to appreciate all her help and support through my research.

Contents

1	Introduction	1
1.1	Power-Efficient Architectures for Large Antenna Arrays	2
1.1.1	Hybrid Beamforming	2
1.1.2	One-Bit Precoding	5
1.2	Thesis Outline and Contributions	7
1.2.1	Hybrid Beamforming for Narrowband Flat-Fading Channels	7
1.2.2	Hybrid Beamforming for mmWave Wideband Channels	10
1.2.3	One-Bit Precoding for Rich-Scattering Channels	11
1.3	Related Work	14
1.3.1	Hybrid Beamforming for Narrowband Flat-Fading Channels	14
1.3.2	Hybrid Beamforming for mmWave Wideband Channels	17
1.3.3	One-Bit Precoding for Rich-Scattering Channels	18
1.4	Notations	20
2	Hybrid Beamforming for Narrowband Flat-Fading Channels	21
2.1	Chapter Organization	21
2.2	System Model	23
2.2.1	Signal Model in Hybrid Beamforming	23
2.2.2	Structure of Analog Beamformer	25
2.2.3	Problem Formulation	26
2.3	Minimum Number of RF Chains to Realize Fully Digital Beamformers	26
2.4	Hybrid Beamforming Design for Large-Scale SU-MIMO Systems	29

2.4.1	Digital Precoder Design for $N_{\text{RF}} = N_s$	30
2.4.2	Analog Precoder Design for $N_{\text{RF}} = N_s$	31
2.4.3	Hybrid Combining Design for $N_{\text{RF}} = N_s$	33
2.4.4	Hybrid Beamforming Design for $N_s < N_{\text{RF}} < 2N_s$	34
2.5	Hybrid Beamforming Design for Massive MU-MISO Systems	36
2.5.1	Digital Precoder Design	38
2.5.2	Analog Precoder Design	38
2.6	Hybrid Beamforming with Finite Resolution Phase Shifters	43
2.7	Numerical Results	45
2.7.1	Performance Analysis of a SU-MIMO System with Hybrid Beamforming	46
2.7.2	Performance Analysis of a MU-MISO System with Hybrid Beamforming	50
2.8	Summary	52
3	Hybrid Beamforming for mmWave Wideband Channels	54
3.1	Chapter Organization	54
3.2	System Model for SU-MIMO	56
3.2.1	Signal Model in OFDM-based Hybrid Beamforming	56
3.2.2	Structure of Analog Beamformer	58
3.2.3	Problem Formulation	59
3.2.4	Channel Model	60
3.3	Asymptotic Beamforming Design for SU-MIMO	62
3.4	Hybrid Beamforming Design for SU-MIMO	63
3.4.1	Transmitter Design	64
3.4.2	Receiver Design	69
3.5	Hybrid Precoding Design for MU-MISO	71
3.6	Numerical Results	75
3.6.1	Asymptotic Hybrid Beamforming Design Performance Analysis for SU-MIMO systems	75
3.6.2	Hybrid Beamforming Performance Analysis in SU-MIMO systems	77
3.6.3	Hybrid Beamforming Performance Analysis in MU-MISO systems	79

3.7	Summary	83
4	One-Bit Precoding for Rich-Scattering Channels	84
4.1	Chapter Organization	84
4.2	System Model	86
4.3	SER Characterization for Symbol-Level Precoding	90
4.4	Constellation Range Design for Single-User Scenario	91
4.4.1	Infinite Resolution Precoding with Total Power Constraint	92
4.4.2	Infinite Resolution Precoding with Per-Antenna Power Constraint	94
4.4.3	One-Bit Precoding	95
4.5	One-Bit Precoding Design for Single-User Scenario	99
4.6	Constellation Range and One-Bit Precoding Design for Multi-User Scenario . . .	101
4.6.1	Constellation Range Design	101
4.6.2	One-Bit Precoding Design	104
4.6.3	Performance Gap of One-Bit Precoding vs. Conventional ZF	105
4.7	Numerical Results	107
4.7.1	MSE Analysis for Choosing M_2	107
4.7.2	MSE Analysis for Constellation Range Design	107
4.7.3	SER of One-Bit Precoding	111
4.8	Summary	114
5	Conclusion and Future Work	116
Bibliography		120

List of Figures

2.8	Sum rate achieved by different methods in an 8-user MISO system with $M_t = 64$. For hybrid beamforming methods, the use of infinite resolution phase shifters is assumed.	52
2.9	Sum rate achieved by different methods in a 4-user MISO system with $M_t = 64$. For the methods with finite resolution phase shifters, $b = 1$.	53
3.1	A block diagram of an OFDM-based large-scale SU-MIMO system with hybrid analog and digital beamforming architecture at the transceivers.	57
3.2	(a) The architecture of an analog precoder with fully-connected structure. (b) The architecture of an analog precoder with partially-connected structure.	59
3.3	A block diagram of a downlink OFDM-based MU-MISO system with hybrid analog and digital beamforming architecture at the BS.	71
3.4	Comparison between the achievable rates of asymptotic design and the optimal fully digital beamforming for an $M \times M$ SU-MIMO system with $N_s = N_{\text{RF}} = 4$, $N = 32$ and SNR = 20dB.	76
3.5	Spectral efficiencies versus SNR of different methods for a 64×32 OFDM-based SU-MIMO system in which hybrid architecture with infinite resolution phase shifters is employed at both transceiver sides and $N_s = 2$, $N_{\text{RF}} = 4$, and $N = 64$.	77
3.6	Spectral efficiencies versus SNR of different methods for a 64×8 OFDM-based SU-MIMO system in which hybrid architecture with infinite resolution phase shifters is employed at the transmitter and $N_s = 8$, $N_{\text{RF}} = 8$, and $N = 64$.	78
3.7	Spectral efficiencies versus SNR of different methods for a 64×8 OFDM-based SU-MIMO system in which hybrid architecture with 1-bit resolution phase shifters is employed at the transmitter and $N_s = 8$, $N_{\text{RF}} = 8$, and $N = 64$.	80
3.8	Weighted sum rate versus transmit power spectral density for different methods in an OFDM-based MU-MISO system with $K = 4$, $M_t = 64$, and $N = 32$.	81
3.9	Empirical CDF of the average rate of the users for different methods in an OFDM-based MU-MISO system with $K = 4$ and $N = 32$.	82
4.1	A MU-MISO system with symbol-level precoding.	87
4.2	An example of N^2 -QAM constellation for $N = 4$.	89

4.3 Fix one random channel realization with $M = 8$ and $P = 4$. The data points are the 4^M possible realizations of $\mathbf{h}^H \mathbf{x}$, and the dashed black and solid red lines are circles with radius of $c_{\text{inf},t}^* = \sqrt{2P} \ \mathbf{h}\ _2$ and $\sqrt{2/\pi} c_{\text{inf},t}^*$, respectively. Most data points are confined within the solid red circle.	98
4.4 The MSE versus γ for a single-user system with $M = 8$ and $P = 4$. There is a phase transition at $\gamma = \sqrt{2/\pi} \approx 0.8$	99
4.5 Average MSE versus M_2 in a single-user system where $M = 128$, $N = 4$, and $P = 1$	108
4.6 Average MSE versus λ in a single-user system for different numbers of antennas, M , when $P = 1$ and $M_2 = 8$	109
4.7 Average MSE versus λ in a 8-user system for different numbers of antennas, M , when $P = 1$ and $M_2 = 8$	110
4.8 Average SER versus SNR for different methods in a SU-MISO system with $M = 256$ and $N = 16$	112
4.9 Average SER versus the number of antennas, M , for different methods in a SU-MISO system with SNR = -4dB and $N = 4$	113
4.10 Average SER versus SNR for different methods in a 8-user MISO system with $M = 512$ and $N = 4$	114

List of Abbreviations

ADC	Analog-to-Digital Converter
BS	Base Station
CDF	Cumulative Distribution Function
CSI	Channel State Information
DAC	Digital-to-Analog Converter
MIMO	Multiple-Input Multiple-Output
MISO	Multiple-Input Single-Output
MU	Multi-User
mmWave	Millimeter Wave
MSE	Mean Squared Error
MMSE	Minimum Mean Squared Error
OFDM	Orthogonal Frequency Division Multiplexing
PSK	Phase Shift Keying
QAM	Quadrature Amplitude Modulation
QPSK	Quadrature Phase Shift Keying
RF	Radio Frequency
SDP	Semidefinite Program
SER	Symbol Error Rate
SNR	Signal-to-Noise Ratio
SU	Single-User
WMMSE	Weighted Minimum Mean Squared Error
ZF	Zero-Forcing

Chapter 1

Introduction

Employing large-scale antenna arrays is a promising candidate for the next generation wireless networks to achieve high spectral efficiency, reliability, and connectivity requirements [1]. However, the advantages of massive MIMO technology come at a cost of increase in hardware complexity. A number of references such as [2, 3] provide an extensive overview of the opportunities and the challenges with the large-scale antenna arrays.

One of the main challenges in designing systems with large-scale antenna arrays is that the implementation of the conventional digital beamforming strategies such as [4–6] may not be practical, because conventional beamforming schemes require one dedicated high resolution RF chains for each antenna element. When a transceiver is equipped with large number of antennas, the fully digital beamforming architecture leads to high hardware complexity and excessive circuit power consumption.

To address the challenge of high power consumption in RF chain circuits, different architectures are proposed in the literature. Analog or RF beamforming schemes implemented using analog circuitry are introduced in [7–10]. They typically use analog phase shifters, which impose a constant modulus constraint on the elements of the beamformer. The constant modulus constraint causes analog beamforming to have poor performance as compared to the fully digital beamforming designs. Another approach for limiting the number of RF chains is antenna subset selection which is implemented using simple analog switches [11, 12]. However, antenna selection scheme provides limited array gain and still has poor performance in correlated channels [13, 14].

To address the hardware limitation of fully digital beamforming, this thesis adopts two alternative architectures:

1. Hybrid Beamforming Architecture: in which the overall beamformer consists of a low-dimensional digital beamformer and a high-dimensional analog beamformer implemented using a network of simple analog phase shifters. In hybrid beamfoming structure, the power consumption of RF chain circuitry is reduced as compared to fully digital beamforming by reducing the number of RF chains.
2. One-Bit Beamforming Architecture: in which one RF chain is dedicated to each antenna element but with only 1-bit resolution digital-to-analog converters (DACs) per complex dimension. In one-bit beamforming structure, the power consumption of RF chain circuitry is reduced as compared to fully digital beamforming by reducing the resolution of the RF chains.

This thesis also notes that the other low-complexity architectures are proposed in the literature to decrease the power consumption in massive MIMO systems such as load modulated arrays [15, 16] and parasitic antenna arrays [17]. In the load modulated array architecture, a constant envelope power amplifier drives a large-scale antenna array and different antenna elements transmits different signals by adjusting their corresponding impedance. In parasitic array architecture, only a single active element is fed by an RF chain while the other antennas, called parasitics, are activated based on the mutual coupling between the antennas.

1.1 Power-Efficient Architectures for Large Antenna Arrays

This section aims to introduce the details of the hybrid beamforming architecture as well as 1-bit precoding architecture which are two possible candidates for mitigating the power consumption of the RF chain circuitry at the terminals with large-scale antenna arrays.

1.1.1 Hybrid Beamforming

The idea of hybrid beamforming architecture which employs a combination of analog beamformer in the RF domain and digital beamformer in the baseband, connected to each other via

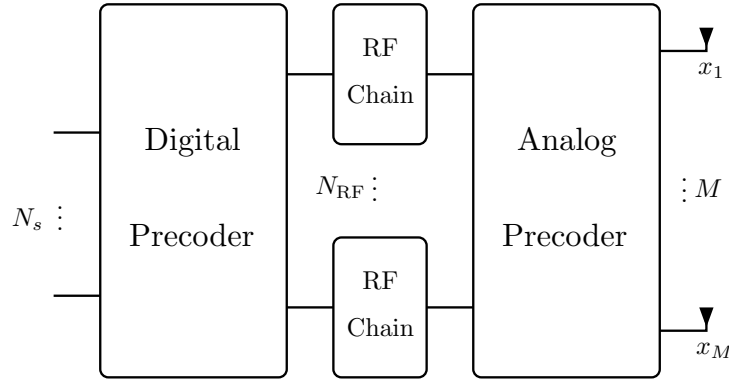


Fig. 1.1: Block diagram of a hybrid beamforming architecture at the transmitter.

a small number of RF chains, is first introduced under the name of “RF-baseband codesign” in [18, 19]. The main advantage of this architecture is that the number of RF chains needs to be in the order of the number of data streams, while the beamforming gain and diversity order are given by the number of antennas [20]. This unique feature of hybrid beamforming architecture makes it a promising technique for mmWave systems. This is because, on one hand, the large antenna arrays employed in the hybrid beamforming structure can be used to combat the severe pathloss and absorption in mmWave frequencies, and on the other hand, the number of data streams that can be transmitted in mmWave systems is already limited due to the sparse nature of the mmWave channels. Motivated by this, a mmWave channel model is considered throughout this thesis for hybrid beamforming.

To describe the structure of the hybrid beamforming, this section focuses on the hybrid architecture at the transmitter. A generic block diagram of a transmitter with hybrid architecture is shown in Fig. 1.1. It can be seen from Fig. 1.1 that the transmitter first modifies the N_s data streams at baseband using digital precoder and constructs a N_{RF} -dimensional digital signal. The transmitter then up-converts this signal to the carrier frequency using N_{RF} RF chains. Finally, it modifies the analog signal using an $M \times N_{\text{RF}}$ analog precoder to construct the final signal that is transmitted from M transmit antennas. The regime of interest for hybrid beamforming is that the number of RF chains is much smaller than the number of antennas, i.e., $N_{\text{RF}} \ll M$. Hence, a low-dimensional digital beamformer and a high-dimensional analog beamformer are employed in the hybrid beamforming architecture.

The analog part of the hybrid beamformer is typically implemented using simple analog

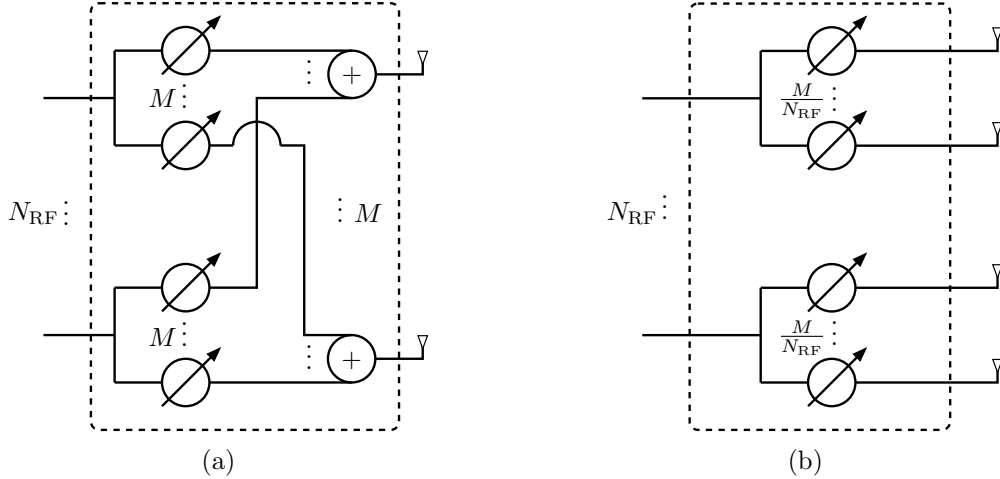


Fig. 1.2: (a) The architecture of an analog precoder with fully-connected structure. (b) The architecture of an analog precoder with partially-connected structure.

components such as analog adders and analog phase shifters which can only modify the phase of signals. This results in some constraints on the analog beamforming matrix depending on the structure of the analog beamformer. The two widely used analog beamforming structures that have been considered in this thesis are the fully-connected and the partially-connected structures.

The schematic of a hybrid transmitter with fully-connected and partially-connected structures is depicted in Fig. 1.2(a) and Fig. 1.2(b), respectively. It can be seen from Fig. 1.2(a) that in the fully-connected architecture structure, each RF chain is connected with all antennas, such that each of N_{RF} digital signals goes through M different phase shifters. This structure is a natural combination of analog beamforming and digital beamforming in which the full beamforming gain for each of digital signals can be achieved. However, the complexity of the fully-connected structure is relatively high, i.e., the total number of phase shifters in this architecture is the number of antennas times the number of RF chains.

An alternative analog beamformer structure is partially-connected structure in which each RF chain is connected only to a subarray of antennas with M/N_{RF} elements as shown in Fig. 1.2(b). It can be seen that the total number of phase shifters in this structure is now given by the number of antennas which means that the hardware complexity of the analog beamformer is reduced by a factor of the number of RF chains.

There is a performance-complexity trade off in choosing the above structures. The fully-

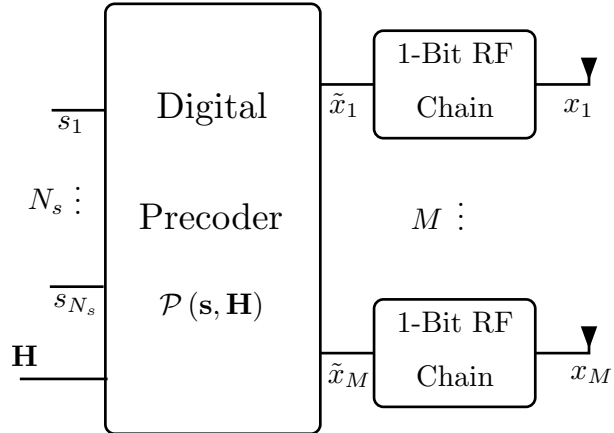


Fig. 1.3: Block diagram of a 1-bit symbol-level precoding architecture in which 1-bit DACs are employed in the RF chains.

connected structure can achieve full beamforming gain with full phase control, while the partially-connected structure has limited phase control, thus cannot achieve full beamforming gain in all cases. On the other hand, the hardware implementation complexity and power consumption of the partially-connected architecture are much lower as compared to those of the fully-connected structure.

This thesis first aims to study the conditions in which the hybrid beamforming with the maximum degrees of freedom, i.e., the fully-connected structure, can approach the performance of the fully digital beamforming baselines. Further, this thesis seeks to provide practical hybrid beamforming designs which can handle both analog beamformer structures for two scenarios: 1) narrowband flat-fading channels, 2) mmWave wideband channels. The detailed summary of the contributions of this thesis on hybrid beamforming will be provided later in Section 1.2.

1.1.2 One-Bit Precoding

Although this thesis shows that hybrid precoding scheme is capable of approaching the performance of the conventional fully digital precoding baselines, hybrid precoding still requires RF chains with high resolution DACs. As the power consumption of DAC grows exponentially with its resolution [21, 22], the use of high resolution DACs would lead to high power consumption, especially when the base station (BS) needs to transmit a large number of data streams. Moreover, the good performance of the hybrid precoding scheme for wideband systems is restricted to the mmWave frequencies. This is because the sparsity of the mmWave channels can be

exploited to show that one common analog beamformer across all the subcarriers is typically sufficient for achieving a good performance, while for rich-scattering environments, one common analog beamformer may not provide enough degrees of freedom for hybrid beamforming to approach the performance of the fully digital beamforming.

In order to address these difficulties, this thesis further considers an alternative precoding architecture called 1-bit precoding in which one RF chain is dedicated to each antenna element but with only 1-bit resolution DAC per complex dimension. The 1-bit precoding scheme enables the transmitter to reduce the circuit power consumption of the DACs, which are one of the most power hungry components in the transmitter. Moreover, the 1-bit precoding satisfies the condition of constant envelop transmission, hence it can prevent the possible amplitude distortions which may occur in the practical systems when the power amplifiers work in the saturation region [23].

A generic block diagram of the 1-bit precoding architecture is depicted in Fig. 1.3. It can be seen that the transmitter first modifies N_s data streams at the baseband using a digital precoder to construct a M -dimensional digital signal, $\tilde{\mathbf{x}}$. Then, this signal passes through M RF chains, each of which equipped with a 1-bit resolution DAC for each complex dimension, to construct the final analog transmitted signal, \mathbf{x} . Some earlier work on 1-bit precoding architecture employs linear precoders such as zero-forcing (ZF) precoder as the digital precoder in Fig. 1.3. Due to the poor performance of those linear precoders in some scenarios, this thesis however considers a non-linear precoding scheme in which the transmitted signal is designed as the non-linear function of the intended symbols, \mathbf{s} , and the channel state information (CSI), \mathbf{H} , namely,

$$\tilde{\mathbf{x}} = \mathcal{P}(\mathbf{s}, \mathbf{H}), \quad (1.1)$$

where the function \mathcal{P} represents the precoder. It is clear that due to the use of 1-bit DACs, the amplitude of each element of $\tilde{\mathbf{x}}$ is not important. Hence, it is desirable to choose each element of $\tilde{\mathbf{x}}$ from a finite alphabet $\tilde{\mathcal{X}}$ as

$$\tilde{\mathcal{X}} = \left\{ \sqrt{\frac{P}{2M}} (\pm 1 \pm i) \right\}, \quad (1.2)$$

where P is the total power budget at the transmitter and i is the imaginary unit.

This thesis aims to design and investigate the performance of this architecture in a downlink multi-user system in which a BS with 1-bit precoding architecture serves multiple single antenna users. It should be mentioned that the design of the non-linear precoder, \mathcal{P} , falls into the symbol-level precoding paradigm which is pioneered in earlier works [24–27] for the infinite resolution case and it is adopted for the 1-bit DAC in this thesis. Therefore, similar to the symbol-level precoding schemes, a faster precoder calculation is required for 1-bit precoding, which translates to more complex algorithms at the transmitter side [26] and it may not be feasible to perform such calculation with current hardware.

The detailed summary of the contributions of this thesis for 1-bit precoding architecture is provided in the following section.

1.2 Thesis Outline and Contributions

This thesis consists of three main parts:

- Chapter 2: Hybrid Beamforming for Narrowband Flat-Fading Channels.
- Chapter 3: Hybrid Beamforming for mmWave Wideband Channels.
- Chapter 4: One-Bit Precoding for Rich-Scattering Channels.

This section summarizes the contributions of this thesis on each of those three parts.

1.2.1 Hybrid Beamforming for Narrowband Flat-Fading Channels

Chapter 2 considers hybrid beamforming design for narrowband flat-fading channels. The results of Chapter 2 are stated when a fully-connected hybrid beamforming structure is employed at the terminals with large antenna arrays. However, most of the algorithms developed in Chapter 2, can be easily extended to the partially-connected structure as well. The main contributions of this thesis in Chapter 2 on hybrid beamforming for narrowband channels are:

Conditions on Optimality of Fully-Connected Hybrid Beamforming

For narrowband flat-fading channels, Chapter 2 first aims to investigate the conditions in which the fully-connected hybrid beamforming architecture can exactly achieve the performance of the fully digital beamforming while it is equipped with much fewer number of RF chains. Specifically, Chapter 2 shows that to realize a generic fully digital beamforming matrix using a hybrid structure, it is necessary for the number of RF chains in the hybrid beamforming structure to be greater than or equal to the number of active data streams. More interestingly, Chapter 2 establishes that if the number of RF chains is twice the total number of data streams, the hybrid beamforming structure has enough degrees of freedom to realize any fully digital beamformer exactly, regardless of the number of antenna elements in the system.

Hybrid Beamforming Design for SU-MIMO Systems

Next, Chapter 2 considers the hybrid beamforming design problem when the number of RF chains is less than twice the number of data streams, in which the hybrid beamforming structure cannot necessarily realize the optimal fully digital beamforming matrix. For such a scenario, Chapter 2 initially considers precoder and combiner design problem for maximizing spectral efficiency under the total power constraint when the hybrid beamforming structure is used at both the transmitter and the receiver of a SU-MIMO system.

The main challenge in solving this problem is the coupling among analog and digital beamformers, and between the beamformers at the transmitter (precoders) and the receiver (combiners). To decouple the design of the beamformers at the transmitter and the receiver, this thesis proposes to design the hybrid precoders assuming the optimal receiver is used. Then, for already designed transmitter, it seeks to design the hybrid combiners. Further, it is shown that the design of the analog beamformers can be decoupled from the design of the digital beamformers using the properties of the large-scale antenna arrays. Subsequently, a simple iterative coordinate descent algorithm is proposed to design the analog beamformers. With the known analog beamformers, a closed-form expression of the digital counterparts is then obtained. The numerical results are provided to show that the proposed hybrid beamforming design with the number of RF chains equal to the number of data streams can achieve spectral efficiency close

to that of the optimal fully digital solution.

Hybrid Beamforming Design for MU-MISO Systems

Chapter 2 further considers the multi-user case, more specifically, the hybrid precoding design problem in a MU-MISO system to maximize the downlink weighted sum rate under a total power constraint. This problem differs from spectral efficiency maximization in a SU-MIMO system in two respects. First, in the MU-MISO scenario the receiving antennas are not collocated, therefore the beamforming design for MU-MISO case should consider the effect of inter-user interference. Second, the priority weights of the data streams of different users may be unequal in a MU-MISO system, while different data streams in a SU-MIMO system have the same priority weights. In order to tackle this problem, ZF beamforming with power allocation is considered as the digital part of the hybrid precoder. It is shown that the optimal digital precoder with such a structure can be found for a fixed analog precoder. In addition, for a fixed power allocation, an approximately locally optimal analog precoder is obtained using an iterative coordinate descent algorithm for the cases in which the number of RF chains is strictly larger than the number of data streams. By iterating between those designs, the final designs of the analog and digital precoders are obtained. The numerical results suggest that the proposed hybrid beamforming design in the MU-MISO scenario can approach the performance of the optimal fully digital ZF precoding with much smaller number of RF chains.

Hybrid Beamforming Design for Finite Resolution Phase Shifters

All the aforementioned designs in Chapter 2 assume the availability of the infinite resolution phase shifters. However, the components required for realizing such accurate phase shifters can be expensive and hence finite resolution phase shifters are typically used in practice. Motivated by this, the final part of Chapter 2 presents a modification of the proposed algorithms for a more practical scenario in which only finite resolution phase shifters are available to construct the analog beamformers. It is numerically shown that the achievable spectral efficiency of the proposed design is close to the spectral efficiency of the optimal solution obtained by exhaustive search, while being significantly better than the spectral efficiency of quantized version of the existing hybrid beamforming designs when very low resolution phase shifters are used.

1.2.2 Hybrid Beamforming for mmWave Wideband Channels

As it was mentioned earlier, mmWave systems can be considered as one of the main applications of hybrid beamforming technique. The mmWave systems are expected to operate on broadband channels with frequency selectivity. The main challenge in designing hybrid beamforming for frequency-selective channels is that of how to design a common analog beamformer shared across all the subcarriers while adopting digital beamforming weights on a per-subcarrier basis. This important feature differentiates hybrid beamforming design in wideband frequency-selective channels from that in narrowband flat-fading channels and motivates this thesis to consider the hybrid beamforming design for mmWave systems with orthogonal frequency division multiplexing (OFDM) modulation in Chapter 3.

Asymptotically Optimal Hybrid Beamforming Design for SU-MIMO Systems

For wideband frequency-selective channels, Chapter 3 first considers the beamforming design in a mmWave SU-MIMO system in which both transmitter and receiver employ large-scale antenna arrays with fully-connected hybrid beamforming structure. In such a system, it is shown that with a sufficiently large number of antennas the sample covariance matrices of the mmWave channel at different subcarriers are asymptotically the same and hence they share the same set of eigenvectors. This asymptotic feature, which is due to the sparsity of the mmWave channels, suggests that the optimal fully digital eigen-beamformers at all subcarriers are the same in the massive MIMO regime. Based on this property, a hybrid beamforming design is proposed that can asymptotically realize the optimal fully digital eigen-beamforming. Although this result is valid only for extremely large number of antennas, it provides intuition as to why hybrid beamforming can approach the performance of the fully digital beamforming in broadband frequency-selective mmWave channels.

Efficient Hybrid Beamforming Design for SU-MIMO Systems

Chapter 3 also considers hybrid beamforming design for practical size of antenna arrays, e.g., arrays with 32-128 antennas, in a typical mmWave propagation environment. In particular, a unified heuristic algorithm is proposed for beamforming design of two different hybrid ar-

chitectures, the fully-connected and partially-connected architectures, to maximize the overall rate under power spectral density constraint in each sub-band. Towards developing this algorithm, Chapter 3 shows that it is possible to transform the analog precoding design problem for frequency-selective channels into an analog precoding design problem for flat-fading channels in which the sample covariance matrix is given by the average of the sample covariance matrices of frequency domain channels, i.e., $\frac{1}{N} \sum_n \mathbf{H}[n]^H \mathbf{H}[n]$, where $\mathbf{H}[n]$ is the channel at n^{th} subcarrier and N is the total number of subcarriers. This transformation enables Chapter 3 to employ the analog beamforming design algorithm already proposed in the Chapter 2 for single-carrier systems with narrowband flat-fading channel model. Finally, the optimal closed-form solution for the digital beamformers at each sub-carrier for the already designed analog beamformers is obtained.

Efficient Hybrid Beamforming Design for MU-MISO Systems

Chapter 3 further considers hybrid precoding design problem in a mmWave MU-MISO system to maximize the downlink weighted sum rate under a power constraint per subcarrier. As explained earlier, this problem differs from spectral efficiency maximization in a SU-MIMO system because of the existence of the inter-user interference and the possibility of having different priority weights for different data streams. In order to tackle this problem, Chapter 3 proposes the following simple design strategy. First, the analog precoder is designed based on the algorithm developed for SU-MIMO scenario assuming that the users are cooperative and have equal priority weights. When the analog precoder is fixed, the iterative weighted minimum mean squared error (WMMSE) approach is employed to design the digital precoders at each subcarrier to deal with the inter-user interference and also the different priority weights of different data streams. Numerical results show that the fully-connected hybrid architecture with this design can already approach the performance of the fully digital WMMSE beamforming.

1.2.3 One-Bit Precoding for Rich-Scattering Channels

In Chapter 2 and Chapter 3, this thesis shows that the hybrid beamforming architecture achieves a promising performance especially in mmWave frequencies in which the channels are sparse. However, the wideband hybrid beamforming results for mmWave systems with sparse channels

cannot be extended to the wideband systems in rich-scattering environments. To address this issue, Chapter 4 introduces an alternative precoding architecture, called 1-bit precoding, for systems with rich-scattering channels.

In particular, Chapter 4 considers the precoder design problem for the downlink of a MU-MISO system where only 1-bit resolution DACs are available at the transmitter. Chapter 4 recognizes that due to the 1-bit DAC, precoding needs to be done on a symbol-by-symbol basis. Moreover, for the QAM signalling, Chapter 4 observes that it is crucial to design the QAM constellation range for each given channel realization in order to perform 1-bit precoding. Chapter 4 focuses on the massive MIMO regime and uses the average symbol error rate of uncoded transmission at the receiver as the design criterion. Chapter 4 makes the following main technical contributions toward the goal of optimizing the constellation range and subsequently 1-bit symbol-level precoding for the massive MIMO downlink:

Deriving a Tight Expression for the SER in Symbol-Level Precoding

Chapter 4 first derives a tight expression for the SER in 1-bit symbol-level precoding. Due to the low resolution transmit DAC, the noiseless receive signal may not line up exactly at the intended constellation location. The derived expression suggests that there is a reduction in the minimum constellation symbol distance in this case. The minimum distance is effectively reduced by the twice of the distance between the noiseless received signal and the intended constellation symbol.

QAM Constellation and One-Bit Precoding Design for SU-MISO Systems

Chapter 4 points out the importance of optimizing the QAM constellation range for 1-bit symbol-level precoding. Inspired by the results from the case where the infinite resolution DACs are available, this thesis concludes that the constellation range should be restricted to the regime where the noiseless received signal of 1-bit precoding can approach all the points in the designed constellation. The analytical result shows that a reasonable choice for the QAM constellation range for 1-bit precoding should be about $\sqrt{2/\pi} \approx 0.8$ times the optimal constellation range in the infinite resolution case with instantaneous power constraint.

In 1-bit precoding, the transmitting signal of each antenna is selected from a quadrature

phase shift keying (QPSK) like alphabet and hence the transmitting signal design problem is a combinatorial optimization problem for which exhaustive search would have exponential complexity. To address that, Chapter 4 proposes a low-complexity two-step heuristic algorithm which finds a high-quality solution for the 1-bit symbol-level precoding problem. Inspired by the observation that 1-bit precoder can realize the constellation points closer to the origin of the complex plane more accurately, the first step of the proposed algorithm iteratively designs the transmitted signal at each antenna such that the overall received signal is as close to the origin of the complex plane as possible. This process is repeated until the transmit signals of all the antennas except last few, i.e., about 5 – 10 antennas, are designed. In the second step, the proposed algorithm performs an exhaustive search on the transmit signals of the remaining few antennas in order to find the best configuration.

QAM Constellation and One-Bit Precoding Design for MU-MISO Systems

Next, the proposed constellation range and 1-bit precoder designs are generalized to the multi-user case. Chapter 4 first designs the constellation range for the multi-user ZF precoder with per-symbol power constraint but assuming infinite resolution DACs. It is observed that in the limit of large number of users, the constellation range for the multi-user case should be set to that of the single-user case multiplied by a factor which is a function of the number of constellation points and the number of users. For the 1-bit precoding case, Chapter 4 proposes to further scale the proposed constellation range design by $\sqrt{2/\pi} \approx 0.8$, the same factor as for the single-user 1-bit precoding. The low-complexity precoding design algorithm is likewise generalized to the multi-user scenario.

Performance Characterization of the Proposed One-Bit Precoding Designs

Finally, Chapter 4 analytically characterizes the performance of the proposed 1-bit symbol-level precoding design and show that there is about 2dB gap between the proposed 1-bit precoding scheme and infinite resolution precoding under the same per-symbol power constraint in the massive MIMO regime. This 2dB gap is true for both single-user and multi-user precoding designs. Moreover, Chapter 4 shows that this 2dB gap can be translated to about 50% more required number of antennas for the 1-bit precoding architecture as compared to the conven-

tional infinite resolution architecture for achieving the same performance. Numerical results are also provided to show that the promising performances can be achieved by the proposed designs.

1.3 Related Work

This section provides a brief review of the literature related to each of the three main parts of this thesis. To have a broader picture on hybrid beamforming and other signal processing techniques for mmWave systems, this thesis refers to the recent surveys in [20, 28].

1.3.1 Hybrid Beamforming for Narrowband Flat-Fading Channels

The idea of hybrid beamforming is introduced under the names of “RF-baseband codesign” and “antenna soft selection” for a point-to-point SU-MIMO scenario in [18] and [29], respectively. It is shown in [18] that for a SU-MIMO system with diversity transmission, i.e., the number of data streams is one, hybrid beamforming can realize the optimal fully digital beamformer if and only if the number of RF chains at each end is at least two. This thesis generalizes the above result for spatial multiplexing transmission for MU-MIMO systems. In particular, this thesis shows that hybrid structure can realize any fully digital beamformer if the number of RF chains is twice the number of data streams. It is mentioned that the recent work of [30] also addressed the question of how many RF chains are needed for hybrid beamforming structure to realize digital beamforming. The authors of [30] propose a hybrid beamforming structure which is slightly different from the conventional fully-connected hybrid beamforming structure in [18, 29, 31–36]. In the conventional fully-connected hybrid beamforming structure the number of phase shifters is $N_{\text{PS}} = N_{\text{RF}}M$ where N_{RF} is the number of RF chains and M is the number of antennas. The proposed hybrid structure in [30] with $N_{\text{RF}} = N_s$ RF chains and about $2N_s M$ phase shifters is shown to be able to realize any fully digital beamforming.

The idea of antenna soft selection is reintroduced under the name of hybrid beamforming for mmWave frequencies [31–33]. For a point-to-point large-scale SU-MIMO system, [31] proposes an algorithm based on the sparse nature of mmWave channels. It is shown that the spectral efficiency maximization problem for mmWave channels can be approximately solved by

addressing a matrix approximation problem, i.e., minimizing the Frobenius norm of the difference between the optimal fully digital beamformer and the overall hybrid beamformer. Using a compressed sensing algorithm called basis pursuit, [31] is able to design hybrid beamformers which achieve good performance when (i) extremely large number of antennas is used at both ends; (ii) the number of RF chains is strictly greater than the number of data streams; (iii) extremely correlated channel matrix is assumed. But in other cases, there is a significant gap between the theoretical maximum capacity and the achievable rate of the algorithm of [31]. This thesis devises a heuristic algorithm that reduces this gap for the case that the number of RF chains is equal to the number of data streams; it is also compatible with any channel model.

It is noted that some other recent work also observes the performance gap between the hybrid beamforming method proposed in [31] and the optimal fully digital beamforming and consequently seeks to reduce this performance gap. For example, [37] proposes an alternating minimization algorithm to approximate the solution of matrix approximation problem. In the algorithm of [37], manifold optimization is employed to tackle the problem of analog beamforming design problem which involves constant modulus constraints.

For the downlink of K -user MISO systems, it is shown in [35, 36] that hybrid beamforming with K RF chains at the BS can achieve a reasonable sum rate as compared to the sum rate of fully digital ZF beamforming which is near optimal for massive MIMO systems [3]. The design of [35, 36] involves matching the analog precoder to the phase of the channel and setting the digital precoder to be the ZF beamformer for the effective channel. However, there is still a gap between the rate achieved with this particular hybrid design and the maximum capacity. This thesis proposes a method to design hybrid precoders for the case that the number of RF chains is slightly greater than K and numerically shows that the proposed design can be used to reduce the gap to capacity.

This thesis also notes some other recent references which consider multi-user hybrid beamforming design [38–40]. The authors in [38] devise a two-stage hybrid precoding algorithm for the downlink multi-user MIMO systems with limited feedback channel. The first step of the algorithm in [38] seeks to design the transmit/receive analog beamformers by maximizing the power of desired signal while the inter-user interference is neglected. The second stage of the algorithm in [38] designs the digital transmit/receive beamformers to manage the inter-user

interference. In [39], a hybrid beamforming design is proposed in which the phase-only analog beamforming is combined with block diagonalization based digital beamforming to maximize the spectral efficiency in a MU-MIMO system with a generic channel model. Further, the authors of [40] exploit the sparsity of the mmWave channels to propose an iterative matrix decomposition based block diagonalization hybrid beamforming scheme for multi-user mmWave systems.

The aforementioned existing hybrid beamforming designs typically assume the use of infinite resolution phase shifters for implementing analog beamformers. However, the components required for realizing accurate phase shifters can be expensive [41, 42]. More cost-effective low resolution phase shifters are typically used in practice. The straightforward way to design beamformers with finite resolution phase shifters is to design the analog beamformer assuming infinite resolution first, then to quantize the value of each phase shifter to a finite set [36]. However, the numerical results of this thesis reveal that this approach is not effective for systems with very low resolution phase shifters. To address that, this thesis further presents a modification to the proposed method for the SU-MIMO scenario as well as the MU-MISO scenario when only finite resolution phase shifters are available. Numerical results show that the proposed method is effective even for the very low resolution phase shifter scenario.

This thesis considers the availability of the perfect CSI for hybrid beamforming design in order to study the ultimate performance of the hybrid architecture. However, in practice, a channel estimation phase is required to obtain the CSI. The authors in [33] propose an efficient channel estimation algorithm for hybrid architecture operating in mmWave frequencies using the sparse nature of the channel in those frequencies.

It should be noted that this thesis focuses on spectral efficiency maximization for hybrid beamforming, however hybrid beamforming architecture has been also used for other applications. For example, the authors in [43] propose a novel hybrid beamforming design in order to enhance the secrecy in multi-antenna transmission systems and the authors in [44] consider hybrid structure for simultaneously transferring wireless information and power.

1.3.2 Hybrid Beamforming for mmWave Wideband Channels

Several recent works have considered the use of hybrid beamforming architecture for frequency-selective channels [37, 45–48]. In [45], the problem of hybrid beamforming design for maximizing the spectral efficiency in a SU-MIMO mmWave system with limited feedback is considered. The authors of [45] first develop a hybrid analog-digital codebook design scheme for broadband mmWave systems, then propose a hybrid precoding algorithm for the given codebook based on Gram-Schmidt orthogonalization.

The reference [37] also considers the spectral efficiency maximization problem for a SU-MIMO system, but unlike [45] the beamformers are not restricted to come from a fixed codebook. The algorithm in [37] seeks to minimize the norm distance between the optimal fully digital beamformers and the overall hybrid beamformers instead of tackling the original problem of spectral efficiency maximization directly.

In [46], a heuristic algorithm is devised to design the hybrid precoders to maximize the overall rate for a SU-MIMO system in which hybrid architecture is only employed at the transmitter. Taking different approach as compared to this thesis, it is also shown in [46] that the average of the sample covariance matrices of frequency domain channels is an important metric in designing the analog precoder.

Through numerical simulations, this thesis shows that under typical parameter settings the proposed algorithm for SU-MIMO scenario achieves a better performance as compared to the algorithms in [37] and [46].

The weighted sum rate maximization problem under the total power constraint for the downlink of OFDM-based MU-MISO systems is recently considered in [47]. The authors in [47] devise an alternating optimization algorithm based on the equivalence between the sum rate maximization problem and the weighted sum mean squared error (MSE) minimization. That algorithm is only applicable to the setting where the total power constraint is considered. However, in practice for wideband systems it is desirable to design the precoders such that the per subcarrier power constraint; i.e. power spectrum density constraint, is satisfied due to the spectral mask limitations [49–52]. In contrast to [47], the proposed algorithm in this thesis addresses the hybrid precoding design problem for per subcarrier power constraint.

As mentioned before, the results of this thesis suggest that the analog part of the hybrid beamforming in a wideband systems should be designed based on the average of the sample covariance matrices of frequency domain channels. On the other hand, a number of papers on narrowband hybrid beamforming (e.g., [19], [53], and [54] for SU-MIMO, MU-MISO, and MU-MIMO, respectively) proposes to update the design of analog and digital beamformers on different time scales in order to reduce the overhead of CSI acquisition for large-scale antenna arrays. In particular, they propose to design the analog beamformers based on the second order channel statistics and the digital beamformers based on the reduced-dimension instantaneous channel. By considering the results of this thesis and the two-time-scale hybrid beamforming designs in [19,53,54] at the same time, one can see that for a wideband system with large number of subcarriers and with pedestrians mobility where the average of sample covariance of frequency domain channels converges to the time domain second order channel statistics, designing the analog beamformers according to the second order channel statistics is an appropriate choice.

Throughout the part of hybrid beamforming design for mmWave wideband channels, the availability of the perfect CSI is assumed. This assumption is made in order to understand the capability of the hybrid architecture for supporting mmWave wideband systems, but it can also be reasonable in certain cases. In [48], it is shown that the channel coefficients can be estimated accurately by exploiting the intrinsic low-rank structure of the mmWave channels.

The very recent work of [55] implements partially-connected hybrid beamforming architecture in 60 GHz for a wideband 2-user MIMO system in which the transmitter is equipped with 32 antennas and 2 RF chains while each receiver is equipped with 4 antennas and a single RF chain. The preliminary results of [55] suggest that hybrid structure is an appropriate choice to achieve spatial multiplexing with reasonable hardware complexity.

1.3.3 One-Bit Precoding for Rich-Scattering Channels

Most of the existing literatures on 1-bit beamforming focuses on the uplink scenario in which the BS is equipped with 1-bit analog-to-digital converters (ADCs). The performance analysis of such systems for narrowband channels are provided in [56–59] while those for wideband channels are presented in [60,61].

For downlink precoding with 1-bit DAC, the authors of [62,63] propose a quantized ZF

method. Although, this method can approach the performance of the infinite resolution precoding in low signal-to-noise ratio (SNR) regime, it suffers from high symbol error floor in the high SNR regime. In [64], the authors propose some methods for slightly perturbing the transmitted signal of the quantized ZF scheme in order to improve performance at higher SNRs and numerically show that those perturbations can provide significant gains for QPSK signalling. More sophisticated precoding methods have been proposed in [65–67] for the scenario where both the receivers and the transmitter are equipped with 1-bit ADCs and DACs, respectively. However, these methods are applicable only for QPSK signalling and for the case where the receiver has 1-bit ADC. This thesis observes that in practice the user terminal is often equipped with only one antenna, so the power consumption of high resolution ADCs at the downlink receiver is not unreasonable. For this reason, this thesis considers the scenario with 1-bit DAC at the transmitter, but high resolution ADC at the receiver.

The authors of [68] generalize the algorithm in [65] for the infinite resolution receivers and introduce a technique to transmit 16-QAM symbols with 1-bit transmitters based on the idea of superposition coding. Unlike the algorithm in [68], the proposed scheme in this thesis can be applied to the QAM constellations with any size. More importantly, this thesis points out the crucial role played by QAM constellation range design, which is not considered in prior work [65].

The recent contributions of [69, 70] consider designing the constellation range, as well as a non-linear precoder scheme with higher order modulations. The algorithms in [69, 70], which seek to minimize the mean squared error at the user side, achieve excellent performance within few dB gap to the infinite-resolution precoding benchmarks. However, in the algorithm of [69, 70], the constellation range is designed for each symbol transmission, which means that the range information needs to be communicated to the receiver as side information on a symbol-by-symbol basis. This is a significant overhead. The recent work [71] extends the algorithm in [70] by considering the constellation range design for T symbol transmissions in which the channel remains constant. However, the high computational complexity of the algorithm in [71] (which is $O(M^3T^3)$ for a system with M transmit antennas) prohibits its use for the typical massive MIMO systems in which M and T are both large.

By recognizing that the coherence time of the wireless channel in practice is typically large

enough to allow at least several hundreds of symbol transmissions, this thesis proposes to design the constellation range for each fading block such that it is suitable for all possible symbol vector choices from the constellation. Furthermore, this thesis shows that for large-scale antenna arrays the proposed constellation range design can be approximated by a constant value which is independent of the channel realization thanks to the “channel hardening” phenomenon in massive MIMO systems [72]. Therefore, the QAM constellation range can be predetermined a priori with no need for instantaneous channel state information (CSI) at the receivers.

Finally, this thesis notes some other references which have considered 1-bit precoding architecture for other constellations rather than QAM constellation. The authors of [73, 74] propose novel 1-bit precoding designs for phase shift keying (PSK) constellation. However, they do not address the problem of designing the PSK constellation in those papers.

1.4 Notations

This thesis uses normal face letters for scalars, lower-case bold face letters for vectors and upper-case bold face letters for matrices. The real part and the imaginary part of a complex scalar s are denoted by $\text{Re}\{s\}$ and $\text{Im}\{s\}$, respectively. For a matrix \mathbf{A} , the element in the i^{th} row and the j^{th} column is denoted by $\mathbf{A}(i, j)$. For a column vector \mathbf{v} , $\text{diag}(\cdot)$ returns a diagonal matrix with elements of \mathbf{v} as the diagonal elements. Further, this thesis uses the superscript H to denote the Hermitian transpose of a matrix and superscript \dagger or $*$ to denote the complex conjugate. The identity and all-one matrices with appropriate dimensions are denoted by \mathbf{I} and $\mathbf{1}$, respectively; $\mathbb{C}^{m \times n}$ denotes an m by n dimensional complex space; $\mathcal{CN}(\mathbf{0}, \mathbf{R})$ represents the zero-mean circularly symmetric complex Gaussian distribution with covariance matrix \mathbf{R} ; $\mathcal{N}(\boldsymbol{\mu}, \boldsymbol{\Sigma})$ represents a real Gaussian distribution with mean $\boldsymbol{\mu}$ and covariance matrix $\boldsymbol{\Sigma}$. The notations $\text{Tr}(\cdot)$, $\log_2(\cdot)$, $\log_{10}(\cdot)$, and $\mathbb{E}\{\cdot\}$ represent the trace, binary logarithm, decimal logarithm, and expectation operators, respectively. Moreover, $|\cdot|$ represents the determinant of a matrix or the absolute value of a scalar depending on context while $\|\cdot\|_p$ indicates the p -norm of a vector. Finally, $\frac{\partial f}{\partial x}$ is used to denote the partial derivative of the function f with respect to x .

Chapter 2

Hybrid Beamforming for Narrowband Flat-Fading Channels

2.1 Chapter Organization

This chapter considers a narrowband system in which the transceivers with large-scale antenna arrays are equipped with limited number of RF chains. To address the difficulty of limited number of RF chains, this chapter proposes a two-stage hybrid beamforming architecture in which the beamformer is constructed by concatenation of a low-dimensional digital (baseband) beamformer and an analog (RF) beamformer which is typically implemented using phase shifters. In particular, this chapter seeks to design the fully-connected hybrid beamforming architecture in order to maximize the overall spectral efficiency of the system under total power constraint when the perfect CSI is available. The details of the system model and the problem formulation are provided in Section 2.2.

This chapter begins with studying the conditions on the number of required RF chains such that the fully-connected hybrid beamforming architecture would be able to construct any fully digital beamformer. In particular, Section 2.3 shows that to accomplish that aim, it is necessary that the number of RF chains in hybrid architecture exceeds the number of data streams. More interestingly, Section 2.3 establishes that the number of RF chains in hybrid structure only needs to scale as twice the total number of data streams for it to achieve the exact

same performance as that of any fully digital beamforming scheme regardless of the number of antenna elements.

The following parts of this chapter consider the hybrid beamforming design when the number of RF chains is less than twice the number of data streams. For the case that the number of RF chains is exactly equal to the number of data streams, Section 2.4 provides the design of the hybrid beamformers in a SU-MIMO system in which both transceivers are equipped with hybrid-structure large-scale antenna arrays. This design is further generalized in Section 2.4 for the cases where the number of RF chains is larger than the number of data streams.

This chapter also considers hybrid beamforming design problem for massive MU-MISO systems in which a BS with hybrid beamforming architecture transmits to multiple single-antenna users. By adopting zero-forcing beamforming as the digital beamformer, Section. 2.5 presents hybrid beamforming design for the downlink MU-MIMO system when the number of RF chains is strictly larger than the number of data streams.

The aforementioned designs are all restricted to the scenarios that infinite resolution phase shifters are available. However, due to the cost of such accurate phase shifters, only finite resolution phase shifters may be available in the practical systems. Section. 2.6 modifies the proposed hybrid beamforming designs when the low resolution phase shifters are used.

The numerical results presented in Section 2.7 show that for both SU-MIMO and MU-MISO scenarios the fully-connected hybrid beamforming with infinite resolution phase shifters can achieve spectral efficiency close to that of the fully digital solution with the number of RF chains approximately equal to the number of data streams. Further, it is shown that the proposed design for hybrid beamforming with finite resolution phase shifters is more effective as compared to the existing solutions. Finally, the summary of this chapter is provided in Section 2.8.

It should be emphasized that throughout this chapter it is assumed that the transceivers have access to perfect CSI. The availability of perfect CSI is an idealistic assumption which rarely occurs in practice, especially for systems implementing large-scale antenna arrays. However, the algorithms proposed in this chapter are still useful as a reference point for studying the performance of hybrid beamforming architecture in comparison with fully digital beamforming. Moreover, for imperfect CSI scenario, one way to design the hybrid beamformers is to first design

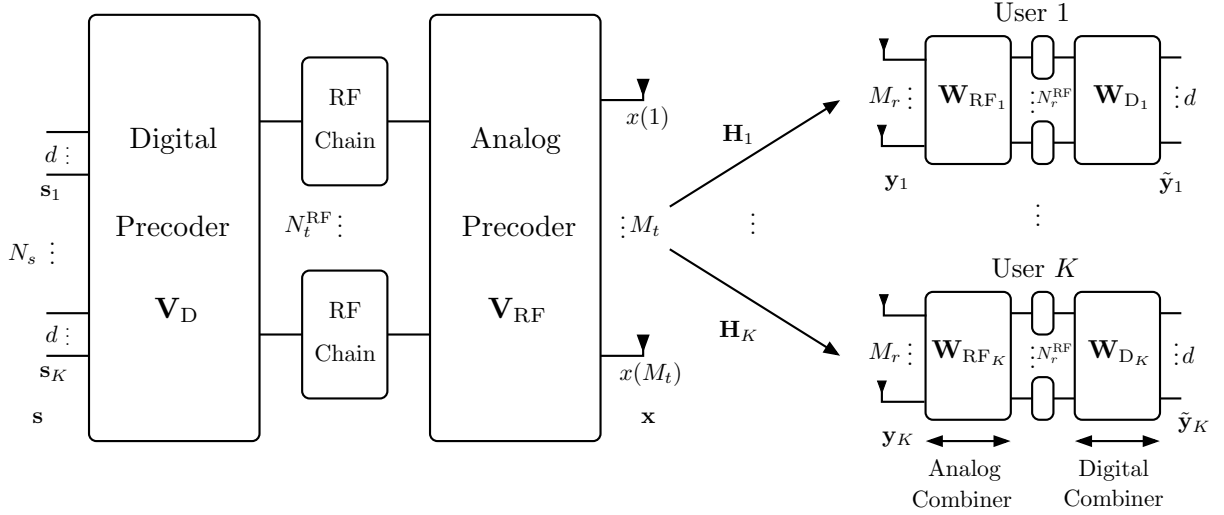


Fig. 2.1: Block diagram of a downlink MU-MIMO system with hybrid beamforming architecture at the BS and the user terminals.

the analog beamformers assuming perfect CSI, and then to design the digital beamformers employing robust beamforming techniques [75–79] to deal with imperfect CSI. It is therefore still of interest to study the analog beamformer design problem in perfect CSI.

2.2 System Model

Consider a narrowband downlink single-cell MU-MIMO system in which a BS with M_t antennas and N_t^{RF} transmit RF chains serves K users, each equipped with M_r antennas and N_r^{RF} receive RF chains. Further, it is assumed that each user requires d data streams and that $Kd \leq N_t^{RF} \leq M_t$ and $d \leq N_r^{RF} \leq M_r$. Since the number of transmit/receive RF chains is limited, the implementation of fully digital beamforming which requires one dedicated RF chain per antenna element, is not possible. Instead, a two-stage hybrid digital and analog beamforming architecture is considered at the BS and the user terminals as shown in Fig. 2.1.

2.2.1 Signal Model in Hybrid Beamforming

In hybrid beamforming structure, the BS first modifies the data streams digitally at baseband using an $N_t^{RF} \times N_s$ digital precoder, \mathbf{V}_D , where $N_s = Kd$, then up-converts the processed signals to the carrier frequency by passing through N_t^{RF} RF chains. After that, the BS uses an $M_t \times N_t^{RF}$ analog precoder, \mathbf{V}_{RF} , which is implemented using analog phase shifters, i.e., with

$|\mathbf{V}_{\text{RF}}(i,j)|^2 = 1$, to construct the final transmitted signal. Mathematically, the transmitted signal can be written as

$$\mathbf{x} = \mathbf{V}_{\text{RF}} \mathbf{V}_{\text{D}} \mathbf{s} = \sum_{\ell=1}^K \mathbf{V}_{\text{RF}} \mathbf{V}_{\text{D}_\ell} \mathbf{s}_\ell, \quad (2.1)$$

where $\mathbf{V}_{\text{D}} = [\mathbf{V}_{\text{D}_1}, \dots, \mathbf{V}_{\text{D}_K}]$, and $\mathbf{s} \in \mathbb{C}^{N_s \times 1}$ is the vector of data symbols which is the concatenation of each user's data stream vector such as $\mathbf{s} = [\mathbf{s}_1^T, \dots, \mathbf{s}_K^T]^T$, where \mathbf{s}_ℓ is the data stream vector for user ℓ . Further, it is assumed that $\mathbb{E}\{\mathbf{s}\mathbf{s}^H\} = \mathbf{I}_{N_s}$. For user k , the received signal can be modelled as

$$\mathbf{y}_k = \mathbf{H}_k \mathbf{V}_{\text{RF}} \mathbf{V}_{\text{D}_k} \mathbf{s}_k + \mathbf{H}_k \sum_{\ell \neq k} \mathbf{V}_{\text{RF}} \mathbf{V}_{\text{D}_\ell} \mathbf{s}_\ell + \mathbf{z}_k, \quad (2.2)$$

where $\mathbf{H}_k \in \mathbb{C}^{M_r \times M_t}$ is the matrix of complex channel gains from the transmit antennas of the BS to the k^{th} user antennas and $\mathbf{z}_k \sim \mathcal{CN}(\mathbf{0}, \sigma^2 \mathbf{I}_{M_r})$ denotes additive white Gaussian noise. The user k first processes the received signals using an $M_r \times N_r^{\text{RF}}$ analog combiner, \mathbf{W}_{RF_k} , implemented using phase shifters such that $|\mathbf{W}_{\text{RF}_k}(i,j)|^2 = 1$, then down-converts the signals to the baseband using N_r^{RF} RF chains. Finally, using a low-dimensional digital combiner, $\mathbf{W}_{\text{D}_k} \in \mathbb{C}^{N_r^{\text{RF}} \times d}$, the final processed signals are obtained as

$$\tilde{\mathbf{y}}_k = \underbrace{\mathbf{W}_{\text{t}_k}^H \mathbf{H}_k \mathbf{V}_{\text{t}_k} \mathbf{s}_k}_{\text{desired signals}} + \underbrace{\mathbf{W}_{\text{t}_k}^H \mathbf{H}_k \sum_{\ell \neq k} \mathbf{V}_{\text{t}_\ell} \mathbf{s}_\ell}_{\text{effective interference}} + \underbrace{\mathbf{W}_{\text{t}_k}^H \mathbf{z}_k}_{\text{effective noise}}, \quad (2.3)$$

where $\mathbf{V}_{\text{t}_k} = \mathbf{V}_{\text{RF}} \mathbf{V}_{\text{D}_k}$ and $\mathbf{W}_{\text{t}_k} = \mathbf{W}_{\text{RF}_k} \mathbf{W}_{\text{D}_k}$ are the overall hybrid precoder and combiner for the k^{th} user, respectively. In such a system, the overall spectral efficiency (rate) of user k assuming Gaussian signalling is [80]

$$R_k = \log_2 |\mathbf{I}_{M_r} + \mathbf{W}_{\text{t}_k} \mathbf{C}_k^{-1} \mathbf{W}_{\text{t}_k}^H \mathbf{H}_k \mathbf{V}_{\text{t}_k} \mathbf{V}_{\text{t}_k}^H \mathbf{H}_k^H|, \quad (2.4)$$

where

$$\mathbf{C}_k = \mathbf{W}_{\text{t}_k}^H \mathbf{H}_k \left(\sum_{\ell \neq k} \mathbf{V}_{\text{t}_\ell} \mathbf{V}_{\text{t}_\ell}^H \right) \mathbf{H}_k^H \mathbf{W}_{\text{t}_k} + \sigma^2 \mathbf{W}_{\text{t}_k}^H \mathbf{W}_{\text{t}_k}, \quad (2.5)$$

is the covariance of the interference plus noise at user k .

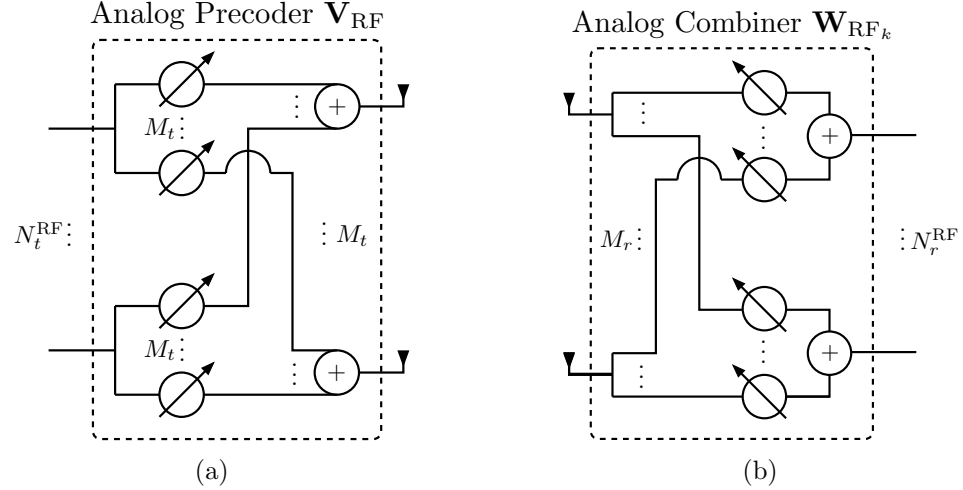


Fig. 2.2: (a) The architecture of an analog precoder with fully-connected structure. (b) The architecture of an analog combiner with fully-connected structure.

2.2.2 Structure of Analog Beamformer

The analog part of the hybrid beamformer is typically implemented using simple analog components such as analog adders and analog phase shifters which can only change the phase of signals. This imposes some constraints on the analog beamforming matrix depending on the structure of the analog beamformer. This chapter focuses on one specific analog beamforming structure with the maximum degrees of freedom called the fully-connected structure. However, most the designs of this chapter can be easily extended to the partially-connected structure described in Chapter 1.

The schematics of the fully-connected hybrid beamforming architecture at the transmitter and the receiver are shown in Fig. 2.2(a) and Fig. 2.2(b), respectively. As shown in Fig. 2.2, in the fully-connected structure, each RF chain is connected to all the antenna elements via a network of phase shifters. This results in constant modulus norm constraint on all elements of the analog beamforming matrices, i.e., $|\mathbf{V}_{RF}(i,j)|^2 = |\mathbf{W}_{RF}(i,j)|^2 = 1, \forall i, j$. Further, it can be seen from Fig. 2.2 that the total number of phase shifters used in this architecture is $M_t N_t^{RF}$ and $M_r N_r^{RF}$ at the transmitter and the receiver, respectively.

2.2.3 Problem Formulation

The problem of interest in this chapter is to maximize the overall spectral efficiency under total transmit power constraint, assuming perfect knowledge of \mathbf{H}_k , i.e., this thesis aims to find the optimal hybrid precoders at the BS and the optimal hybrid combiners for each user by solving the following problem:

$$\underset{\mathbf{V}_{\text{RF}}, \mathbf{V}_{\text{D}}, \mathbf{W}_{\text{RF}_k}, \mathbf{W}_{\text{D}_k}}{\text{maximize}} \quad \sum_{k=1}^K \beta_k R_k \quad (2.6a)$$

$$\text{subject to} \quad \text{Tr}(\mathbf{V}_{\text{RF}} \mathbf{V}_{\text{D}} \mathbf{V}_{\text{D}}^H \mathbf{V}_{\text{RF}}^H) \leq P, \quad (2.6b)$$

$$|\mathbf{V}_{\text{RF}}(i, j)|^2 = 1, \quad \forall i, j, \quad (2.6c)$$

$$|\mathbf{W}_{\text{RF}_k}(i, j)|^2 = 1, \quad \forall i, j, k, \quad (2.6d)$$

where P is the total power budget at the BS and the weight β_k represents the priority of user k ; i.e., the larger $\frac{\beta_k}{\sum_{\ell=1}^K \beta_\ell}$ implies greater priority for user k .

The system model in this section is described for a general setting. The next section characterizes the minimum number of RF chains in hybrid beamforming architecture for realizing a fully digital beamformer for the general system model. The subsequent parts of this chapter focus on two specific scenarios:

1. SU-MIMO system with large antenna arrays at both ends, i.e., $K = 1$ and $\min(M_t, M_r) \gg N_s$.
2. Downlink MU-MISO system with large number of antennas at the BS and single antenna at the user side, i.e., $M_t \gg K$ and $M_r = 1$.

2.3 Minimum Number of RF Chains to Realize Fully Digital Beamformers

The first part of this chapter establishes theoretical bounds on the minimum number of RF chains that are required for the fully-connected hybrid beamforming structure to be able to realize any fully digital beamforming schemes. Recall that without the hybrid structure constraints, fully digital beamforming schemes can be easily designed with $N_t^{\text{RF}} = M_t$ RF chains

at the BS and $N_r^{\text{RF}} = M_r$ RF chains at the user side [4–6, 81, 82]. This section aims to show that hybrid beamforming architecture can realize fully digital beamforming schemes with potentially smaller number of RF chains. Toward this aim, this section begins by presenting a necessary condition on the number of RF chains for implementing a fully digital beamformer, $\mathbf{F}_{\text{FD}} \in \mathbb{C}^{M \times N_s}$. Note that in order to emphasize that the results of this section are valid for both the transmitter side and the receiver side, throughout this section, the subscripts in the notation of the number of antennas and the number of RF chains are dropped and they are denoted by M and N_{RF} , respectively.

Proposition 1. *To realize a full-rank fully digital beamforming matrix, it is necessary that the number of RF chains in the hybrid architecture (shown in Fig. 2.2) is greater than or equal to the number of active data streams, i.e., $N_{\text{RF}} \geq N_s$.*

Proof. Let denote the analog beamformer and digital beamformer in hybrid structure with \mathbf{F}_{RF} and \mathbf{F}_{D} , respectively. It is easy to see that $\text{rank}(\mathbf{F}_{\text{RF}}\mathbf{F}_{\text{D}}) \leq N_{\text{RF}}$ and $\text{rank}(\mathbf{F}_{\text{FD}}) = N_s$. Therefore, hybrid beamforming structure requires at least $N_{\text{RF}} \geq N_s$ RF chains to implement \mathbf{F}_{FD} . \square

The following part addresses how many RF chains are sufficient in the hybrid structure for implementing any fully digital beamformer $\mathbf{F}_{\text{FD}} \in \mathbb{C}^{M \times N_s}$. It is already known that for the case of $N_s = 1$, the hybrid beamforming structure can realize any fully digital beamformer if and only if $N_{\text{RF}} \geq 2$ [18]. Proposition 2 generalizes this result for any arbitrary value of N_s .

Proposition 2. *To realize any fully digital beamforming matrix, it is sufficient that the number of RF chains in hybrid architecture (shown in Fig. 2.2) is greater than or equal to twice the number of data streams, i.e., $N_{\text{RF}} \geq 2N_s$.*

Proof. Let $N_{\text{RF}} = 2N_s$ and denote $\mathbf{F}_{\text{FD}}(i, j) = \nu_{i,j} e^{j\phi_{i,j}}$ and $\mathbf{F}_{\text{RF}}(i, j) = e^{j\theta_{i,j}}$ where j is the complex unit satisfying $j^2 = -1$. The following solution is proposed to satisfy $\mathbf{F}_{\text{RF}}\mathbf{F}_{\text{D}} = \mathbf{F}_{\text{FD}}$. Choose the k^{th} column of the digital beamformer as $\mathbf{f}_{\text{D}}^{(k)} = [\mathbf{0}^T \ f_{2k-1} \ f_{2k} \ \mathbf{0}^T]^T$. Then,

satisfying $\mathbf{F}_{\text{RF}}\mathbf{F}_{\text{D}} = \mathbf{F}_{\text{FD}}$ is equivalent to

$$\begin{bmatrix} & & & \\ \dots & e^{j\theta_{i,2k-1}} & e^{j\theta_{i,2k}} & \dots \end{bmatrix} \begin{bmatrix} 0 \\ \vdots \\ f_{2k-1} \\ f_{2k} \\ \vdots \\ 0 \end{bmatrix} = \nu_{i,k} e^{j\phi_{i,k}},$$

or

$$f_{2k-1} e^{j\theta_{i,2k-1}} + f_{2k} e^{j\theta_{i,2k}} = \nu_{i,k} e^{j\phi_{i,k}}, \quad (2.7)$$

for all $i = 1, \dots, M$ and $k = 1, \dots, N_s$. This non-linear system of equations has multiple solutions [18]. If it is further chosen to set $f_{2k-1} = f_{2k} = \nu_{\max}^{(k)}$ where $\nu_{\max}^{(k)} = \max_i \{\nu_{i,k}\}$, it can be verified after several algebraic steps that the following is a solution to (2.7):

$$\begin{aligned} \theta_{i,2k-1} &= \phi_{i,k} - \cos^{-1} \left(\frac{\nu_{i,k}}{2\nu_{\max}^{(k)}} \right), \\ \theta_{i,2k} &= \phi_{i,k} + \cos^{-1} \left(\frac{\nu_{i,k}}{2\nu_{\max}^{(k)}} \right). \end{aligned} \quad (2.8)$$

Thus for the case that $N_{\text{RF}} = 2N_s$, a solution to $\mathbf{F}_{\text{RF}}\mathbf{F}_{\text{D}} = \mathbf{F}_{\text{FD}}$ can be readily found. The validity of the proposition for $N_{\text{RF}} > 2N_s$ is obvious since the same parameters can be used as for $N_{\text{RF}} = 2N_s$ by setting the extra parameters to be zero in \mathbf{F}_{D} . \square

Remark 1. The solution given in Proposition 2 is one possible set of solutions to the equations in (2.7). The interesting property of that specific solution is that as two digital gains of each data stream are identical; i.e., $f_{2k-1} = f_{2k}$, it is possible to convert one realization of the scaled data symbol to RF signal and then use it twice. Therefore, it is in fact possible to realize any fully digital beamformer using the hybrid structure with N_s RF chains and $2N_sM$ phase shifters. This leads this thesis to the similar result but with different design as in [30]. However, in the rest of this chapter, the conventional configuration of fully-connected hybrid structure in which the number of phase shifters are $N_{\text{RF}}M$ is considered. It is shown that near

optimal performance can be obtained with $N_{\text{RF}} \approx N_s$, thus further reducing the number of phase shifters as compared to the solution above is possible.

Remark 2. Proposition 2 is stated for a generic \mathbf{F}_{FD} which can be a full-rank matrix, i.e., $\text{rank}(\mathbf{F}_{\text{FD}}) = N_s$. In the case that \mathbf{F}_{FD} is a rank-deficient matrix, which is a common scenario in the low SNR regime, it can always be decomposed as $\mathbf{F}_{\text{FD}} = \mathbf{A}_{M \times r} \mathbf{B}_{r \times N_s}$ where $r = \text{rank}(\mathbf{F}_{\text{FD}})$. Since \mathbf{A} is a full-rank matrix, it can be realized using the procedure in the proof of Proposition 2 as $\mathbf{A} = \mathbf{F}_{\text{RF}} \mathbf{F}'_{\text{D}}$ with hybrid structure using $2r$ RF chains. Therefore, $\mathbf{F}_{\text{FD}} = \mathbf{F}_{\text{RF}} (\mathbf{F}'_{\text{D}} \mathbf{B})$ can be realized by hybrid structure using $2r$ RF chains with \mathbf{F}_{RF} as analog beamformer and $\mathbf{F}'_{\text{D}} \mathbf{B}$ as digital beamformer.

2.4 Hybrid Beamforming Design for Large-Scale SU-MIMO Systems

The second part of this chapter considers the design of hybrid beamformers. First, a large-scale SU-MIMO system in which a BS with M_t antennas sends N_s data symbols to a user with M_r antennas where $\min(M_t, M_r) \gg N_s$ is considered. Without loss of generality, identical number of transmit/receive RF chains is assumed, i.e., $N_t^{\text{RF}} = N_r^{\text{RF}} = N_{\text{RF}}$, to simplify the notation. For such a system with hybrid structure, the expression of the spectral efficiency in (2.4) can be simplified to

$$R = \log_2 \left| \mathbf{I}_{M_r} + \frac{1}{\sigma^2} \mathbf{W}_t (\mathbf{W}_t^H \mathbf{W}_t)^{-1} \mathbf{W}_t^H \mathbf{H} \mathbf{V}_t \mathbf{V}_t^H \mathbf{H}^H \right|. \quad (2.9)$$

where $\mathbf{V}_t = \mathbf{V}_{\text{RF}} \mathbf{V}_{\text{D}}$ and $\mathbf{W}_t = \mathbf{W}_{\text{RF}} \mathbf{W}_{\text{D}}$ are the overall hybrid precoder and combiner, respectively.

This section first focuses on hybrid beamforming design for the case that the number of RF chains is equal to the number of data streams; i.e., $N_{\text{RF}} = N_s$. This critical case is important because according to Proposition 1, the hybrid structure requires at least N_s RF chains to be able to realize the fully digital beamformer. For this case, a heuristic algorithm is proposed which achieves a rate close to the capacity. At the end of this section, it is shown that by further approximations, the proposed hybrid beamforming design algorithm for $N_{\text{RF}} = N_s$, can

be used for the case of $N_s < N_{\text{RF}} < 2N_s$ as well.

The problem of the spectral efficiency maximization in (2.6) involves joint optimization over the hybrid precoders and combiners. However, the joint transmit-receive beamforming matrix design, for similarly constrained optimization problem is usually found to be difficult to solve [83]. Further, the non-convex constraints on the elements of the analog beamformers in (2.6c) and (2.6d) make developing low-complexity algorithm for finding the exact optimal solution unlikely [31]. So, this thesis considers the following strategy instead. First, this thesis seeks to design the hybrid precoders, assuming that the optimal receiver is used. Then, for the already designed transmitter, it seeks to design the hybrid combiners.

Assuming that the optimal fully digital MMSE combiner is employed, the spectral efficiency can be expressed in terms of the precoders [5] and the transmitter design problem can be written as

$$\max_{\mathbf{V}_{\text{RF}}, \mathbf{V}_D} \log_2 \left| \mathbf{I}_{M_r} + \frac{1}{\sigma^2} \mathbf{H} \mathbf{V}_{\text{RF}} \mathbf{V}_D \mathbf{V}_D^H \mathbf{V}_{\text{RF}}^H \mathbf{H}^H \right| \quad (2.10a)$$

$$\text{s.t.} \quad \text{Tr} (\mathbf{V}_{\text{RF}} \mathbf{V}_D \mathbf{V}_D^H \mathbf{V}_{\text{RF}}^H) \leq P, \quad (2.10b)$$

$$|\mathbf{V}_{\text{RF}}(i, j)|^2 = 1, \quad \forall i, j. \quad (2.10c)$$

This problem is non-convex. This thesis proposes the following heuristic algorithm for obtaining a good solution to (2.10). First, the closed-form solution of the digital precoder in problem (2.10) for a fixed analog precoder, \mathbf{V}_{RF} , is derived. It is shown that regardless of the value of \mathbf{V}_{RF} , the digital precoder approximately satisfies $\mathbf{V}_D \mathbf{V}_D^H \propto \mathbf{I}$. Then, assuming such a digital precoder, an iterative algorithm to find a locally optimal analog precoder is proposed.

2.4.1 Digital Precoder Design for $N_{\text{RF}} = N_s$

The first part of the algorithm considers the design of \mathbf{V}_D assuming that \mathbf{V}_{RF} is fixed. For a fixed analog precoder, $\mathbf{H}_{\text{eff}} = \mathbf{H} \mathbf{V}_{\text{RF}}$ can be considered as an effective channel and the digital precoder design problem can be written as

$$\max_{\mathbf{V}_D} \log_2 \left| \mathbf{I}_{M_r} + \frac{1}{\sigma^2} \mathbf{H}_{\text{eff}} \mathbf{V}_D \mathbf{V}_D^H \mathbf{H}_{\text{eff}}^H \right| \quad (2.11a)$$

$$\text{s.t.} \quad \text{Tr} (\mathbf{Q} \mathbf{V}_D \mathbf{V}_D^H) \leq P, \quad (2.11b)$$

where $\mathbf{Q} = \mathbf{V}_{\text{RF}}^H \mathbf{V}_{\text{RF}}$. This problem has a well-known water-filling solution as

$$\mathbf{V}_D = \mathbf{Q}^{-1/2} \mathbf{U}_e \boldsymbol{\Gamma}_e, \quad (2.12)$$

where \mathbf{U}_e is the set of right singular vectors corresponding to the N_s largest singular values of $\mathbf{H}_{\text{eff}} \mathbf{Q}^{-1/2}$ and $\boldsymbol{\Gamma}_e$ is the diagonal matrix of allocated powers to each stream.

Now, this thesis seeks to exploit the structure of the digital precoder in (2.12) in order to simplify the analog precoding design problem. Toward this aim, this thesis observes that most of the existing hybrid precoding designs for analog precoding matrix satisfy $\mathbf{Q} = \mathbf{V}_{\text{RF}}^H \mathbf{V}_{\text{RF}} \approx M_t \mathbf{I}$, e.g., it is shown in [31] that for a channel with fixed number of scatterers if $M_t \rightarrow \infty$ then the asymptotically optimal analog precoder satisfies $\mathbf{Q} = \mathbf{V}_{\text{RF}}^H \mathbf{V}_{\text{RF}} = M_t \mathbf{I}$. Moreover, for moderate and high SNR regime, it is possible to adopt an equal power allocation for all the streams without significant performance degradation, $\boldsymbol{\Gamma}_e = \sqrt{P/N_{\text{RF}}} \mathbf{I}$. Using these observations, it can be seen that the optimal digital precoder approximately satisfies $\mathbf{V}_D \approx \gamma \mathbf{U}_e$ where $\gamma^2 = P/(M_t N_{\text{RF}})$. Since \mathbf{U}_e is a unitary matrix for the case that $N_{\text{RF}} = N_s$, it can be easily shown that $\mathbf{V}_D \mathbf{V}_D^H \approx \gamma^2 \mathbf{I}$.

2.4.2 Analog Precoder Design for $N_{\text{RF}} = N_s$

Now, this part seeks to design the analog precoder assuming $\mathbf{V}_D \mathbf{V}_D^H \approx \gamma^2 \mathbf{I}$. Under this assumption, the transmitter power constraint (2.10b) is automatically satisfied for any design of \mathbf{V}_{RF} . Therefore, the analog precoder can be obtained by solving

$$\max_{\mathbf{V}_{\text{RF}}} \log_2 \left| \mathbf{I} + \frac{\gamma^2}{\sigma^2} \mathbf{V}_{\text{RF}}^H \mathbf{F}_1 \mathbf{V}_{\text{RF}} \right| \quad (2.13a)$$

$$\text{s.t. } |\mathbf{V}_{\text{RF}}(i, j)|^2 = 1, \quad \forall i, j, \quad (2.13b)$$

where $\mathbf{F}_1 = \mathbf{H}^H \mathbf{H}$. This problem is still non-convex, since the objective function (2.13a) is not concave in \mathbf{V}_{RF} . However, the decoupled nature of the constraints in this formulation enables us to devise an iterative coordinate descent algorithm over the elements of the analog precoder.

In order to extract the contribution of $\mathbf{V}_{\text{RF}}(i, j)$ to the objective function of (2.13), it is

shown in [84] that the objective function in (2.13) can be rewritten as

$$\log_2 \left| \mathbf{I} + \frac{\gamma^2}{\sigma^2} \mathbf{V}_{\text{RF}}^H \mathbf{F}_1 \mathbf{V}_{\text{RF}} \right| = \log_2 \begin{vmatrix} 1 + \frac{\gamma^2}{\sigma^2} \mathbf{v}_{\text{RF},j}^H \mathbf{F}_1 \mathbf{v}_{\text{RF},j} & \frac{\gamma^2}{\sigma^2} \mathbf{v}_{\text{RF},j}^H \mathbf{F}_1 \bar{\mathbf{V}}_{\text{RF}}^j \\ \frac{\gamma^2}{\sigma^2} (\bar{\mathbf{V}}_{\text{RF}}^j)^H \mathbf{F}_1 \mathbf{v}_{\text{RF},j} & \mathbf{I} + \frac{\gamma^2}{\sigma^2} (\bar{\mathbf{V}}_{\text{RF}}^j)^H \mathbf{F}_1 \bar{\mathbf{V}}_{\text{RF}}^j \end{vmatrix} \quad (2.14a)$$

$$= \log_2 |\mathbf{C}_j| + \log_2 \left(1 + \mathbf{v}_{\text{RF},j}^H \mathbf{G}_j \mathbf{v}_{\text{RF},j} \right) \quad (2.14b)$$

$$= \log_2 |\mathbf{C}_j| + \log_2 (2 \operatorname{Re} \{ \mathbf{V}_{\text{RF}}^*(i,j) \eta_{ij} \} + \zeta_{ij} + 1) \quad (2.14c)$$

where $\mathbf{v}_{\text{RF},j}$ is the j^{th} column of the analog precoder,

$$\mathbf{C}_j = \mathbf{I} + \frac{\gamma^2}{\sigma^2} (\bar{\mathbf{V}}_{\text{RF}}^j)^H \mathbf{F}_1 \bar{\mathbf{V}}_{\text{RF}}^j, \quad (2.15)$$

and $\bar{\mathbf{V}}_{\text{RF}}^j$ is the sub-matrix of \mathbf{V}_{RF} with j^{th} column removed,

$$\eta_{ij} = \sum_{\ell \neq i} \mathbf{G}_j(i, \ell) \mathbf{V}_{\text{RF}}(\ell, j), \quad (2.16a)$$

$$\zeta_{ij} = \mathbf{G}_j(i, i) + 2 \operatorname{Re} \left\{ \sum_{m \neq i, n \neq i} \mathbf{V}_{\text{RF}}^*(m, j) \mathbf{G}_j(m, n) \mathbf{V}_{\text{RF}}(n, j) \right\}, \quad (2.16b)$$

and $\mathbf{G}_j = \frac{\gamma^2}{\sigma^2} \mathbf{F}_1 - \frac{\gamma^4}{\sigma^4} \mathbf{F}_1 \bar{\mathbf{V}}_{\text{RF}}^j \mathbf{C}_j^{-1} (\bar{\mathbf{V}}_{\text{RF}}^j)^H \mathbf{F}_1$. Note that (2.14b) is written by using the equation

for determinants of block matrices, i.e., $\begin{vmatrix} A & B \\ C & D \end{vmatrix} = |A - BD^{-1}C| |D|$, and (2.14c) is obtained by simply expanding the term $\mathbf{v}_{\text{RF},j}^H \mathbf{G}_j \mathbf{v}_{\text{RF},j}$ in (2.14b).

Since \mathbf{C}_j , ζ_{ij} and η_{ij} are independent of $\mathbf{V}_{\text{RF}}(i, j)$, if it is assumed that all the elements of the analog precoder are fixed except $\mathbf{V}_{\text{RF}}(i, j)$, the optimal value for the element of the analog precoder at the i^{th} row and j^{th} column is given by

$$\mathbf{V}_{\text{RF}}(i, j) = \begin{cases} 1, & \text{if } \eta_{ij} = 0, \\ \frac{\eta_{ij}}{|\eta_{ij}|}, & \text{otherwise.} \end{cases} \quad (2.17)$$

This enables us to propose an iterative algorithm that starts with an initial feasible analog precoder satisfying (2.13b), i.e., $\mathbf{V}_{\text{RF}}^{(0)} = \mathbf{1}_{M_t \times N_{\text{RF}}}$, then sequentially updates each element of the

Algorithm 1 Design of the analog beamformer, \mathbf{V}_{RF} , by solving the problem in (2.13)

Require: $\mathbf{F}_1, \gamma^2, \sigma^2$

- 1: Initialize $\mathbf{V}_{\text{RF}} = \mathbf{1}_{M_t \times N_{\text{RF}}}$.
 - 2: **for** $j = 1 \rightarrow N_{\text{RF}}$ **do**
 - 3: Calculate $\mathbf{C}_j = \mathbf{I} + \frac{\gamma^2}{\sigma^2} (\bar{\mathbf{V}}_{\text{RF}}^j)^H \mathbf{F}_1 \bar{\mathbf{V}}_{\text{RF}}^j$.
 - 4: Calculate $\mathbf{G}_j = \frac{\gamma^2}{\sigma^2} \mathbf{F}_1 - \frac{\gamma^4}{\sigma^4} \mathbf{F}_1 \bar{\mathbf{V}}_{\text{RF}}^j \mathbf{C}_j^{-1} (\bar{\mathbf{V}}_{\text{RF}}^j)^H \mathbf{F}_1$.
 - 5: **for** $i = 1 \rightarrow M_t$ **do**
 - 6: Find $\eta_{ij} = \sum_{\ell \neq i} \mathbf{G}_j(i, \ell) \mathbf{V}_{\text{RF}}(\ell, j)$.
 - 7: $\mathbf{V}_{\text{RF}}(i, j) = \begin{cases} 1, & \text{if } \eta_{ij} = 0, \\ \frac{\eta_{ij}}{|\eta_{ij}|}, & \text{otherwise.} \end{cases}$
 - 8: **end for**
 - 9: **end for**
 - 10: Check convergence. If yes, stop; if not go to Step 2.
-

analog precoder according to (2.17) until the algorithm converges to a locally optimal solution of \mathbf{V}_{RF} of the problem (2.13). Note that since in each element update step of the proposed algorithm, the objective function of (2.13) increases (or at least does not decrease), therefore the convergence of the algorithm is guaranteed. The proposed algorithm for designing the analog beamformer in (2.13) is summarized in Algorithm 1. It should be mentioned that the proposed algorithm is inspired by the algorithm in [84] that seeks to solve the problem of transmitter precoder design with per-antenna power constraint which happens to have the same form as the problem in (2.13).

2.4.3 Hybrid Combining Design for $N_{\text{RF}} = N_s$

Finally, this part aims to design the hybrid combiners that maximize the overall spectral efficiency in (2.9) assuming that the hybrid precoders are already designed. For a fixed analog combiner, the optimal digital combiner is given by the minimum mean squared error (MMSE) combiner as

$$\mathbf{W}_D = \mathbf{J}^{-1} \mathbf{W}_{\text{RF}}^H \mathbf{H} \mathbf{V}_t, \quad (2.18)$$

where

$$\mathbf{J} = \mathbf{W}_{\text{RF}}^H \mathbf{H} \mathbf{V}_t \mathbf{V}_t^H \mathbf{H}^H \mathbf{W}_{\text{RF}} + \sigma^2 \mathbf{W}_{\text{RF}}^H \mathbf{W}_{\text{RF}}. \quad (2.19)$$

Analogous to the argument made in Section 2.4.1 for the analog precoder, it can be shown that

the analog combiner typically satisfies $\mathbf{W}_{\text{RF}}^H \mathbf{W}_{\text{RF}} \approx M_r \mathbf{I}$, for large values of M_r . This leads to the conclusion that the effective noise after the analog combiner approximately remains white. Now, using the property of MMSE digital combiner under white background noise, the analog combiner design problem can be written as

$$\max_{\mathbf{W}_{\text{RF}}} \log_2 \left| \mathbf{I} + \frac{1}{\sigma^2} (\mathbf{W}_{\text{RF}}^H \mathbf{W}_{\text{RF}})^{-1} \mathbf{W}_{\text{RF}}^H \mathbf{F}_2 \mathbf{W}_{\text{RF}} \right| \quad (2.20a)$$

$$\text{s.t. } |\mathbf{W}_{\text{RF}}(i, j)|^2 = 1, \quad \forall i, j, \quad (2.20b)$$

where $\mathbf{F}_2 = \mathbf{H} \mathbf{V}_t \mathbf{V}_t^H \mathbf{H}^H$. This problem is very similar to the analog precoder design problem in (2.13), except the extra term $(\mathbf{W}_{\text{RF}}^H \mathbf{W}_{\text{RF}})^{-1}$. Now using $\mathbf{W}_{\text{RF}}^H \mathbf{W}_{\text{RF}} \approx M_r \mathbf{I}$, the problem (2.20) can be approximated in the form of analog precoder design problem in (2.13) and Algorithm 1 can be used to design \mathbf{W}_{RF} by substituting \mathbf{F}_2 and $\frac{1}{M_r}$ by \mathbf{F}_1 and γ^2 , respectively, i.e.,

$$\max_{\mathbf{W}_{\text{RF}}} \log_2 \left| \mathbf{I} + \frac{1}{M_r \sigma^2} \mathbf{W}_{\text{RF}}^H \mathbf{F}_2 \mathbf{W}_{\text{RF}} \right| \quad (2.21a)$$

$$\text{s.t. } |\mathbf{W}_{\text{RF}}(i, j)|^2 = 1, \quad \forall i, j. \quad (2.21b)$$

2.4.4 Hybrid Beamforming Design for $N_s < N_{\text{RF}} < 2N_s$

In Section 2.3, it has been shown how to optimally design the hybrid beamformers for the case $N_{\text{RF}} \geq 2N_s$ for which the fully-connected hybrid structure can achieve the same rate as the rate of optimal fully digital beamforming. Earlier in this section, a heuristic hybrid beamforming design algorithm is proposed for $N_{\text{RF}} = N_s$. Now, this part aims to design the hybrid beamformers for the case of $N_s < N_{\text{RF}} < 2N_s$.

For $N_s < N_{\text{RF}} < 2N_s$, the transmitter design problem can still be formulated as in (2.10). For a fixed analog precoder, it can be seen that the optimal digital precoder can still be found according to (2.12), however now it satisfies

$$\mathbf{V}_D \mathbf{V}_D^H \approx \gamma^2 \mathbf{U} \tilde{\mathbf{I}}_{N_{\text{RF}}} \mathbf{U}^H, \quad (2.22)$$

where $\tilde{\mathbf{I}}_{N_{\text{RF}}} = \begin{bmatrix} \mathbf{I}_{N_s} & \mathbf{0} \\ \mathbf{0} & \mathbf{0} \end{bmatrix}$ and $\mathbf{U} \in \mathbb{C}^{N_{\text{RF}} \times N_{\text{RF}}}$ is a unitary matrix. For such a digital precoder,

the objective function of (2.10) that should be maximized over \mathbf{V}_{RF} can be upper-bounded as

$$\begin{aligned} \log_2 \left| \mathbf{I}_{N_{\text{RF}}} + \frac{\gamma^2}{\sigma^2} \mathbf{U}^H \mathbf{V}_{\text{RF}}^H \mathbf{H}^H \mathbf{H} \mathbf{V}_{\text{RF}} \mathbf{U} \tilde{\mathbf{I}}_{N_{\text{RF}}} \right| &\stackrel{(a)}{\leq} \log_2 \left| \mathbf{I}_{N_{\text{RF}}} + \frac{\gamma^2}{\sigma^2} \mathbf{U}^H \mathbf{V}_{\text{RF}}^H \mathbf{H}^H \mathbf{H} \mathbf{V}_{\text{RF}} \mathbf{U} \mathbf{I}_{N_{\text{RF}}} \right| \\ &\stackrel{(b)}{=} \log_2 \left| \mathbf{I} + \frac{\gamma^2}{\sigma^2} \mathbf{V}_{\text{RF}}^H \mathbf{H}^H \mathbf{H} \mathbf{V}_{\text{RF}} \right|, \end{aligned} \quad (2.23)$$

where (a) is satisfied with equality if $N_{\text{RF}} = N_s$ and (b) is due to the properties of the unitary matrices, i.e., for a unitary matrix \mathbf{U} , we have $|\mathbf{I} + \mathbf{U}^H \mathbf{A} \mathbf{U}| = |\mathbf{I} + \mathbf{A}|$.

Now it is proposed to design the analog precoder such that it maximizes the upper-bound of the spectral efficiency in (2.23), yielding

$$\max_{\mathbf{V}_{\text{RF}}} \log_2 \left| \mathbf{I} + \frac{\gamma^2}{\sigma^2} \mathbf{V}_{\text{RF}}^H \mathbf{H}^H \mathbf{H} \mathbf{V}_{\text{RF}} \right| \quad (2.24a)$$

$$\text{s.t. } |\mathbf{V}_{\text{RF}}(i, j)|^2 = 1, \quad \forall i, j. \quad (2.24b)$$

Using this strategy, the analog precoder design problem is now in the form of (2.13). Hence, Algorithm 1 can be used to obtain the analog precoder. In summary, it is suggested to first design the analog precoder assuming that the number of data streams is equal to the number of RF chains, then for that analog precoder, to obtain the digital precoder for the actual N_s .

At the receiver, this thesis still suggests to design the analog combiner first, then set the digital combiner to the MMSE solution. This decoupled optimization of analog combiner and digital combiner is approximately optimal for the following reason. Assume that all the beamformers are already designed except the digital combiner. Since $\mathbf{W}_{\text{RF}}^H \mathbf{W}_{\text{RF}} \approx M_r \mathbf{I}$, the effective noise after the analog combiner can be considered as an uncolored noise with covariance matrix $\sigma^2 M_r \mathbf{I}$. Under this condition, by choosing the digital combiner as the MMSE solution, the mutual information between the data symbols and the processed signals before digital combiner is approximately equal to the mutual information between the data symbols and the final processed signals. Therefore, it is approximately optimal to first design the analog combiner using Algorithm 1, then set the digital combiner to the MMSE solution.

The summary of the overall proposed procedure for designing the hybrid beamformers for spectral efficiency maximization in a large-scale SU-MIMO system is given in Algorithm 2. By assuming that the number of antennas at both ends are in the same range, i.e., $M_r = O(M_t)$, it

Algorithm 2 Design of Hybrid Beamformers for large-scale SU-MIMO systems

Require: \mathbf{H} , σ^2 , P

- 1: Assuming $\mathbf{V}_D \mathbf{V}_D^H = \gamma \mathbf{I}$ where $\gamma = \sqrt{P/(M_t N_{RF})}$, find \mathbf{V}_{RF} by solving the problem in (2.13) using Algorithm 1.
 - 2: Calculate $\mathbf{V}_D = (\mathbf{V}_{RF}^H \mathbf{V}_{RF})^{-1/2} \mathbf{U}_e \boldsymbol{\Gamma}_e$ where \mathbf{U}_e and $\boldsymbol{\Gamma}_e$ are defined as following (2.12).
 - 3: Find \mathbf{W}_{RF} by solving the problem in (2.21) using Algorithm 1.
 - 4: Calculate $\mathbf{W}_D = \mathbf{J}^{-1} \mathbf{W}_{RF}^H \mathbf{H} \mathbf{V}_{RF} \mathbf{V}_D$ where $\mathbf{J} = \mathbf{W}_{RF}^H \mathbf{H} \mathbf{V}_{RF} \mathbf{V}_D \mathbf{V}_D^H \mathbf{V}_{RF}^H \mathbf{H}^H \mathbf{W}_{RF} + \sigma^2 \mathbf{W}_{RF}^H \mathbf{W}_{RF}$.
-

can be shown that the overall complexity of Algorithm 2 is $O(M_t^3)$ which is similar to the most of the existing hybrid beamforming designs, e.g., the hybrid beamforming designs in [18, 31].

Numerical results presented in the simulation part of this chapter suggest that for the case of $N_{RF} = N_s$ and infinite resolution phase shifters, the achievable rate of the proposed algorithm is very close the maximum capacity. The case of $N_s < N_{RF} < 2N_s$ is of most interest when the finite resolution phase shifters are used. It is shown in the simulation part of this chapter that the extra number of RF chains can be used to trade off the accuracy of the phase shifters.

2.5 Hybrid Beamforming Design for Massive MU-MISO Systems

This section considers the design of hybrid precoders for the downlink MU-MISO system in which a BS with large number of antennas M_t , but limited number of RF chains N_{RF} , supports K single-antenna users where $M_t \gg K$. For such a system with hybrid precoding architecture at the BS, the rate expression for user k in (2.4) can be expressed as

$$R_k = \log_2 \left(1 + \frac{|\mathbf{h}_k^H \mathbf{V}_{RF} \mathbf{v}_{D_k}|^2}{\sigma^2 + \sum_{\ell \neq k} |\mathbf{h}_k^H \mathbf{V}_{RF} \mathbf{v}_{D_\ell}|^2} \right), \quad (2.25)$$

where \mathbf{h}_k^H is the channel from the BS to the k^{th} user and \mathbf{v}_{D_ℓ} denotes the ℓ^{th} column of the digital precoder \mathbf{V}_D . The problem of overall spectral efficiency maximization for the MU-MISO systems differs from the spectral efficiency maximization problem in point-to-point SU-MIMO systems in two respects. First, in the MU-MISO case the receiving antennas are not collocated, therefore it is not possible to use the rate expression in (2.9), which assumes cooperation

between the receivers. The hybrid beamforming design for MU-MISO systems must account for the effect of inter-user interference. Second, the priority of the streams may be unequal in a MU-MISO system, while different streams in a point-to-point SU-MIMO systems have the same priority. This section considers the hybrid beamforming design of a MU-MISO system to maximize the weighted sum rate.

In [35,36], it is shown for the case $N_{\text{RF}} = K$ and $M_t \rightarrow \infty$, that by matching the analog precoder to the overall channel (or the strongest paths of the channel) and using a low-dimensional ZF digital precoder, the hybrid beamforming structure can achieve a reasonable sum rate as compared to the sum rate of fully digital ZF scheme, which is shown to be near optimal in massive MIMO systems [3]. However, for practical values of M_t , there is still a gap between the achievable rates of the hybrid beamforming designs in [35,36] and the capacity. One possible way to reduce this gap is to increase the number of RF chains. But the proposed designs in [35,36] are restricted to the case that $N_{\text{RF}} = K$. This motivates us to propose a design for the scenarios where $N_{\text{RF}} > K$ in order to increase the overall performance of the system.

The problem of interest for a MU-MIMO system can be written as

$$\underset{\mathbf{V}_{\text{RF}}, \mathbf{V}_{\text{D}}}{\text{maximize}} \quad \sum_{k=1}^K \beta_k \log_2 \left(1 + \frac{|\mathbf{h}_k^H \mathbf{V}_{\text{RF}} \mathbf{v}_{\text{D},k}|^2}{\sigma^2 + \sum_{\ell \neq k} |\mathbf{h}_\ell^H \mathbf{V}_{\text{RF}} \mathbf{v}_{\text{D},\ell}|^2} \right) \quad (2.26a)$$

$$\text{subject to} \quad \text{Tr}(\mathbf{V}_{\text{RF}} \mathbf{V}_{\text{D}} \mathbf{V}_{\text{D}}^H \mathbf{V}_{\text{RF}}^H) \leq P, \quad (2.26b)$$

$$|\mathbf{V}_{\text{RF}}(i, j)|^2 = 1, \quad \forall i, j. \quad (2.26c)$$

Solving this problem involves a joint optimization over \mathbf{V}_{RF} and \mathbf{V}_{D} which is challenging. This thesis again decouples the design of \mathbf{V}_{RF} and \mathbf{V}_{D} by considering ZF beamforming with power allocation as the digital precoder. It is shown that the optimal digital precoder with such a structure can be found for a fixed analog precoder. In addition, for a fixed power allocation, an approximately locally optimal analog precoder can be obtained. By iterating between those designs, a good solution of the problem (2.26) for MU-MISO systems can be found.

2.5.1 Digital Precoder Design

This thesis considers ZF beamforming with power allocation as the low-dimensional digital precoder part of the BS's precoder to manage the inter-user interference. For a fixed analog precoder, such a digital precoder can be found as [81]

$$\mathbf{V}_D^{ZF} = \mathbf{V}_{RF}^H \mathbf{H}^H (\mathbf{H} \mathbf{V}_{RF} \mathbf{V}_{RF}^H \mathbf{H}^H)^{-1} \mathbf{P}^{\frac{1}{2}} = \tilde{\mathbf{V}}_D \mathbf{P}^{\frac{1}{2}}, \quad (2.27)$$

where $\mathbf{H} = [\mathbf{h}_1, \dots, \mathbf{h}_K]^H$, $\tilde{\mathbf{V}}_D = \mathbf{V}_{RF}^H \mathbf{H}^H (\mathbf{H} \mathbf{V}_{RF} \mathbf{V}_{RF}^H \mathbf{H}^H)^{-1}$ and $\mathbf{P} = \text{diag}(p_1, \dots, p_K)$ with p_k denoting the received power at the k^{th} user. For a fixed analog precoder, the only design variables of ZF digital precoder are the received powers, $[p_1, \dots, p_K]$. Using the properties of ZF beamforming; i.e., $|\mathbf{h}_k^H \mathbf{V}_{RF} \mathbf{v}_{D_k}^{ZF}| = \sqrt{p_k}$ and $|\mathbf{h}_k^H \mathbf{V}_{RF} \mathbf{v}_{D_\ell}^{ZF}| = 0$ for all $\ell \neq k$, problem (2.26) for designing those powers assuming a feasible analog precoder is reduced to

$$\max_{p_1, \dots, p_K \geq 0} \sum_{k=1}^K \beta_k \log_2 \left(1 + \frac{p_k}{\sigma^2} \right) \quad (2.28a)$$

$$\text{s.t.} \quad \text{Tr}(\tilde{\mathbf{Q}} \mathbf{P}) \leq P, \quad (2.28b)$$

where $\tilde{\mathbf{Q}} = \tilde{\mathbf{V}}_D^H \mathbf{V}_{RF}^H \mathbf{V}_{RF} \tilde{\mathbf{V}}_D$. The optimal solution of this problem can be found by water-filling as

$$p_k = \frac{1}{\tilde{q}_{kk}} \max \left\{ \frac{\beta_k}{\tilde{\lambda}} - \tilde{q}_{kk} \sigma^2, 0 \right\}, \quad (2.29)$$

where \tilde{q}_{kk} is k^{th} diagonal element of $\tilde{\mathbf{Q}}$ and $\tilde{\lambda}$ is chosen such that $\sum_{k=1}^K \max \left\{ \frac{\beta_k}{\tilde{\lambda}} - \tilde{q}_{kk} \sigma^2, 0 \right\} = P$.

2.5.2 Analog Precoder Design

This part seeks to design the analog precoder assuming the ZF digital precoding as in (2.27). The overall proposed strategy is to iterate between the design of ZF precoder and the analog precoder. Observe that the achievable weighted sum rate with ZF precoding in (2.28) depends on the analog precoder \mathbf{V}_{RF} only through the power constraint (2.28b). Now, this thesis proposes to design the analog precoder such that it minimizes the overall power consumption

in left hand of (2.28b) for a fixed \mathbf{P} as

$$\min_{\mathbf{V}_{\text{RF}}} f(\mathbf{V}_{\text{RF}}) \quad (2.30\text{a})$$

$$\text{s.t. } |\mathbf{V}_{\text{RF}}(i, j)|^2 = 1, \quad \forall i, j. \quad (2.30\text{b})$$

where

$$f(\mathbf{V}_{\text{RF}}) = \text{Tr} \left(\mathbf{V}_{\text{RF}} \tilde{\mathbf{V}}_{\text{D}} \mathbf{P} \tilde{\mathbf{V}}_{\text{D}}^H \mathbf{V}_{\text{RF}}^H \right). \quad (2.31)$$

The intuition behind the problem formulation (2.30) is that if after designing the analog precoder for a given \mathbf{P} , we are just allowed to equally scale all the elements of \mathbf{P} , then the optimal solution for \mathbf{V}_{RF} in (2.26) is also the optimal solution for the problem (2.30).

The problem in (2.30) is still difficult to solve since the expression $f(\mathbf{V}_{\text{RF}})$ in term of \mathbf{V}_{RF} is very complicated. But, using the fact that the analog precoder typically satisfies $\mathbf{V}_{\text{RF}}^H \mathbf{V}_{\text{RF}} \approx M_t \mathbf{I}$ when M_t is large [31], this can be simplified as

$$f(\mathbf{V}_{\text{RF}}) = \text{Tr} \left(\mathbf{V}_{\text{RF}}^H \mathbf{V}_{\text{RF}} \tilde{\mathbf{V}}_{\text{D}} \mathbf{P} \tilde{\mathbf{V}}_{\text{D}}^H \right) \quad (2.32\text{a})$$

$$\approx M_t \text{Tr} \left(\mathbf{P}^{\frac{1}{2}} \tilde{\mathbf{V}}_{\text{D}}^H \tilde{\mathbf{V}}_{\text{D}} \mathbf{P}^{\frac{1}{2}} \right) \quad (2.32\text{b})$$

$$= M_t \text{Tr} \left(\left(\tilde{\mathbf{H}} \mathbf{V}_{\text{RF}} \mathbf{V}_{\text{RF}}^H \tilde{\mathbf{H}}^H \right)^{-1} \right) = \hat{f}(\mathbf{V}_{\text{RF}}), \quad (2.32\text{c})$$

where $\tilde{\mathbf{H}} = \mathbf{P}^{-\frac{1}{2}} \mathbf{H}$. Now, analogous to the procedure for the SU-MIMO case, this thesis aims to extract the contribution of $\mathbf{V}_{\text{RF}}(i, j)$ in the objective function (here the approximation of the objective function), $\hat{f}(\mathbf{V}_{\text{RF}})$, then seeks to find the optimal value of $\mathbf{V}_{\text{RF}}(i, j)$ assuming all other elements are fixed.

Toward this aim, let $\mathbf{A}_j = \tilde{\mathbf{H}} \bar{\mathbf{V}}_{\text{RF}}^j (\bar{\mathbf{V}}_{\text{RF}}^j)^H \tilde{\mathbf{H}}^H$ where $\bar{\mathbf{V}}_{\text{RF}}^j$ is the sub-matrix of \mathbf{V}_{RF} with j^{th} column $\mathbf{v}_{\text{RF}}^{(j)}$ removed. It is easy to see that $\hat{f}(\mathbf{V}_{\text{RF}})$ in (2.32c) can be written as

$$\hat{f}(\mathbf{V}_{\text{RF}}) = M_t \text{Tr} \left(\left(\mathbf{A}_j + \tilde{\mathbf{H}} \mathbf{v}_{\text{RF}}^{(j)} \mathbf{v}_{\text{RF}}^{(j)H} \tilde{\mathbf{H}}^H \right)^{-1} \right), \quad (2.33)$$

where $\tilde{\mathbf{H}} \mathbf{v}_{\text{RF}}^{(j)} \mathbf{v}_{\text{RF}}^{(j)H} \tilde{\mathbf{H}}^H$ is a rank one matrix and \mathbf{A}_j is a full-rank matrix for $N_{\text{RF}} > N_s$. This

enables us to write

$$\frac{\hat{f}(\mathbf{V}_{\text{RF}})}{M_t} \stackrel{(a)}{=} \text{Tr} \left(\mathbf{A}_j^{-1} - \frac{\mathbf{A}_j^{-1} \tilde{\mathbf{H}} \mathbf{v}_{\text{RF}}^{(j)H} \tilde{\mathbf{H}}^H \mathbf{A}_j^{-1}}{1 + \text{Tr} \left(\mathbf{A}_j^{-1} \tilde{\mathbf{H}} \mathbf{v}_{\text{RF}}^{(j)H} \tilde{\mathbf{H}}^H \right)} \right) \quad (2.34a)$$

$$\stackrel{(b)}{=} \text{Tr} \left(\mathbf{A}_j^{-1} \right) - \frac{\text{Tr} \left(\mathbf{A}_j^{-1} \tilde{\mathbf{H}} \mathbf{v}_{\text{RF}}^{(j)H} \tilde{\mathbf{H}}^H \mathbf{A}_j^{-1} \right)}{1 + \text{Tr} \left(\mathbf{A}_j^{-1} \tilde{\mathbf{H}} \mathbf{v}_{\text{RF}}^{(j)H} \tilde{\mathbf{H}}^H \right)} \quad (2.34b)$$

$$\stackrel{(c)}{=} \text{Tr} \left(\mathbf{A}_j^{-1} \right) - \frac{\mathbf{v}_{\text{RF}}^{(j)H} \mathbf{B}_j \mathbf{v}_{\text{RF}}^{(j)}}{1 + \mathbf{v}_{\text{RF}}^{(j)H} \mathbf{D}_j \mathbf{v}_{\text{RF}}^{(j)}} \quad (2.34c)$$

$$\stackrel{(d)}{=} \text{Tr} \left(\mathbf{A}_j^{-1} \right) - \frac{\zeta_{ij}^B + 2 \text{Re} \left\{ \mathbf{V}_{\text{RF}}^*(i, j) \eta_{ij}^B \right\}}{1 + \zeta_{ij}^D + 2 \text{Re} \left\{ \mathbf{V}_{\text{RF}}^*(i, j) \eta_{ij}^D \right\}} \quad (2.34d)$$

where

$$\zeta_{ij}^B = \mathbf{B}_j(i, i) + 2 \text{Re} \left\{ \sum_{m \neq i, n \neq i} \mathbf{V}_{\text{RF}}^*(m, j) \mathbf{B}_j(m, n) \mathbf{V}_{\text{RF}}(n, j) \right\}, \quad (2.35a)$$

$$\zeta_{ij}^D = \mathbf{D}_j(i, i) + 2 \text{Re} \left\{ \sum_{m \neq i, n \neq i} \mathbf{V}_{\text{RF}}^*(m, j) \mathbf{D}_j(m, n) \mathbf{V}_{\text{RF}}(n, j) \right\}, \quad (2.35b)$$

$$\eta_{ij}^B = \sum_{\ell \neq i} \mathbf{B}_j(i, \ell) \mathbf{V}_{\text{RF}}(\ell, j), \quad (2.35c)$$

$$\eta_{ij}^D = \sum_{\ell \neq i} \mathbf{D}_j(i, \ell) \mathbf{V}_{\text{RF}}(\ell, j), \quad (2.35d)$$

where $b_{i\ell}^j$ and $d_{i\ell}^j$ are the i^{th} row and ℓ^{th} column element of $\mathbf{B}_j = \tilde{\mathbf{H}}^H \mathbf{A}_j^{-2} \tilde{\mathbf{H}}$ and $\mathbf{D}_j = \tilde{\mathbf{H}}^H \mathbf{A}_j^{-1} \tilde{\mathbf{H}}$, respectively. In (2.34), the first equality, (a), is written using the Sherman Morrison formula [85]; i.e., $(\mathbf{A} + \mathbf{B})^{-1} = \mathbf{A}^{-1} - \frac{\mathbf{A}^{-1} \mathbf{B} \mathbf{A}^{-1}}{1 + \text{Tr}(\mathbf{A}^{-1} \mathbf{B})}$ for a full-rank matrix \mathbf{A} and a rank-one matrix \mathbf{B} . Since $\text{Tr}(\cdot)$ is a linear function, equation (b) can be obtained. Equation (c) is based on the fact that the trace is invariant under cyclic permutations; i.e., $\text{Tr}(\mathbf{AB}) = \text{Tr}(\mathbf{BA})$ for any arbitrary matrices \mathbf{A} and \mathbf{B} with appropriate dimensions. Finally, (d) is obtained by expanding the terms.

Now, if it is assumed that all elements of the analog precoder are fixed except $\mathbf{V}_{\text{RF}}(i, j) = e^{-i\theta_{i,j}}$, the optimal value for $\theta_{i,j}$ should satisfy $\frac{\partial \hat{f}(\mathbf{V}_{\text{RF}})}{\partial \theta_{i,j}} = 0$. In order to find the solutions of

$\frac{\partial \hat{f}(\mathbf{V}_{\text{RF}})}{\partial \theta_{i,j}} = 0$, consider the following function of θ ,

$$g(\theta) = \frac{a_1 + 2 \operatorname{Re}\{b_1 e^{i\theta}\}}{a_2 + 2 \operatorname{Re}\{b_2 e^{i\theta}\}}, = \frac{a_1 + b_1 e^{i\theta} + b_1^* e^{-i\theta}}{a_2 + b_2 e^{i\theta} + b_2^* e^{-i\theta}} \quad (2.36)$$

where a_1 and a_2 are real constants and b_1 and b_2 are complex constants. The maxima and minima of $g(\theta)$ can be found by solving $\frac{\partial g(\theta)}{\partial \theta} = 0$ or equivalently

$$\frac{\partial g(\theta)}{\partial \theta} = \frac{(jb_1 e^{i\theta} - jb_1^* e^{-i\theta})(a_2 + b_2 e^{i\theta} + b_2^* e^{-i\theta})}{(a_2 + b_2 e^{i\theta} + b_2^* e^{-i\theta})^2} - \frac{(jb_2 e^{i\theta} - jb_2^* e^{-i\theta})(a_1 + b_1 e^{i\theta} + b_1^* e^{-i\theta})}{(a_1 + b_1 e^{i\theta} + b_1^* e^{-i\theta})^2} = 0. \quad (2.37)$$

By some further algebra, it can be shown that (2.37) is equivalent to

$$\operatorname{Im}\{ce^{i\theta}\} = \operatorname{Im}\{c\} \cos(\theta) + \operatorname{Re}\{c\} \sin(\theta) = z, \quad (2.38)$$

where $z = \operatorname{Im}\{2b_1^* b_2\}$ and $c = a_2 b_1 - a_1 b_2$. The equation (2.38) can be further simplified to

$$|c| \sin(\theta + \phi) = z, \quad (2.39)$$

where

$$\phi = \begin{cases} \sin^{-1} \left(\frac{\operatorname{Im}\{c\}}{|c|} \right), & \text{if } \operatorname{Re}\{c\} \geq 0, \\ \pi - \sin^{-1} \left(\frac{\operatorname{Im}\{c\}}{|c|} \right), & \text{if } \operatorname{Re}\{c\} < 0. \end{cases} \quad (2.40)$$

It is easy to show that the (2.39) has only two solutions over one period of 2π as follows:

$$\theta^{(1)} = -\phi + \sin^{-1} \left(\frac{z}{|c|} \right), \quad (2.41a)$$

$$\theta^{(2)} = \pi - \phi - \sin^{-1} \left(\frac{z}{|c|} \right). \quad (2.41b)$$

Since $\hat{f}(\mathbf{V}_{\text{RF}})$ as function of $\theta_{i,j}$ is in the format of $g(\theta)$, it is possible to use the above results, i.e., it can be seen that it is always the case that only two $\theta_{i,j} \in [0, 2\pi)$ satisfy $\frac{\partial \hat{f}(\mathbf{V}_{\text{RF}})}{\partial \theta_{i,j}} = 0$,

namely:

$$\theta_{i,j}^{(1)} = -\phi_{i,j} + \sin^{-1} \left(\frac{z_{ij}}{|c_{ij}|} \right), \quad (2.42a)$$

$$\theta_{i,j}^{(2)} = \pi - \phi_{i,j} - \sin^{-1} \left(\frac{z_{ij}}{|c_{ij}|} \right), \quad (2.42b)$$

where $c_{ij} = (1 + \zeta_{ij}^D) \eta_{ij}^B - \zeta_{ij}^B \eta_{ij}^D$, $z_{ij} = \text{Im} \left\{ 2(\eta_{ij}^B)^* \eta_{ij}^D \right\}$ and

$$\phi_{i,j} = \begin{cases} \sin^{-1} \left(\frac{\text{Im}\{c_{ij}\}}{|c_{ij}|} \right), & \text{if } \text{Re}\{c_{ij}\} \geq 0, \\ \pi - \sin^{-1} \left(\frac{\text{Im}\{c_{ij}\}}{|c_{ij}|} \right), & \text{if } \text{Re}\{c_{ij}\} < 0. \end{cases} \quad (2.43)$$

Since $\hat{f}(\mathbf{V}_{\text{RF}})$ is periodic over $\theta_{i,j}$, only one of those solutions is the minimizer of $\hat{f}(\mathbf{V}_{\text{RF}})$.

The optimal $\theta_{i,j}$ can be written as

$$\theta_{ij}^{\text{opt}} = \underset{\theta_{i,j}^{(1)}, \theta_{i,j}^{(2)}}{\operatorname{argmin}} \left(\hat{f} \left(\theta_{i,j}^{(1)} \right), \hat{f} \left(\theta_{i,j}^{(2)} \right) \right). \quad (2.44)$$

Now, it is possible to devise an iterative algorithm starting from an initially feasible analog precoder and sequentially updating each entry of the analog precoder according to (2.44) until the algorithm converges to a local minimizer of $\hat{f}(\mathbf{V}_{\text{RF}})$.

The overall algorithm is to iterate between the design of \mathbf{V}_{RF} and the design of \mathbf{P} . First, starting with a feasible \mathbf{V}_{RF} and $\mathbf{P} = \mathbf{I}$, the algorithm seeks to sequentially update the phase of each element of the analog precoder according to (2.44) until convergence. Then, assuming the current analog precoder, the algorithm finds the optimal power allocation \mathbf{P} using (2.29). The iteration between these two steps continues until convergence. The overall proposed algorithm for designing the hybrid digital and analog precoder to maximize the weighted sum rate in the downlink of a massive MU-MISO system is summarized in Algorithm 3.

Algorithm 3 Design of Hybrid Precoders for massive MU-MISO systems**Require:** \mathbf{H} , β_k , P , σ^2

- 1: Start with a feasible \mathbf{V}_{RF} and $\mathbf{P} = \mathbf{I}_K$.
- 2: **for** $j = 1 \rightarrow N_{\text{RF}}$ **do**
- 3: Calculate $\mathbf{A}_j = \mathbf{P}^{-\frac{1}{2}} \mathbf{H} \bar{\mathbf{V}}_{\text{RF}}^j (\bar{\mathbf{V}}_{\text{RF}}^j)^H \mathbf{H}^H \mathbf{P}^{-\frac{1}{2}}$.
- 4: **for** $i = 1 \rightarrow M_t$ **do**
- 5: Find ζ_{ij}^B , ζ_{ij}^D , η_{ij}^B , η_{ij}^D as defined in (2.35).
- 6: Calculate $\theta_{i,j}^{(1)}$ and $\theta_{i,j}^{(2)}$ according to (2.42).
- 7: Find $\theta_{ij}^{\text{opt}} = \text{argmin} \left(\hat{f} \left(\theta_{i,j}^{(1)} \right), \hat{f} \left(\theta_{i,j}^{(2)} \right) \right)$.
- 8: Set $\mathbf{V}_{\text{RF}}(i, j) = e^{-i\theta_{ij}^{\text{opt}}}$.
- 9: **end for**
- 10: **end for**
- 11: Check convergence of analog precoder. If yes, continue; if not go to Step 2.
- 12: Find $\mathbf{P} = \text{diag}[p_1, \dots, p_k]$ using water-filling as in (2.29).
- 13: Check convergence of the overall algorithm. If yes, stop; if not go to Step 2.
- 14: Set $\mathbf{V}_{\text{D}} = \mathbf{V}_{\text{RF}}^H \mathbf{H}^H (\mathbf{H} \mathbf{V}_{\text{RF}} \mathbf{V}_{\text{RF}}^H \mathbf{H}^H)^{-1} \mathbf{P}^{\frac{1}{2}}$.

2.6 Hybrid Beamforming with Finite Resolution Phase Shifters

Finally, this chapter considers the hybrid beamforming design with finite resolution phase shifters for the two scenarios of interest in this chapter, the SU-MIMO system with large antenna arrays at both ends and the MU-MISO system with large arrays at the BS. So far, it is assumed that infinite resolution phase shifters are available in the hybrid structure, so the elements of analog beamformers can have any arbitrary phase angles. However, components required for accurate phase control can be expensive [42]. Since the number of phase shifters in hybrid structure is proportional to the number of antennas, the assumption of having infinite resolution phase shifters is not always practical for systems with large antenna array terminals. This section considers the impact of finite resolution phase shifters with $\mathbf{V}_{\text{RF}}(i, j) \in \mathcal{G}$ and $\mathbf{W}_{\text{RF}}(i, j) \in \mathcal{G}$ where

$$\mathcal{G} = \{1, \omega, \omega^2, \dots, \omega^{n_{\text{PS}}-1}\}, \quad (2.45)$$

and $\omega = e^{i\frac{2\pi}{n_{\text{PS}}}}$ and n_{PS} is the number of realizable phase angles which is typically $n_{\text{PS}} = 2^b$, where b is the number of bits in the resolution of phase shifters.

With finite resolution phase shifters, the general weighted sum rate maximization problem

can be written as

$$\underset{\mathbf{V}_{\text{RF}}, \mathbf{V}_{\text{D}}, \mathbf{W}_{\text{RF}_k}, \mathbf{W}_{\text{D}_k}}{\text{maximize}} \sum_{k=1}^K \beta_k R_k \quad (2.46a)$$

$$\text{subject to } \text{Tr}(\mathbf{V}_{\text{RF}} \mathbf{V}_{\text{D}} \mathbf{V}_{\text{D}}^H \mathbf{V}_{\text{RF}}^H) \leq P, \quad (2.46b)$$

$$\mathbf{V}_{\text{RF}}(i, j) \in \mathcal{G}, \forall i, j, \quad (2.46c)$$

$$\mathbf{W}_{\text{RF}_k}(i, j) \in \mathcal{G}, \forall i, j, k. \quad (2.46d)$$

For a set of fixed analog beamformers, the design of digital beamformers is a well-studied problem in the literature. However, the combinatorial nature of optimization over analog beamformers in (2.46) makes the design of analog beamformers more challenging. Theoretically, since the set of feasible analog beamformers are finite, it is possible to exhaustively search over all feasible choices. But, as the number of feasible analog beamformers is exponential in the number of antennas and the resolution of the phase shifters, this approach is not practical for systems with large number of antennas.

The other straightforward approach for finding the feasible solution for (2.46) is to first solve the problem under the infinite resolution phase shifter assumption, then to quantize the elements of the obtained analog beamformers to the nearest points in the set \mathcal{G} . However, our numerical results suggest that for low resolution phase shifters, this approach is not effective. This section aims to show that it is possible to account for the finite resolution phase shifter directly in the optimization procedure to get better performance.

For hybrid beamforming design of a SU-MIMO system with finite resolution phase shifters, Algorithm 2 for solving the spectral efficiency maximization problem can be adapted as follows. According to the procedure in Algorithm 2, assuming all of the elements of the analog beamformer are fixed except $\mathbf{V}_{\text{RF}}(i, j)$, the term $\text{Re}\{\mathbf{V}_{\text{RF}}^*(i, j)\eta_{ij}\}$ needs to be maximized for designing $\mathbf{V}_{\text{RF}}(i, j)$. This is equivalent to minimizing the angle between $\mathbf{V}_{\text{RF}}(i, j)$ and η_{ij} on the complex plane. Since $\mathbf{V}_{\text{RF}}(i, j)$ is constrained to be chosen from the set \mathcal{G} , the optimal design is given by

$$\mathbf{V}_{\text{RF}}^{\text{MIMO}}(i, j) = \mathcal{Q}(\psi(\eta_{ij})), \quad (2.47)$$

where for a non-zero complex variable a , $\psi(a) = \frac{a}{|a|}$ and for $a = 0$, $\psi(a) = 1$, and the function

$\mathcal{Q}(\cdot)$ quantizes a complex unit-norm variable to the nearest point in the set \mathcal{G} . Note that this quantization is performed in each element update step which can lead to a different analog beamforming design as compared to quantizing the final solution of the infinite resolution design. Later in this section, it will numerically be shown that performing the quantization in each element update step results in a much better performance.

By assuming that the number of antennas at both ends in the same range, i.e., $M_r = O(M_t)$, it can be shown that the complexity of the proposed algorithm is polynomial in the number of antennas, $O(M_t^3)$, while the complexity of finding the optimal beamformers using exhaustive search method is exponential, $O(M_t^2 2^{bM_t})$.

Similarly, for hybrid beamforming design of a MU-MISO system with finite resolution phase shifters, Algorithm 3 can likewise be modified as follows. Since the set of feasible phase angles are limited, instead of (2.44), it is possible to find $\mathbf{V}_{\text{RF}}(i, j)$ in each iteration by minimizing $\hat{f}(\mathbf{V}_{\text{RF}})$ using one-dimensional exhaustive search over the set \mathcal{G} , i.e.,

$$\mathbf{V}_{\text{RF}}^{\text{MU-MISO}}(i, j) = \underset{\mathbf{V}_{\text{RF}}(i, j) \in \mathcal{G}}{\operatorname{argmin}} \hat{f}(\mathbf{V}_{\text{RF}}). \quad (2.48)$$

The overall complexity of the proposed algorithm for hybrid beamforming design of a MU-MISO system with finite resolution phase shifters is $O(M_t^2 2^b)$, while the complexity of finding the optimal beamforming using exhaustive search method is $O(M_t 2^{bM_t})$. Note that accounting for the effect of phase quantization is most important when low resolution phase shifters are used, i.e., $b = 1$ or $b = 2$. Since in these cases, the number of possible choices for each element of analog beamformer is small, the proposed one-dimensional exhaustive search approach is not computationally demanding.

2.7 Numerical Results

In this section, simulation results are presented to show the performance of the proposed algorithms for SU-MIMO systems and MU-MISO systems and also to compare them with the existing hybrid beamforming designs and the optimal (or nearly-optimal) fully digital schemes. In the simulations, the propagation environment between each user terminal and the BS is mod-

eled as a sparse channel with L paths [36] which is a typical channel model for mmWave systems. Further, uniform linear array antenna configuration is considered. For such an environment, the channel matrix of the k^{th} user can be written as

$$\mathbf{H}_k = \sqrt{\frac{M_t M_r}{L}} \sum_{\ell=1}^L \alpha_k^\ell \mathbf{a}_r(\phi_{r_k}^\ell) \mathbf{a}_t(\phi_{t_k}^\ell)^H, \quad (2.49)$$

where $\alpha_k^\ell \sim \mathcal{CN}(0, 1)$ is the complex gain of the ℓ^{th} path between the BS and the user k , and $\phi_{r_k}^\ell \in [0, 2\pi)$ and $\phi_{t_k}^\ell \in [0, 2\pi)$. Further, $\mathbf{a}_r(\cdot)$ and $\mathbf{a}_t(\cdot)$ are the antenna array response vectors at the receiver and the transmitter, respectively. In a uniform linear array configuration with M antenna elements, the antenna array response vector can be written as

$$\mathbf{a}(\phi) = \frac{1}{\sqrt{M}} \left[1, e^{j\frac{2\pi}{\lambda}\tilde{d}\sin(\phi)}, \dots, e^{j\frac{2\pi}{\lambda}\tilde{d}(M-1)\sin(\phi)} \right]^T, \quad (2.50)$$

where λ denotes the wavelength and \tilde{d} is the antenna spacing.

In the following simulations, an environment with $L = 15$ scatterers (unless otherwise mentioned) between the BS and each user terminal is considered. Further, it is assumed that angles of arrival and departure are drawn from a uniform distribution on the interval $[0, 2\pi)$ and the antenna spacing is set to be $\tilde{d} = \lambda/2$. For each simulation, the average spectral efficiency is plotted versus signal-to-noise-ratio, defined as $\text{SNR} = \frac{P}{\sigma^2}$, over 500 channel realizations.

2.7.1 Performance Analysis of a SU-MIMO System with Hybrid Beamforming

The first simulation considers a 64×16 MIMO system with $N_s = 6$. For hybrid beamforming schemes, it is assumed that the number of RF chains at each end is $N_{\text{RF}} = N_s = 6$ and infinite resolution phase shifters are used at both ends. Fig. 2.3 shows that the proposed algorithm has a better performance as compared to hybrid beamforming algorithms in [18] and [31]: about 1 – 1.5dB gain as compared to the algorithms in [18] and [31]. Moreover, the performance of the proposed algorithm is very close to the rate of optimal fully digital beamforming scheme. This indicates that the proposed algorithm is nearly optimal.

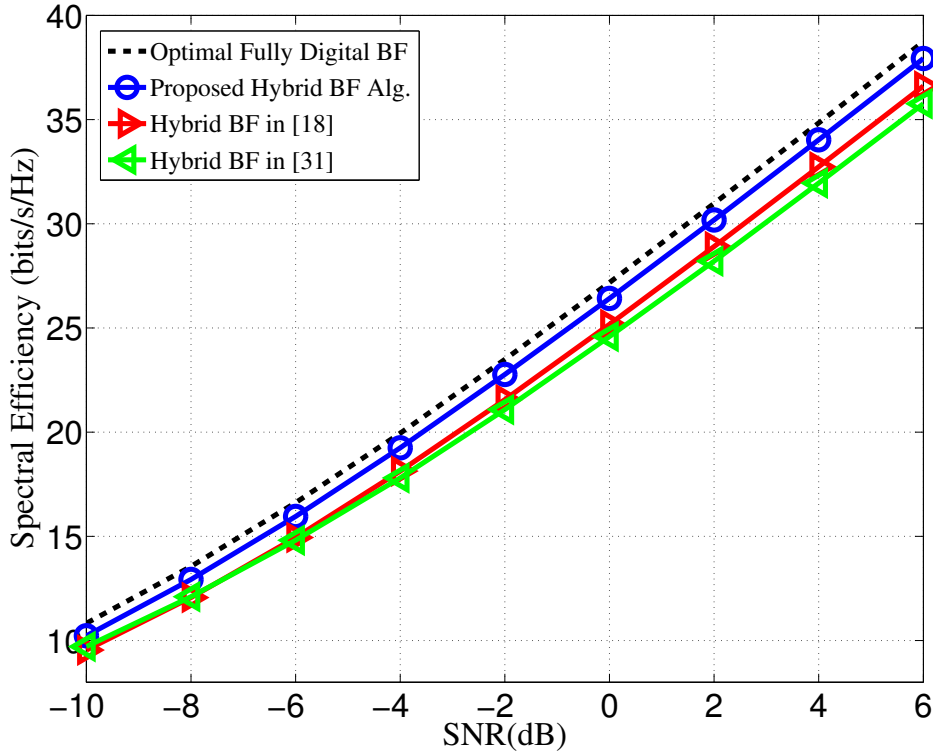


Fig. 2.3: Spectral efficiencies achieved by different methods in a 64×16 MIMO system where $N_{\text{RF}} = N_s = 6$ and $L = 15$. For hybrid beamforming methods, the use of infinite resolution phase shifters is assumed.

The proposed narrowband hybrid beamforming algorithm in this chapter does not depend on the sparse channel model and it can also be applied to the scenarios with rich scattering environments. To show the performance of the proposed algorithm in an environment with rich scattering channels, the next simulation considers a system with similar parameters to the previous experiment except that the number of scatters is now set to be $L = 1000$ in order to model a rich scattering environment. It can be seen from Fig. 2.4 that the proposed algorithm and the algorithm in [18] still achieve a good performance in rich scattering channels while the hybrid beamforming algorithm in [31] which is based on the sparse channel model assumption fails to retain its performance.

The next simulations illustrate the performance of the proposed algorithm when only low resolution phase shifters are available. To do so, the second experiment considers a relatively small 10×10 MIMO system with hybrid beamforming architecture where the analog beamformers are

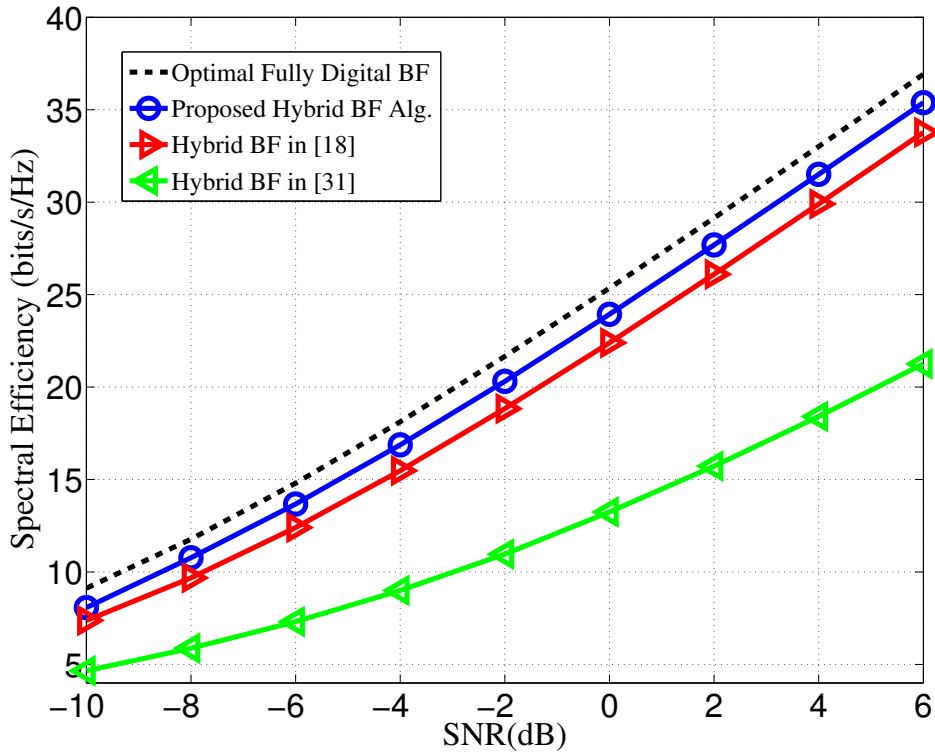


Fig. 2.4: Spectral efficiencies achieved by different methods in a 64×16 MIMO system where $N_{\text{RF}} = N_s = 6$ and $L = 1000$. For hybrid beamforming methods, the use of infinite resolution phase shifters is assumed.

constructed using 1-bit resolution phase shifters. Further, it is assumed that $N_{\text{RF}} = N_s = 2$. The number of antennas at each end is chosen to be relatively small in order to be able to compare the performance of the proposed algorithm with the exhaustive search method. This experiment also compares the performance of the proposed algorithm in Section 2.6, which considers the finite resolution phase shifter constraint in the analog beamformer design, to the performance of the quantized version of the algorithms in Section 2.4, and in [18, 31], where the analog beamformers are first designed under the assumption of infinite resolution phase shifters, then each entry of the analog beamformers is quantized to the nearest point of the set \mathcal{G} . Fig. 2.5 shows that the performance of the proposed algorithm for $b = 1$ has a better performance, at least 1.5dB gain, as compared to the quantized version of the other algorithms that design the analog beamformers assuming accurate phase shifters first. Moreover, the spectral efficiency achieved by the proposed algorithm is very close to that of the optimal exhaustive

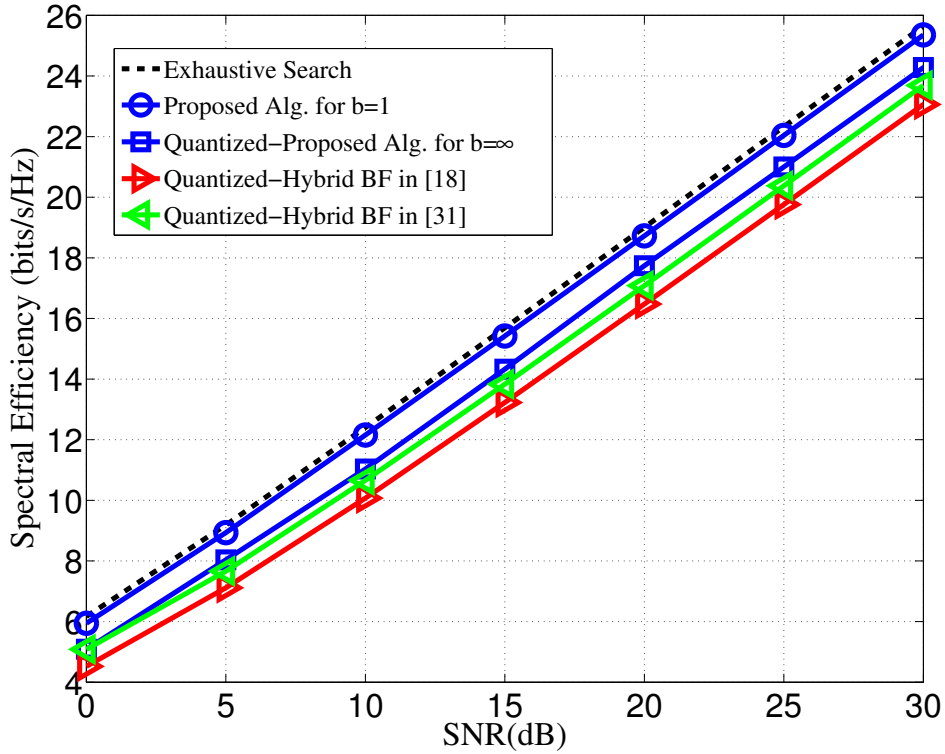


Fig. 2.5: Spectral efficiencies versus SNR for different methods in a 10×10 system where $N_{\text{RF}} = N_s = 2$ and $b = 1$.

search method, confirming that the proposed methods is near to optimal.

The next simulation of this part considers a 64×16 MIMO system with $N_s = 4$ to investigate the performance degradation of the hybrid beamforming with low resolution phase shifters. Fig. 2.7 shows that the performance degradation of a MIMO system with very low resolution phase shifters as compared to the infinite resolution case is significant—about 5dB in this example. However, Fig. 2.7 verifies that this gap can be reduced by increasing the number of RF chains, and by using the algorithm in Section 2.4.4 to optimize the analog and digital beamformers. Therefore, the number of RF chains can be used to trade off the accuracy of phase shifters in hybrid beamforming design.

For the same system parameters as the previous experiment, Fig. 2.7 shows the performance gain of the proposed algorithm for finite b as compared to the quantized version of the proposed algorithm for $b = \infty$. It can be seen that this performance gain is significant only when very-low-resolution PSs are used. This suggests that designing the hybrid beamformers for finite-

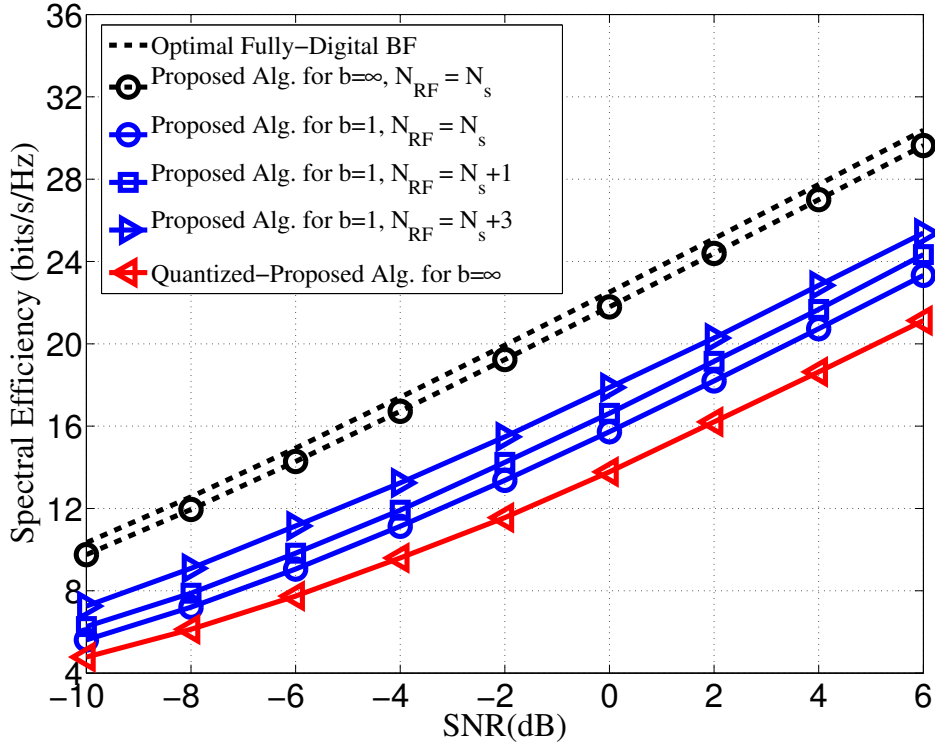


Fig. 2.6: Spectral efficiencies versus SNR for different methods in a 64×16 system where $N_s = 4$.

resolution PSs is crucial when very-low-resolution PSs are used; i.e., here when $b = 1$ or 2. Moreover, Fig. 2.7 indicates that the performance of 3-bit PSs is very close to that of hybrid beamforming with infinite-resolution PSs which matches perfectly with the previous results in [86].

2.7.2 Performance Analysis of a MU-MISO System with Hybrid Beamforming

To study the performance of the proposed algorithm for MU-MISO systems, the first simulation considers an 8-user MISO system with $M_t = 64$ antennas at the BS. Further, it is assumed that the users have the same priority, i.e., $\beta_k = 1, \forall k$. Assuming the use of infinite resolution phase shifters for hybrid beamforming schemes, this experiment compares the performance of the proposed algorithm with $K + 1 = 9$ RF chains to the algorithms in [36] and [35] using $K = 8$ RF chains. In [36] and [35] each column of analog precoder is designed by matching to the

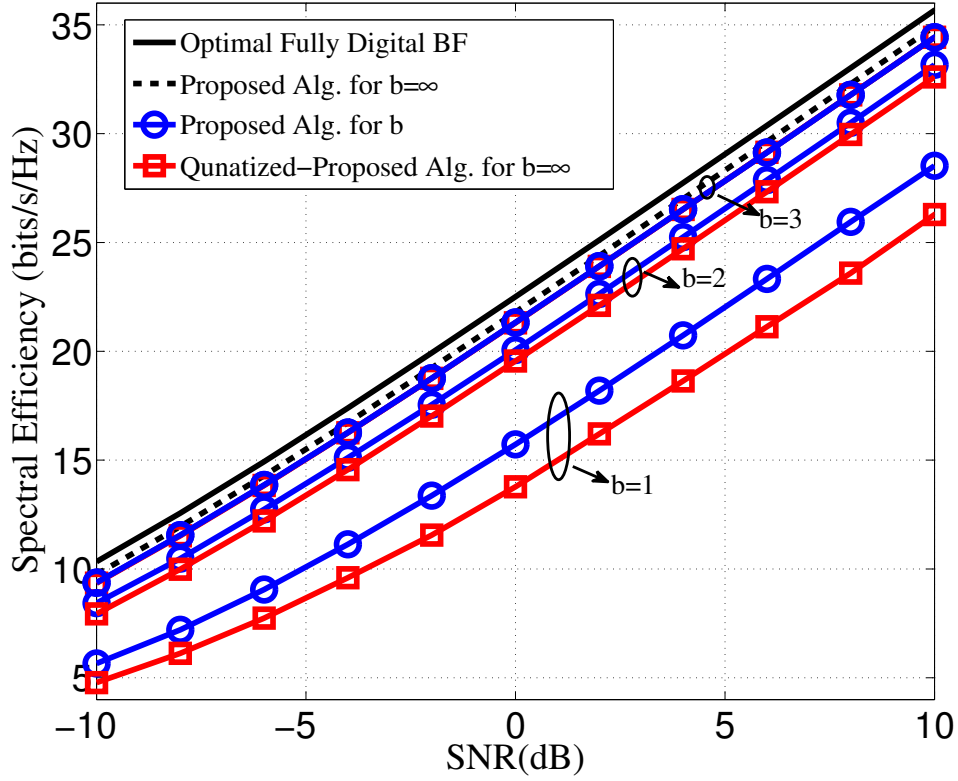


Fig. 2.7: Spectral efficiencies versus SNR for different methods in a 64×16 system where $N_{RF} = N_s = 4$.

phase of the channel of each user and matching to the strongest paths of the channel of each user, respectively. Fig. 2.8 shows that the approach of matching to the strongest paths in [35] is not effective for practical value of M_t ; (here $M_t = 64$). Moreover, the performance of the proposed approach with one extra RF chain is very close to the sum rate upper bound achieved by fully digital ZF beamforming. It improves the method in [36] by about 1dB in this example.

The final experiment studies the effect of finite resolution phase shifters on the performance of the hybrid beamforming in a MU-MISO system. Toward this aim, a MU-MISO system with $M_t = 64$, $K = 4$ and $\beta_k = 1, \forall k$ is considered. Further, it is assumed that only very low resolution phase shifters, i.e., $b = 1$, are available at the BS. Fig. 2.9 shows that the performance of hybrid beamforming with finite resolution phase shifters can be improved by using the proposed approach in Section 2.6; it improves the performance about 1dB, 2dB and 8dB respectively as compared to the quantized version of the algorithms in Section 2.4, [36]

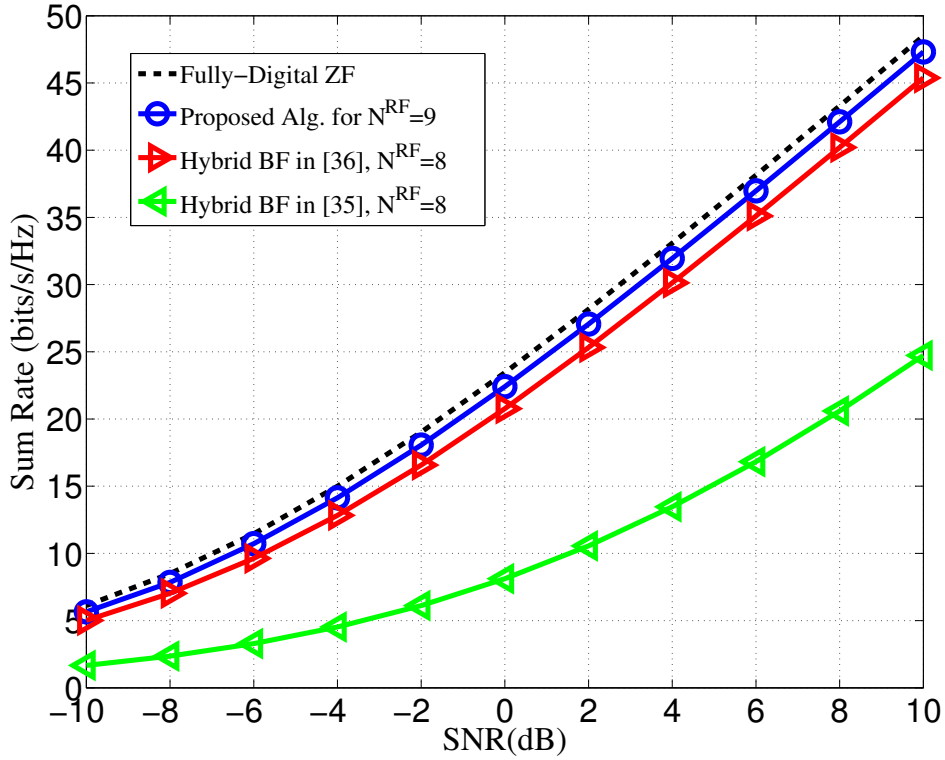


Fig. 2.8: Sum rate achieved by different methods in an 8-user MISO system with $M_t = 64$. For hybrid beamforming methods, the use of infinite resolution phase shifters is assumed.

and [35] .

2.8 Summary

This chapter considers the hybrid beamforming architecture for narrowband wireless communication systems with large-scale antenna arrays. It is shown that fully-connected hybrid beamforming can achieve the same performance of any fully digital beamforming scheme with much fewer number of RF chains; the required number RF chains only needs to be twice the number of active data streams. Further, when the number of RF chains is less than twice the number of data streams, this chapter proposes heuristic algorithms for solving the problem of overall spectral efficiency maximization for the transmission scenario over a SU-MIMO system and over a downlink MU-MISO system. The numerical results show that the proposed approaches achieve a performance close to that of the fully digital beamforming schemes while they achieve a bet-

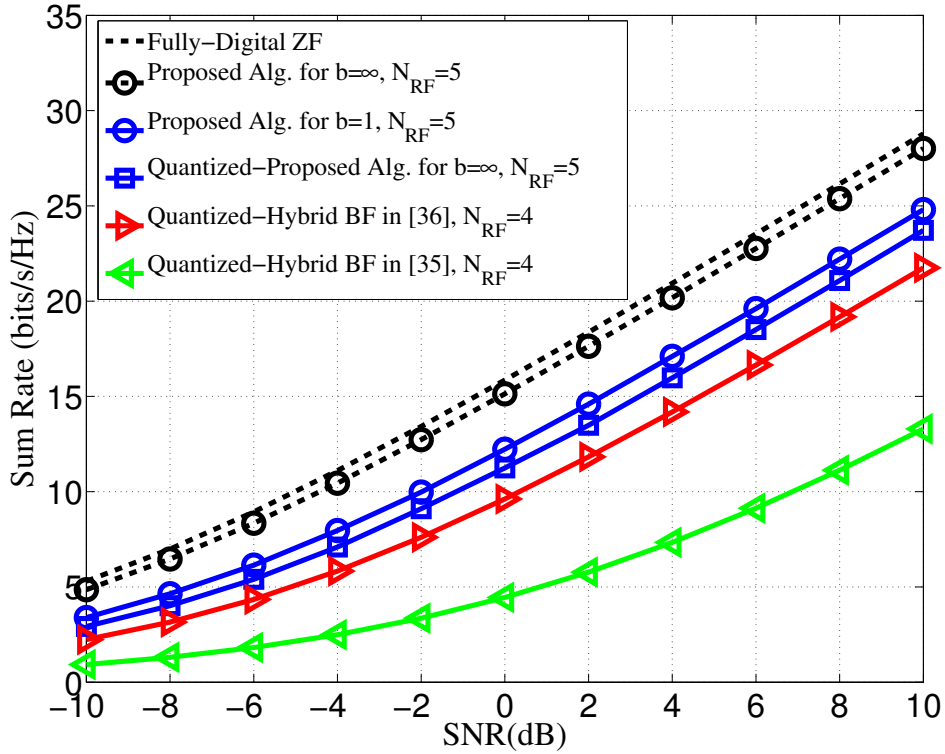


Fig. 2.9: Sum rate achieved by different methods in a 4-user MISO system with $M_t = 64$. For the methods with finite resolution phase shifters, $b = 1$.

ter performance as compared to the other hybrid beamforming baselines. Finally, this chapter modifies the proposed algorithms for systems with finite resolution phase shifters. The numerical results suggest that the proposed modifications can improve the performance significantly, when only very low resolution phase shifters are available.

Chapter 3

Hybrid Beamforming for mmWave Wideband Channels

3.1 Chapter Organization

In the previous chapter, the hybrid analog digital beamforming is introduced to address the challenge of having limited number of RF chains in the systems with narrowband flat-fading channel models. Chapter 2 also recognizes that the mmWave systems can be considered as one of the major applications of the hybrid beamforming architecture. But, since mmWave systems are expected to operate on wideband channels with frequency selectivity, this chapter aims to extend the designs of Chapter 2 to the mmWave frequency-selective channels.

This chapter begins with introducing the system model and the problem formulation in an OFDM-based mmWave SU-MIMO system in which both transmitter and receiver employ large-scale antenna arrays with hybrid structure. In particular, Section 3.2 mentions that the main challenge of hybrid beamforming design in frequency-selective channels is that a common analog beamformer is shared across all the subcarriers. This important feature differentiates hybrid beamforming design in wideband frequency-selective channels from that in narrowband flat-fading channels.

For such a system, Section 3.3 seeks to show that hybrid beamforming can asymptotically achieve the performance of the optimal fully digital beamforming. Toward this aim, Section 3.3

shows that with a sufficiently large number of antenna elements the sample covariance matrices of the channel at different subcarriers asymptotically share the same set of eigenvectors. This feature which is the result of the sparsity in mmWave channels, indicates that the optimal fully digital eigen-beamformers at all subcarriers are asymptotically the same. Further, using this property, Section 3.3 proposes a hybrid precoding and combining design which can asymptotically achieve the capacity of the fully digital beamforming.

The asymptotic proposed design provides an intuition that hybrid beamforming architecture can achieve a performance close to the fully digital beamforming. However, this asymptotic design requires extremely large number of antennas to do so. Motivated by this, Section. 3.4 considers hybrid beamforming design for practical size of antenna arrays. In particular, Section. 3.4 provides a unified algorithm for designing the hybrid precoders and combiners for two hybrid beamforming structures, fully-connected and partially-connected structures, to maximize the overall spectral efficiency under power spectral density constraint in each subcarrier. To develop this algorithm, Section. 3.4 takes several steps to show that it is possible to approximately transform the analog beamforming design problem for frequency-selective channels into the analog beamforming design problem for flat-fading channels. This transformation enables this chapter to employ the analog beamforming algorithms that have been already developed in Chapter 2 for narrowband flat-fading channels.

This chapter also considers hybrid beamforming design for MU-MISO scenario. As discussed earlier in Chapter 2, this problem is different from SU-MIMO case because of the inter-user interference as well as the different priority of different data streams. In order to tackle this problem, Section. 3.5 proposes a simple heuristic algorithm. In the proposed algorithm, the analog precoder is first designed assuming that all the users are cooperative and all the streams have the same priority weights. By this simplifying assumption, the analog precoder can be designed by the algorithm developed in the previous section for a SU-MIMO scenario. Further, when the analog precoder is fixed, Section. 3.5 proposes to employ iterative WMMSE approach to design the digital precoders in different subcarriers to manage both the inter-user interference and the different priority of different data streams.

Section. 3.6 numerically evaluates the performance of the proposed designs. First, Section. 3.6 shows that the performance of the proposed asymptotic design for SU-MIMO scenario

approaches the capacity of the fully digital beamforming when large antenna arrays are employed. Further, for practical number of antennas, it is shown that the proposed heuristic design for SU-MIMO scenario is more effective as compared to the asymptotic design. Finally, the numerical results suggest that the proposed fully-connected hybrid beamforming designs with practical number of RF chains can already approach the performance of the fully digital beamforming baselines for both SU-MIMO and MU-MISO scenarios. Finally, Section. 3.6 provides the summary of this chapter.

3.2 System Model for SU-MIMO

This chapter begins by treating the hybrid beamforming design problem for the single-user mmWave frequency-selective channel. Consider an OFDM-based large-scale SU-MIMO system in which a transmitter equipped with M_t antennas serves a receiver equipped with M_r antennas by sending N_s data symbols per frequency tone. In general, the number of data symbols can be different for different frequency tones, however for simplicity, this chapter restricts attention to the case with an equal number of data streams for all subcarriers. Further, in practical large-scale MIMO systems, the number of available RF chains¹, N_{RF} , is typically much smaller than the number of transceiver antennas, i.e., $N_{RF} \ll \min(M_t, M_r)$. This prohibits the implementation of conventional fully digital beamforming methods which require one RF chain per antenna element. Similar to Chapter 2, this chapter adopts the hybrid analog digital beamforming architecture, shown in Fig. 3.1, to address this hardware limitation challenge. In the hybrid beamforming architecture, the overall beamformer consists of a low-dimensional digital (baseband) beamformer and a high-dimensional analog (RF) beamformer implemented using simple analog components.

3.2.1 Signal Model in OFDM-based Hybrid Beamforming

In the OFDM-based hybrid beamforming architecture shown in Fig. 3.1, the transmitter first precodes N_s data symbols $\mathbf{s}[n]$ at each subcarrier $n = 1, \dots, N$, using a low-dimensional digital precoder, $\mathbf{V}_D[n] \in \mathbb{C}^{N_{RF} \times N_s}$, then transforms the signals to the time domain by using N_{RF}

¹To simplify the notation in this chapter, it is assumed that the number of RF chains at the transmitter and the receiver is identical, however the results can be easily applied to the general setting.

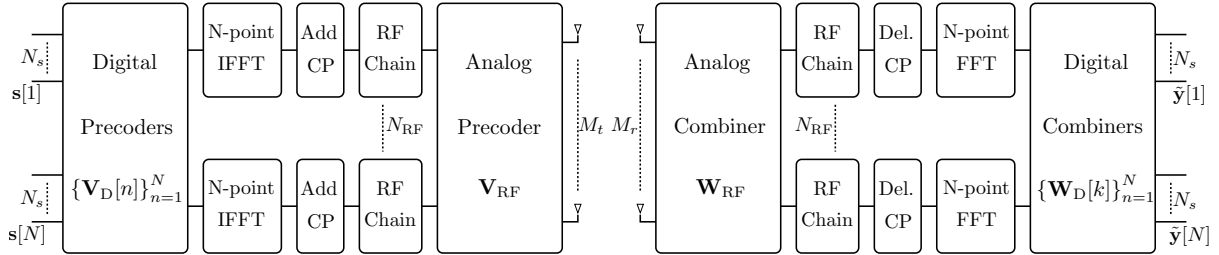


Fig. 3.1: A block diagram of an OFDM-based large-scale SU-MIMO system with hybrid analog and digital beamforming architecture at the transceivers.

N -point inverse fast Fourier transforms (IFFTs). After adding cyclic prefixes, the transmitter employs an analog precoding matrix $\mathbf{V}_{RF} \in \mathbb{C}^{M_t \times N_{RF}}$, to generate the final transmitted signal. Since the analog precoder is a post-IFFT module, the analog precoder is identical for all subcarriers. This is the key challenge in designing the hybrid beamformers in OFDM systems as compared to single-carrier systems. By this consideration, the final transmitted signal at subcarrier n is

$$\mathbf{x}[n] = \mathbf{V}_{RF}\mathbf{V}_D[n]\mathbf{s}[n], \quad (3.1)$$

where $\mathbf{s}[n] \in \mathbb{C}^{N_s \times 1}$ is the vector of transmitted data symbols at subcarrier n with $\mathbb{E}\{\mathbf{s}[n]\mathbf{s}[n]^H\} = \mathbf{I}_{N_s}$. Assuming a block-fading channel model, the received signal at subcarrier n is

$$\mathbf{y}[n] = \mathbf{H}[n]\mathbf{V}_{RF}\mathbf{V}_D[n]\mathbf{s}[n] + \mathbf{z}[n], \quad (3.2)$$

where $\mathbf{H}[n] \in \mathbb{C}^{M_r \times M_t}$ and $\mathbf{z}[n] \sim \mathcal{CN}(\mathbf{0}, \sigma^2 \mathbf{I}_{M_r})$ are the channel matrix and additive white Gaussian noise for subcarrier n , respectively.

At the receiver, the received signals of all subcarriers are initially processed using an analog combiner, $\mathbf{W}_{RF} \in \mathbb{C}^{M_r \times N_{RF}}$. Then, the cyclic prefix is removed and N_{RF} N -point fast Fourier transforms (FFTs) are applied to recover the frequency domain signals. Finally, by employing a low-dimensional digital combiner per subcarrier, $\mathbf{W}_D[n] \in \mathbb{C}^{N_{RF} \times N_s}$, the receiver obtains the final processed signal as

$$\tilde{\mathbf{y}}[n] = \mathbf{W}_t[n]^H \mathbf{H}[n] \mathbf{V}_t[n] \mathbf{s}[n] + \mathbf{W}_t[n]^H \mathbf{z}[n], \quad (3.3)$$

in which $\mathbf{V}_t[n] = \mathbf{V}_{RF}\mathbf{V}_D[n]$ and $\mathbf{W}_t[n] = \mathbf{W}_{RF}\mathbf{W}_D[n]$ are the overall hybrid precoder and

combiner for the n^{th} subcarrier, respectively.

3.2.2 Structure of Analog Beamformer

As discussed in the earlier chapters, the analog part of the hybrid beamformer is typically implemented using simple analog components including analog adders and analog phase shifters which can only adjust the phase of signals. This causes some constraints on the analog beamforming matrix depending on the structure of the analog beamformer. This chapter focuses on two widely used analog beamforming structures: the fully-connected and the partially-connected structures.

Fully-connected Architecture: In this structure, each RF chain is connected to all the antenna elements via a network of phase shifters. As an example the fully-connected hybrid precoder is shown in Fig. 3.2(a). Use of simple analog phase shifters which can only change the phase of the signals imposes a constant modulus norm constraint on each element of the analog beamforming matrices, i.e., $|\mathbf{V}_{\text{RF}}(i, j)| = |\mathbf{W}_{\text{RF}}(i, j)| = 1, \forall i, j$. Moreover, as it can be seen in Fig. 3.2(a), each element of analog beamforming matrix is realized by a single analog phase shifter. Therefore, the total number of phase shifters in this architecture is given by the number of antennas times the number of RF chains which means that in fully-connected structure the transmitter and the receiver require $M_t N_{\text{RF}}$ and $M_r N_{\text{RF}}$ phase shifters, respectively.

Partially-connected Architecture: Unlike the fully-connected structure, in the partially-connected structure, each RF chain is connected only to a subarray with M_t/N_{RF} and M_r/N_{RF} antennas at the transmitter and the receiver, respectively. This is schematically shown in Fig. 3.2(b) for the partially-connected hybrid precoder. This structure implies that the analog beamforming matrix in the partially-connected architecture has a block diagonal format, i.e., the analog precoder has the form,

$$\mathbf{V}_{\text{RF}} = \begin{bmatrix} \mathbf{v}_1 & \mathbf{0} & \cdots & \mathbf{0} \\ \mathbf{0} & \mathbf{v}_2 & & \mathbf{0} \\ \mathbf{0} & \mathbf{0} & \ddots & \mathbf{0} \\ \mathbf{0} & \mathbf{0} & \cdots & \mathbf{v}_{N_{\text{RF}}} \end{bmatrix}, \quad (3.4)$$

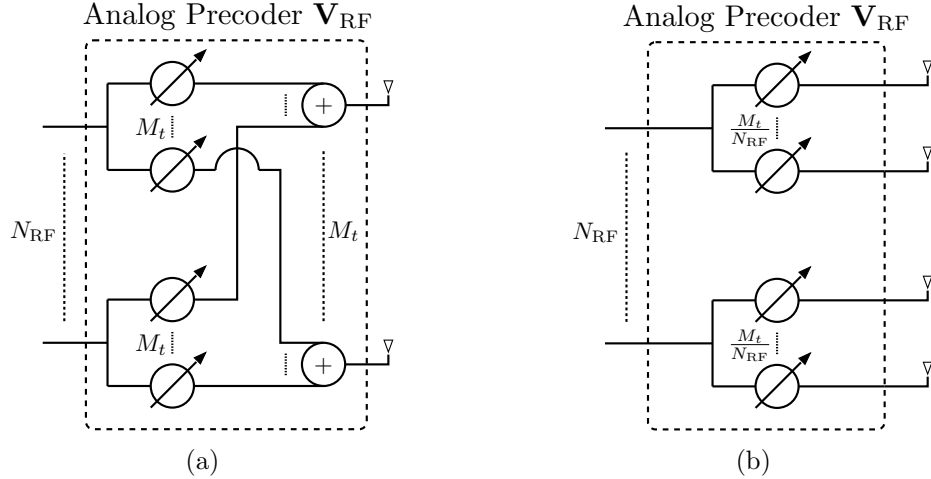


Fig. 3.2: (a) The architecture of an analog precoder with fully-connected structure. (b) The architecture of an analog precoder with partially-connected structure.

where each element of the vector \mathbf{v}_i satisfies the constant modulus constraint. Moreover, the total number of phase shifters in this structure is equal to the number of antennas, i.e., M_t for the precoder and M_r for the combiner. This means that the hardware complexity of the RF beamformer is reduced by a factor of N_{RF} as compared to the fully-connected structure.

It is shown in [37] that there is a performance-complexity trade off in choosing the above structures. The fully-connected structure can achieve full beamforming gain with full phase control, while the partially-connect structure has limited phase control, thus cannot achieve full beamforming gain in all cases. On the other hand, the hardware implementation complexity and power consumption of the partially-connected architecture are much lower as compared to those of the fully-connected structure. This chapter seeks to propose a general design algorithm which can handle the design of hybrid beamforming for both analog beamformer structures.

3.2.3 Problem Formulation

The problem of interest for SU-MIMO case is to design the hybrid analog and digital beamformers under either fully or partially connected structures in order to maximize the overall spectral efficiency of the system under a power spectral density constraint for each subcarrier. Note that, throughout this chapter, it is assumed that the perfect CSI is available. In this case,

the problem can be formulated as

$$\underset{\mathbf{V}_{\text{RF}}, \mathbf{W}_{\text{RF}}, \{\mathbf{V}_D[n], \mathbf{W}_D[n]\}_{n=1}^N}{\text{maximize}} \quad \frac{1}{N} \sum_{n=1}^N R[n] \quad (3.5a)$$

$$\text{subject to} \quad \text{Tr} \left(\mathbf{V}_{\text{RF}} \mathbf{V}_D[n] \mathbf{V}_D[n]^H \mathbf{V}_{\text{RF}}^H \right) \leq P, \quad \forall n, \quad (3.5b)$$

$$|\mathbf{V}_{\text{RF}}(i, j)| = 1, \quad \forall (i, j) \in \mathcal{F}_t, \quad (3.5c)$$

$$|\mathbf{W}_{\text{RF}}(i, j)| = 1, \quad \forall (i, j) \in \mathcal{F}_r, \quad (3.5d)$$

where P is the total transmit power budget per subcarrier, \mathcal{F}_t (\mathcal{F}_r) is the set of non-zero elements of analog precoder (combiner), and $R[n]$ is the overall spectral efficiency of the subcarrier n which for Gaussian signalling is

$$R[n] = \log_2 \left| \mathbf{I}_{M_r} + \frac{1}{\sigma^2} \mathbf{C}[n] \mathbf{H}[n] \mathbf{V}_t[n] \mathbf{V}_t[n]^H \mathbf{H}[n]^H \right|, \quad (3.6)$$

in which

$$\mathbf{C}[n] = \mathbf{W}_t[n] \left(\mathbf{W}_t[n]^H \mathbf{W}_t[n] \right)^{-1} \mathbf{W}_t[n]^H, \quad (3.7)$$

$\mathbf{V}_t[n] = \mathbf{V}_{\text{RF}} \mathbf{V}_D[n]$ and $\mathbf{W}_t[n] = \mathbf{W}_{\text{RF}} \mathbf{W}_D[n]$ are the overall hybrid precoder and combiner in subcarrier n , respectively.

It should be mentioned that this thesis considers the stringent constraint of per subcarrier power constraint motivated by the fact that it is desirable for practical wideband systems to satisfy the power spectrum density constraint [49–52]. However, the proposed algorithms in this thesis can be easily extended to a more relaxed problem with total power constraint.

3.2.4 Channel Model

It is known that the channel of a mmWave propagation environment does not follow the conventional rich-scattering model because the number of scatterers in such an environment is limited [87]. In fact, the mmWave propagation environment is typically modeled as a geometric channel with N_c scattering clusters and N_{sc} scatterers within each cluster. In this model, the

channel matrix of subcarrier n is given as [37]

$$\mathbf{H}[n] = \sum_{c=1}^{N_c} \sum_{\ell=1}^{N_{sc}} \alpha_{c\ell} \mathbf{a}_r(\phi_{c\ell}^r) \mathbf{a}_t(\phi_{c\ell}^t)^H e^{-i2\pi(c-1)\frac{n}{N}}, \quad (3.8)$$

where $\alpha_{c\ell} \sim \mathcal{CN}(0, \frac{M_t M_r}{N_c N_{sc}})$, $\phi_{c\ell}^r$ and $\phi_{c\ell}^t$ are the scaled complex gain, angles of arrival and departure for the ℓ^{th} path in the c^{th} cluster, respectively. Further, $\mathbf{a}_r(\cdot)$ and $\mathbf{a}_t(\cdot)$ are the antenna array response vectors for the receiver and the transmitter, respectively. The antenna array response vectors $\mathbf{a}_r(\cdot)$ and $\mathbf{a}_t(\cdot)$ are functions of the antenna array structure and each element of these vectors typically satisfies a constant modulus norm constraint. This thesis considers a uniform linear array configuration in which the antenna array response vector of an array with M antennas and spacing of \tilde{d} is modeled as

$$\mathbf{a}(\phi) = \frac{1}{\sqrt{M}} [1, e^{i\frac{2\pi}{\lambda}\tilde{d}\sin(\phi)}, \dots, e^{i\frac{2\pi}{\lambda}(M-1)\tilde{d}\sin(\phi)}]^T, \quad (3.9)$$

where λ is the signal wavelength. Note that in this representation it is assumed that the operating frequency is much larger than the total bandwidth of the OFDM system such that the signal wavelength in all subcarriers can approximately be considered equal.

The channel matrix in (3.8) can also be written in a more compact form as

$$\mathbf{H}[n] = \mathbf{A}_r \text{diag}(\boldsymbol{\alpha}[n]) \mathbf{A}_t^H, \quad (3.10)$$

where

$$\mathbf{A}_r = [\mathbf{a}_r(\phi_{11}^r), \mathbf{a}_r(\phi_{12}^r), \dots, \mathbf{a}_r(\phi_{N_c N_{sc}}^r)], \quad (3.11a)$$

$$\mathbf{A}_t = [\mathbf{a}_t(\phi_{11}^t), \mathbf{a}_t(\phi_{12}^t), \dots, \mathbf{a}_t(\phi_{N_c N_{sc}}^t)], \quad (3.11b)$$

$$\boldsymbol{\alpha}[n] = [\alpha_{11} e^{-i\theta_1[n]}, \alpha_{12} e^{-i\theta_1[n]}, \dots, \alpha_{N_c N_{sc}} e^{-i\theta_{N_c}[n]}], \quad (3.11c)$$

and $\theta_c[n] = \frac{2\pi(c-1)n}{N}$.

3.3 Asymptotic Beamforming Design for SU-MIMO

This section exploits the sparse nature of the frequency-selective mmWave propagation environment introduced in Section 3.2.4 to show that for a fixed number of data streams, N_s , hybrid beamforming architecture with only N_s RF chains, i.e., $N_{\text{RF}} = N_s$, can asymptotically realize the optimal fully digital beamformer when $M_t, M_r \rightarrow \infty$. Note that this result is known in the hybrid beamforming literature for single-carrier systems [31, 88]. This section generalizes that result to OFDM-based SU-MIMO systems with frequency-selective channels to explain why the hybrid beamforming is expected to work well in mmWave frequency-selective channels despite being much less complex than conventional fully digital beamforming.

It is well-known that the optimal linear fully digital precoder in each subcarrier, $\mathbf{V}_{\text{opt}}[n] \in \mathbb{C}^{M_t \times N_s}$, that maximizes the overall rate subject to the power constraint is given by matching to the set of eigenvectors corresponding to the N_s largest eigenvalues of the channel sample covariance matrix, $\mathbf{S}[n] = \mathbf{H}[n]^H \mathbf{H}[n]$ [4]. This section takes advantage of the sparsity of the channel in (3.10) to show that the channel sample covariance matrices in different subcarriers are approximately similar, hence they share approximately the same set of eigenvectors.

For mmWave channel model (3.10) when $M_t, M_r \rightarrow \infty$, the matrix $\mathbf{S}[n]$ can be further simplified as

$$\mathbf{S}[n] = \mathbf{A}_t \text{diag}(\boldsymbol{\alpha}^*[n]) \mathbf{A}_r^H \mathbf{A}_r \text{diag}(\boldsymbol{\alpha}[n]) \mathbf{A}_t^H \quad (3.12a)$$

$$\approx \mathbf{A}_t \text{diag}(\boldsymbol{\beta}) \mathbf{A}_t^H, \quad (3.12b)$$

where $\boldsymbol{\beta} = [| \alpha_{11} |^2, | \alpha_{12} |^2, \dots, | \alpha_{N_c N_{\text{sc}}} |^2]$. The approximate equality in (3.12b) is due to the fact that the diagonal elements of $\mathbf{A}_r^H \mathbf{A}_r$ are exactly equal to 1 while the off-diagonal elements of $\mathbf{A}_r^H \mathbf{A}_r$ scales with $\frac{1}{M_t}$ such that for $M_t \rightarrow \infty$, they are going to zero [31]. Using a similar argument, it is possible to show that $\mathbf{A}_t^H \mathbf{A}_t \approx \mathbf{I}$. Now, using this property and the structure of $\mathbf{S}[n]$ in (3.12b), it can be seen that the columns of \mathbf{A}_t are approximately the eigenvectors of $\mathbf{S}[n]$.

Let $\tilde{\mathbf{A}}_t \in \mathbb{C}^{M_t \times N_s}$ denote the set of columns of \mathbf{A}_t corresponding to N_s largest elements of the vector $\boldsymbol{\beta}$, i.e., N_s largest values of the set $\{|\alpha_{c\ell}|^2\}_{\forall c, \ell}$. It can be seen that the optimal

fully digital precoder in each subcarrier is now $\mathbf{V}_{\text{opt}}[n] = \tilde{\mathbf{A}}_t \boldsymbol{\Gamma}[n]$ where $\boldsymbol{\Gamma}[n]$ is the diagonal matrix of the allocated power to each data stream which can be obtained using water-filling approach. Since the elements of $\tilde{\mathbf{A}}_t$ satisfy the constant modulus norm constraint, those optimal fully digital precoders can be realized by the hybrid precoding design in which $\mathbf{V}_{\text{RF}} = \tilde{\mathbf{A}}_t$ and $\mathbf{V}_{\text{D}}[n] = \boldsymbol{\Gamma}[n]$.

At the receiver side, with a similar justification, it is possible to show that the asymptotic optimal analog combiner is given by the set of columns of \mathbf{A}_r corresponding to N_s largest complex gains.

In summary, this section shows that in a mmWave SU-MIMO system with fixed number of scatterers in the environment and fixed number of data streams, if the number of antennas is sufficiently large so that $\mathbf{A}_t^H \mathbf{A}_t \approx \mathbf{I}$ and $\mathbf{A}_r^H \mathbf{A}_r \approx \mathbf{I}$, the hybrid beamforming with only N_s RF chains can realize the optimal fully digital beamforming.

3.4 Hybrid Beamforming Design for SU-MIMO

In the previous section, it is shown that the performance of the hybrid beamforming in frequency-selective channels can asymptotically approach the performance of the optimal fully digital beamforming when the number of antennas at both transmitter and receiver is sufficiently large. Based on the asymptotic analysis, it is shown that the optimal analog beamforming design is to choose the columns of the analog precoder (combiner) from the transmit (receive) antenna array response vectors. However, as numerical results presented in Section 3.6 show, in scenarios with a practical number of antennas in an environment with multiple scatters within each cluster, the performance of this asymptotic design actually has a sizable gap to the performance of fully digital beamforming. Further, this asymptotic design requires fully-connected analog beamforming, and is not applicable to the partially-connected case. The goal of this section is to investigate how to design the hybrid beamformers for the scenarios with practical number of antennas and also with partially-connected structure.

3.4.1 Transmitter Design

In general, maximizing the spectral efficiency in (3.5a) requires a joint optimization over the transmit beamformers and receive beamformers. Joint optimization is, however, computationally complex. This chapter follows the alternative strategy proposed in Chapter 2, in which the transmitter is first designed assuming an ideal fully digital receiver, then the receiver is designed given the already designed transmitter. This strategy leads to a decoupled transmitter and receiver design. Following this strategy, the hybrid beamforming design problem at the transmitter is

$$\max_{\mathbf{V}_{\text{RF}}, \{\mathbf{V}_D[n]\}_{n=1}^N} \frac{1}{N} \sum_{n=1}^N \tilde{R}[n] \quad (3.13a)$$

$$\text{s.t.} \quad \text{Tr} \left(\mathbf{V}_{\text{RF}} \mathbf{V}_D[n] \mathbf{V}_D[n]^H \mathbf{V}_{\text{RF}}^H \right) \leq P, \quad \forall n, \quad (3.13b)$$

$$|\mathbf{V}_{\text{RF}}(i, j)| = 1, \quad \forall (i, j) \in \mathcal{F}_t, \quad (3.13c)$$

where

$$\tilde{R}[n] = \log_2 \left| \mathbf{I} + \frac{1}{\sigma^2} \mathbf{H}[n] \mathbf{V}_{\text{RF}} \mathbf{V}_D[n] \mathbf{V}_D[n]^H \mathbf{V}_{\text{RF}}^H \mathbf{H}[n]^H \right|, \quad (3.14)$$

is the achievable rate of subcarrier n . This optimization problem is challenging since it is not convex even for single-carrier systems with flat-fading channels as discussed in Chapter 2. To develop an algorithm for tackling this optimization problem, this thesis takes the following steps:

- First, for a fixed analog precoder, \mathbf{V}_{RF} , this thesis derives the optimal closed-form solution for digital precoder of each subcarrier, $\mathbf{V}_D[n]$, that maximizes the overall spectral efficiency.
- Second, by exploiting the structure of that optimal digital precoders, this thesis shows that the expression $\mathbf{V}_D[n] \mathbf{V}_D[n]^H$ in (3.14) can be further simplified for large-scale antenna arrays.
- Then, using that simplification and the Jensen's inequality, this thesis derives an upper-bound for the objective function of (3.13).

- Finally, this thesis devises an iterative algorithm to design the analog precoder such that it locally maximizes that upper-bound.

Digital Precoding Design

In this part, the optimal digital precoding design is presented given the analog precoder. When the analog precoder is fixed, the effective channel of subcarrier n can be considered as $\mathbf{H}_{\text{eff}}[n] = \mathbf{H}[n]\mathbf{V}_{\text{RF}}$. Further, it can be seen that the constraints on digital precoders of different subcarriers in (3.13) are decoupled. Therefore, without loss of optimality, the following problem for designing the digital precoder of the subcarrier n can be considered

$$\max_{\mathbf{V}_D[n]} \log_2 \left| \mathbf{I} + \frac{1}{\sigma^2} \mathbf{H}_{\text{eff}}[n] \mathbf{V}_D[n] \mathbf{V}_D[n]^H \mathbf{H}_{\text{eff}}[n]^H \right| \quad (3.15a)$$

$$\text{s.t. } \text{Tr} \left(\mathbf{Q} \mathbf{V}_D[n] \mathbf{V}_D[n]^H \right) \leq P, \quad (3.15b)$$

where $\mathbf{Q} = \mathbf{V}_{\text{RF}}^H \mathbf{V}_{\text{RF}}$. It can be seen that this problem is now in the form of digital precoding design problem of a SU-MIMO system with narrowband channel considered in the previous chapter. Therefore, the problem (3.15) has also a closed-form water-filling solution as

$$\mathbf{V}_D[n] = \mathbf{Q}^{-1/2} \mathbf{U}_e[n] \boldsymbol{\Gamma}_e[n], \quad (3.16)$$

in which $\mathbf{U}_e[n]$ is the set of right singular vectors corresponding to the N_s largest singular values of $\mathbf{H}_{\text{eff}}[n] \mathbf{Q}^{-1/2}$ and $\boldsymbol{\Gamma}_e[n]$ is the diagonal matrix of allocated powers to each symbol of the subcarrier n .

Now, this part seeks to exploit the structure of the optimal digital precoder in (3.16) for large antenna arrays. Similar to the single-carrier setup, it is possible to argue that the analog precoder in fully-connected structure approximately satisfies $\mathbf{V}_{\text{RF}}^H \mathbf{V}_{\text{RF}} \approx M_t \mathbf{I}$ for sufficiently large number of antennas. Further, in partially-connected structure, the analog precoder exactly satisfies $\mathbf{V}_{\text{RF}}^H \mathbf{V}_{\text{RF}} = \frac{M_t}{N_{\text{RF}}} \mathbf{I}$ due to the block diagonal format of the analog beamformer as described in (3.4). Using these observations, this thesis approximates $\mathbf{Q} = \mathbf{V}_{\text{RF}}^H \mathbf{V}_{\text{RF}}$ as proportional to the identity matrix, $\mathbf{Q} \propto \mathbf{I}$ for both fully-connected and partially-connected structures. Moreover, for moderate and high SNR regime, it is possible to adopt an equal

power allocation for all streams in each subcarrier, $\mathbf{\Gamma}_e[n] \propto \mathbf{I}$, without significant performance degradation. Accordingly, the overall digital precoder can be approximated as $\mathbf{V}_D[n] \approx \gamma \mathbf{U}_e[n]$ where γ is a scalar parameter that guarantees that the power constraint in (3.15b) is satisfied, yielding,

$$\gamma = \begin{cases} \sqrt{\frac{P}{M_t N_{RF}}}, & \text{for fully-connected structure,} \\ \sqrt{\frac{P}{M_t}}, & \text{for partially-connected structure.} \end{cases} \quad (3.17)$$

Analog Precoding Design

This part presents an algorithm for designing the analog precoder assuming that the digital precoder in each subcarrier is given as $\mathbf{V}_D[n] \approx \gamma \mathbf{U}_e[n]$. It can be seen that such digital precoders satisfy

$$\mathbf{V}_D[n] \mathbf{V}_D[n]^H \approx \gamma^2 \mathbf{U}[n] \tilde{\mathbf{I}}_{N_{RF}} \mathbf{U}[n]^H, \quad (3.18)$$

where

$$\tilde{\mathbf{I}}_{N_{RF}} = \begin{bmatrix} \mathbf{I}_{N_s} & \mathbf{0} \\ \mathbf{0} & \mathbf{0} \end{bmatrix}, \quad (3.19)$$

and $\mathbf{U}[n] \in \mathbb{C}^{N_{RF} \times N_{RF}}$ is a unitary matrix. Using the approximation in (3.18), the achievable rate of subcarrier n in (3.14) can be approximately upper-bounded as

$$\tilde{R}[n] \approx \log_2 \left| \mathbf{I} + \frac{\gamma^2}{\sigma^2} \mathbf{U}[n]^H \mathbf{V}_{RF}^H \mathbf{H}[n]^H \mathbf{H}[n] \mathbf{V}_{RF} \mathbf{U}[n] \tilde{\mathbf{I}}_{N_{RF}} \right| \quad (3.20a)$$

$$\leq \log_2 \left| \mathbf{I} + \frac{\gamma^2}{\sigma^2} \mathbf{U}[n]^H \mathbf{V}_{RF}^H \mathbf{H}[n]^H \mathbf{H}[n] \mathbf{V}_{RF} \mathbf{U}[n] \mathbf{I}_{N_{RF}} \right| \quad (3.20b)$$

$$= \log_2 \left| \mathbf{I} + \frac{\gamma^2}{\sigma^2} \mathbf{V}_{RF}^H \mathbf{H}[n]^H \mathbf{H}[n] \mathbf{V}_{RF} \right|, \quad (3.20c)$$

where (3.20b) is satisfied with equality if $N_{RF} = N_s$ and (3.20c) is written based on the properties of the unitary matrices. Finally, this thesis derives an upper-bound for the overall spectral

efficiency in the objective of (3.13) using Jensen's inequality as

$$\frac{1}{N} \sum_{n=1}^N \tilde{R}[n] \lesssim \frac{1}{N} \sum_{n=1}^N \log_2 \left| \mathbf{I} + \frac{\gamma^2}{\sigma^2} \mathbf{V}_{\text{RF}}^H \mathbf{H}[n]^H \mathbf{H}[n] \mathbf{V}_{\text{RF}} \right| \quad (3.21a)$$

$$\leq \log_2 \left| \mathbf{I} + \frac{\gamma^2}{\sigma^2} \mathbf{V}_{\text{RF}}^H \mathbf{F}_1 \mathbf{V}_{\text{RF}} \right|, \quad (3.21b)$$

where

$$\mathbf{F}_1 = \frac{1}{N} \sum_{n=1}^N \left(\mathbf{H}[n]^H \mathbf{H}[n] \right), \quad (3.22)$$

is the average of the sample covariance matrices of frequency domain channels, (3.21a) follows (3.20c) and (3.21b) is based on Jensen's inequality; i.e., for a concave function $f(\cdot)$, if $\sum_i \alpha_i = 1$, then $\sum_i \alpha_i f(\mathbf{X}_i) \leq f(\sum_i \alpha_i \mathbf{X}_i)$.

This thesis proposes to design the analog precoder such that it maximizes the upper-bound of the overall spectral efficiency in (3.21b), yielding,

$$\max_{\mathbf{V}_{\text{RF}}} \log_2 \left| \mathbf{I} + \frac{\gamma^2}{\sigma^2} \mathbf{V}_{\text{RF}}^H \mathbf{F}_1 \mathbf{V}_{\text{RF}} \right| \quad (3.23a)$$

$$\text{s.t. } |\mathbf{V}_{\text{RF}}(i, j)| = 1, \quad \forall (i, j) \in \mathcal{F}_t. \quad (3.23b)$$

Interestingly, the problem (3.23) is now in the format of analog precoder design problem for single-carrier systems with flat-fading channels which has considered in Chapter 2. In Chapter 2, it is shown that the analog precoder of a single-carrier system should be designed to maximize the following objective function

$$\log_2 \left| \mathbf{I} + \frac{\gamma^2}{\sigma^2} \mathbf{V}_{\text{RF}}^H (\mathbf{H}^H \mathbf{H}) \mathbf{V}_{\text{RF}} \right|. \quad (3.24)$$

This observation motivates us to replace the sample covariance matrix of the channel, $\mathbf{H}^H \mathbf{H}$, in flat-fading scenario by its average over all subcarriers, i.e., $\mathbf{F}_1 = \frac{1}{N} \sum_{n=1}^N \left(\mathbf{H}[n]^H \mathbf{H}[n] \right)$, and then use the algorithm proposed in Chapter 2 for designing the analog precoder in OFDM-based systems with frequency-selective channels. The rest of this section provides a brief explanation of the iterative algorithm proposed in Chapter 2.

It can be seen that all the constraints in problem (3.23) are decoupled. This enables us to

develop an iterative coordinate descent algorithm over the elements of analog precoder, \mathbf{V}_{RF} , to find a locally optimal solution of the problem (3.23). Mathematically, it is shown in Chapter 2 that the contribution of each element of analog precoder, $\mathbf{V}_{\text{RF}}(i, j)$, to the objective of (3.23) can be extracted as

$$\log_2 |\mathbf{C}_j| + \log_2 (2 \operatorname{Re} \{\mathbf{V}_{\text{RF}}^*(i, j)\eta_{ij}\} + \zeta_{ij} + 1), \quad (3.25)$$

where

$$\mathbf{C}_j = \mathbf{I} + \frac{\gamma^2}{\sigma^2} (\bar{\mathbf{V}}_{\text{RF}}^j)^H \mathbf{F}_1 \bar{\mathbf{V}}_{\text{RF}}^j, \quad (3.26)$$

and $\bar{\mathbf{V}}_{\text{RF}}^j$ is the sub-matrix of \mathbf{V}_{RF} with j^{th} column removed, and

$$\eta_{ij} = \sum_{\ell \neq i} \mathbf{G}_j(i, \ell) \mathbf{V}_{\text{RF}}(\ell, j), \quad (3.27a)$$

$$\zeta_{ij} = \mathbf{G}_j(i, i) + 2 \operatorname{Re} \left\{ \sum_{m \neq i, n \neq i} \mathbf{V}_{\text{RF}}^*(m, j) \mathbf{G}_j(m, n) \mathbf{V}_{\text{RF}}(n, j) \right\}, \quad (3.27b)$$

$$\mathbf{G}_j = \frac{\gamma^2}{\sigma^2} \mathbf{F}_1 - \frac{\gamma^4}{\sigma^4} \mathbf{F}_1 \bar{\mathbf{V}}_{\text{RF}}^j \mathbf{C}_j^{-1} (\bar{\mathbf{V}}_{\text{RF}}^j)^H \mathbf{F}_1. \quad (3.27c)$$

Now, because all parameters \mathbf{C}_j , ζ_{ij} and η_{ij} are independent of the element $\mathbf{V}_{\text{RF}}(i, j)$, the optimal value for this element (when all other elements of \mathbf{V}_{RF} are fixed) is given as

$$\mathbf{V}_{\text{RF}}(i, j) = \begin{cases} \frac{\eta_{ij}}{|\eta_{ij}|}, & \forall (i, j) \in \mathcal{F}_t \text{ s.t. } \eta_{ij} \neq 0, \\ 1, & \forall (i, j) \in \mathcal{F}_t \text{ s.t. } \eta_{ij} = 0, \\ 0, & \forall (i, j) \notin \mathcal{F}_t. \end{cases} \quad (3.28)$$

The final algorithm starts with an initial feasible analog precoder which satisfies (3.23b), then sequentially updates each $\mathbf{V}_{\text{RF}}(i, j)$ based on (3.28). The convergence of this algorithm to the locally optimal solution of (3.23) is guaranteed since in each step of algorithm the objective function increases.

3.4.2 Receiver Design

This part considers the hybrid combining design when the transmit beamforming matrix is already fixed. For a fixed analog combiner, the optimal digital combiner of each subcarrier is known to be the MMSE solution as

$$\mathbf{W}_D[n] = \mathbf{J}[n]^{-1} \mathbf{W}_{RF}^H \mathbf{H}[n] \mathbf{V}_t[n], \quad (3.29)$$

in which

$$\mathbf{J}[n] = \mathbf{W}_{RF}^H \mathbf{H}[n] \mathbf{V}_t[n] \mathbf{V}_t[n]^H \mathbf{H}[n]^H \mathbf{W}_{RF} + \sigma^2 \mathbf{W}_{RF}^H \mathbf{W}_{RF}. \quad (3.30)$$

Using the same argument as for analog precoder, it can be shown that the analog combiner approximately satisfies $\mathbf{W}_{RF}^H \mathbf{W}_{RF} \propto \mathbf{I}$, for both fully-connected and partially-connected structures. This leads to the conclusion that the effective noise after the analog combiner approximately remains white. Now, using the property of MMSE digital combiner under white background noise, the analog combiner design problem can be written as

$$\max_{\mathbf{W}_{RF}} \quad \frac{1}{N} \sum_{n=1}^N \log_2 \left| \mathbf{I} + (\sigma^2 \mathbf{W}_{RF}^H \mathbf{W}_{RF})^{-1} \mathbf{W}_{RF}^H \tilde{\mathbf{F}}[n] \mathbf{W}_{RF} \right| \quad (3.31a)$$

$$\text{s.t.} \quad |\mathbf{W}_{RF}(i, j)| = 1, \quad \forall (i, j) \in \mathcal{F}_r, \quad (3.31b)$$

where

$$\tilde{\mathbf{F}}[n] = \mathbf{H}[n] \mathbf{V}_t[n] \mathbf{V}_t[n]^H \mathbf{H}[n]^H. \quad (3.32)$$

By using the approximation $\mathbf{W}_{RF}^H \mathbf{W}_{RF} \propto \mathbf{I}$, and applying the Jensen's inequality, this thesis can consider maximizing the upper-bound of (3.31) for designing \mathbf{W}_{RF} as

$$\max_{\mathbf{W}_{RF}} \quad \log_2 \left| \mathbf{I} + \frac{1}{\sigma^2 \tau} \mathbf{W}_{RF}^H \mathbf{F}_2 \mathbf{W}_{RF} \right| \quad (3.33a)$$

$$\text{s.t.} \quad |\mathbf{W}_{RF}(i, j)|^2 = 1, \quad \forall (i, j) \in \mathcal{F}_r, \quad (3.33b)$$

in which $\mathbf{F}_2 = \frac{1}{N} \sum_{n=1}^N \tilde{\mathbf{F}}[n]$, $\tau = M_r$ and $\tau = M_r/N_{RF}$ for fully-connected structure and partially-connected structure, respectively. It can be seen that this problem is in the same format as analog precoder design problem in (3.23). Therefore, the analog combiner \mathbf{W}_{RF} can

Algorithm 4 Design of Hybrid Beamformers for OFDM-based SU-MIMO systems

Require: $\sigma^2, P, N, \mathbf{H}[n]$

- 1: Find \mathbf{V}_{RF} by solving the problem in (3.23) using Algorithm 1 in Chapter 2.
 - 2: Calculate $\mathbf{V}_D[n] = (\mathbf{V}_{\text{RF}}^H \mathbf{V}_{\text{RF}})^{-1/2} \mathbf{U}_e[n] \boldsymbol{\Gamma}_e[n]$ where $\mathbf{U}_e[n]$ and $\boldsymbol{\Gamma}_e[n]$ are defined as following (3.16).
 - 3: Find \mathbf{W}_{RF} by solving the problem in (3.31) using Algorithm 1 in Chapter 2.
 - 4: Calculate $\mathbf{W}_D[n] = \mathbf{J}[n]^{-1} \mathbf{W}_{\text{RF}}^H \mathbf{H}[n] \mathbf{V}_{\text{RF}} \mathbf{V}_D[n]$ where $\mathbf{J}[n]$ is defined as in (3.30).
-

be designed using the proposed algorithm in Section 3.4.1.

Note that the receiver design is based on the already designed transmitter. This implies that either a dedicated phase is required to feed forward the designed transmit beamformers to the receiver, or it is required that the receiver first solves the transmitter design problem and then solves the receiver design problem. In the former case, the extra radio communication resource is needed while in the latter case extra computation resource is needed at the receiver.

The summary of the overall proposed algorithm for the hybrid beamforming design to maximize the overall spectral efficiency in an OFDM-based large-scale SU-MIMO system is given in Algorithm 4. Assuming that the number of antennas at both ends are in the same range, i.e., $M_r = O(M_t)$, it can be shown the computational complexity of the overall algorithm is $O(NM_t^3)$.

Remark 3. So far in this chapter, it is assumed that the infinite resolution phase shifters are available at the transceivers. However, as discussed in the previous chapters, in practice the components required for such an accurate phase control may be costly [42]. This arises an interesting question of how to design the analog beamformers if only low resolution phase shifters are available; i.e., $\mathbf{V}_{\text{RF}}(i, j) \in \mathcal{G}$ and $\mathbf{W}_{\text{RF}}(i, j) \in \mathcal{G}$ where

$$\mathcal{G} = \{1, \omega, \omega^2, \dots, \omega^{2^b-1}\}, \quad (3.34)$$

$\omega = e^{j\frac{2\pi}{2^b}}$ and b is the number of bits in the resolution of phase shifters. This thesis has already addressed this problem in Chapter 2 for single-carrier system by quantizing the solution of the analog precoder element in (3.28) in each iteration to the closest point in \mathcal{G} . Since the preceding treatment essentially transforms the multi-carrier analog beamformer design problem to the format of analog precoder design problem for the single-carrier scenario, it is possible to use

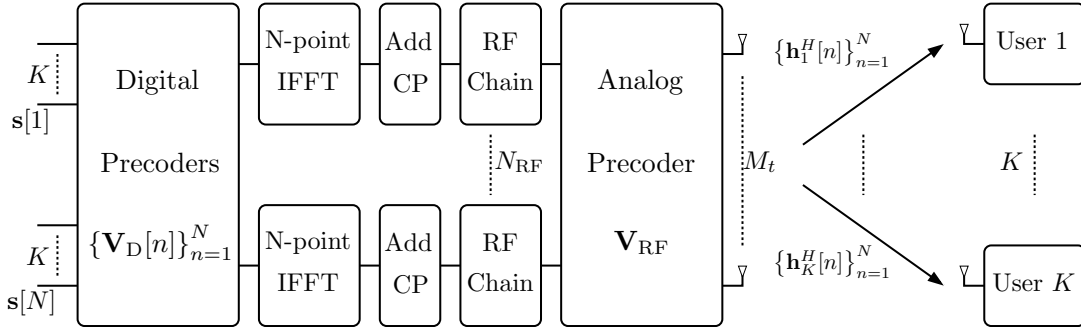


Fig. 3.3: A block diagram of a downlink OFDM-based MU-MISO system with hybrid analog and digital beamforming architecture at the BS.

the same technique.

3.5 Hybrid Precoding Design for MU-MISO

This chapter now considers the hybrid precoding design for a OFDM-based MU-MISO system in which a base station with M_t antennas and N_{RF} RF chains serves K non-cooperative single-antenna users. It is shown in [47] that hybrid beamforming with limited number of RF chains can approach the performance of fully digital beamforming only if the same set of users are scheduled to be served at the entire band for each time slot. This is because when the same users are served in the entire band, the channels of different subcarriers are highly correlated due to the sparse nature of mmWave channels. Accordingly, it is possible to design a common analog beamformer which is appropriate for all the channels. This is more spectrally efficient than the alternative of multiplexing users across the frequencies. For this reason, this section focuses on a MU-MISO design in which the same users are served over all subcarriers.

For such a system, the transmitted signal at subcarrier n is

$$\mathbf{x}[n] = \sum_{k=1}^K \mathbf{V}_{RF} \mathbf{v}_{D_k}[n] s_k[n], \quad (3.35)$$

where $\mathbf{V}_{RF} \in \mathbb{C}^{M_t \times N_{RF}}$ is the analog precoder, $\mathbf{v}_{D_k}[n] \in \mathbb{C}^{N_{RF} \times 1}$ is the digital precoder for user k at subcarrier n and $s_k[n] \in \mathbb{C}$ is the intended data symbol for user k at subcarrier n . Then, the user k receives $y_k[n] = \mathbf{h}_k^H[n] \mathbf{x}[n] + z_k[n]$, where $z_k[n]$ is the additive white Gaussian noise.

The rate expression in n^{th} subcarrier for user k can be expressed as

$$R_k[n] = \log_2 \left(1 + \frac{|\mathbf{h}_k^H[n] \mathbf{V}_{\text{RF}} \mathbf{v}_{D_k}[n]|^2}{\sigma^2 + \sum_{\ell \neq k} |\mathbf{h}_k^H[n] \mathbf{V}_{\text{RF}} \mathbf{v}_{D_\ell}[n]|^2} \right), \quad (3.36)$$

where $\mathbf{h}_k^H[n]$ is the channel of n^{th} subcarrier from the BS to the k^{th} user. Now, the hybrid precoding design problem for maximizing the weighted sum rate is

$$\max_{\mathbf{V}_{\text{RF}}, \{\mathbf{V}_D[n]\}_{n=1}^N} \frac{1}{N} \sum_{n=1}^N \sum_{k=1}^K \beta_k R_k[n] \quad (3.37a)$$

$$\text{s.t.} \quad \text{Tr} \left(\mathbf{V}_{\text{RF}} \mathbf{V}_D[n] \mathbf{V}_D[n]^H \mathbf{V}_{\text{RF}}^H \right) \leq P, \quad \forall n, \quad (3.37b)$$

$$|\mathbf{V}_{\text{RF}}(i,j)| = 1, \quad \forall (i,j) \in \mathcal{F}_t, \quad (3.37c)$$

in which $\mathbf{V}_D[n] = [\mathbf{v}_{D_1}[n], \dots, \mathbf{v}_{D_K}[n]]$ is the overall digital precoder at n^{th} frequency tone and the weight β_k represents the priority of k^{th} user; i.e., larger β_k implies greater priority for k^{th} user.

The problem of weighted sum rate maximization in (3.37) differs from the spectral efficiency maximization for the SU-MIMO systems in two respects. First, the users in MU-MISO scenario are not collocated which results in an inter-user interference term in the rate expression. Second, the different data streams corresponding to different users in a MU-MISO system may have different priority weights, while all the data streams in a SU-MIMO system always have the same priority weights.

These two differences make the analog precoding design much more complicated. In order to tackle the problem (3.37), this thesis proposes the following simple design strategy:

- First, design the analog precoder assuming that the users are cooperative and they have equal priority weights. Loosely speaking, this means that the common analog beamformer is designed to improve the direct channel of the all users while neglecting the effect of the inter-user interference and the different priority weights.
- Second, design the digital beamformers for the effective channel using one of the conventional fully digital beamforming schemes such as the WMMSE approach in [5] which can

manage both the inter-user interference effect and the different priority weights.

In particular, this thesis first considers designing the analog precoder by maximizing

$$\log_2 \left| \mathbf{I} + \frac{\gamma^2}{\sigma^2} \mathbf{V}_{\text{RF}}^H \mathbf{F}_1 \mathbf{V}_{\text{RF}} \right|, \quad (3.38)$$

where $\mathbf{F}_1 = \frac{1}{N} \sum_{n=1}^N (\mathbf{H}[n]^H \mathbf{H}[n])$ and $\mathbf{H}[n] = [\mathbf{h}_1[n], \dots, \mathbf{h}_K[n]]^H$ is the collection of channel vectors of all users at subcarrier n . It is clear that the analog precoder now can be designed using the proposed algorithm in Section 3.4. After designing the analog precoder, this thesis seeks to design the digital precoders using the iterative WMMSE approach which is summarized as follows:

1. Let $\mathbf{g}_k^H[n] = \mathbf{h}_k^H[n] \mathbf{V}_{\text{RF}}$ denote the effective channel for user k in subcarrier n . Initialize all digital precoders, $\mathbf{v}_{\text{D}_k}[n], \forall n, k$, such that the power constraints (3.37b) are satisfied.
2. Calculate the receiver combining filter for each user at each subcarrier as

$$w_k[n] = \frac{\mathbf{g}_k^H[n] \mathbf{v}_{\text{D}_k}[n]}{\sigma^2 + \sum_i |\mathbf{g}_k^H[n] \mathbf{v}_{\text{D}_i}[n]|^2}. \quad (3.39)$$

3. Calculate the mean square error (MSE) as

$$e_k[n] = \sum_i \left(|w_k[n] \mathbf{g}_k^H[n] \mathbf{v}_{\text{D}_i}[n]|^2 - 2 \operatorname{Re} \{ w_k^*[n] \mathbf{g}_k^H[n] \mathbf{v}_{\text{D}_i} \} \right) + |w_k[n]|^2 \sigma^2 + 1, \quad (3.40)$$

and then calculate $t_k[n] = \frac{1}{e_k[n]}$.

4. Design the digital precoder as

$$\mathbf{v}_{\text{D}_k}[n] = \beta_k t_k[n] w_k[n] (\mathbf{J}_k[n])^{-1} \mathbf{g}_k[n], \quad (3.41)$$

where

$$\mathbf{J}_k[n] = \sum_i \left(\beta_i t_i[n] |w_i[n]|^2 \mathbf{g}_i[n] \mathbf{g}_i^H[n] \right) + \lambda[n] \mathbf{V}_{\text{RF}}^H \mathbf{V}_{\text{RF}}, \quad (3.42)$$

and $\lambda[n]$ is the Lagrangian multiplier for subcarrier n which can be optimized based on Karush-Kuhn-Tucker (KKT) conditions [5].

5. Repeat the steps from 2 to 5 until the convergence.

Now, assuming that $\min\{N, M_t\} \gg N_{\text{RF}}$, it can be shown that the dominant term in computational cost is $O(NM_t^2)$ which corresponds to the calculation of the average of the sample covariance matrices of frequency domain channels, $\frac{1}{N} \sum_{n=1}^N (\mathbf{H}[n]^H \mathbf{H}[n])$. As a result, the overall computational complexity of the proposed hybrid beamforming algorithm is $O(NM_t^2)$.

It should be noted that the recent work in [47] also considers hybrid precoding design for weighted sum rate maximization in a OFDM-based MU-MISO system. The general algorithm in [47] uses the WMMSE technique to design the analog precoder as well as the digital precoders. The algorithm of [47] can only be applied to the setting where the total power constraint is considered,

$$\sum_n \text{Tr} \left(\mathbf{V}_{\text{RF}} \mathbf{V}_{\text{D}}[n] \mathbf{V}_{\text{D}}[n]^H \mathbf{V}_{\text{RF}}^H \right) \leq NP. \quad (3.43)$$

However, in practical systems it is desirable that the designed precoders satisfy a per subcarrier power constraint (3.37b). The reason that it is difficult to generalize the algorithm of [47] for the per subcarrier power constraint case is that in the analog precoder design step within WMMSE approach, multiple Lagrangian multipliers would arise, and the resulting optimization problem would be computationally difficult to solve. It should be noted that although the focus of this chapter is on hybrid beamforming design for power spectral density constraint, the proposed algorithm can be easily modified for the total power constraint scenario since it is possible to use WMMSE approach only to design digital precoders. It can be shown that this approach is more computationally efficient as compared to the algorithm in [47] since the analog beamformer in [47] needs to be updated in each iteration of WMMSE method and the expression of the analog beamformer involves a large dimension matrix inversion. Further, since the design of digital and analog precoders are decoupled in the proposed algorithm, when the analog precoder is fixed, other simpler linear beamforming approaches such as zero-forcing and maximum ratio transmission can be employed as the digital precoders to reduce the design complexity.

3.6 Numerical Results

This section presents numerical simulation results for both the asymptotic hybrid beamforming design presented in Section 3.3 and the proposed algorithms for SU-MIMO systems and MU-MISO systems presented in Section 3.4 and Section 3.5, respectively. In the simulations, this chapter considers the uniform linear array antenna configuration with half-wavelength antenna spacing. Further, unless otherwise mentioned, an environment with 5 clusters and 10 scatterers per cluster (as suggested by [89]) is considered in which the angles of arrival (departure) are generated according to Laplacian distribution with random mean cluster angels $\bar{\phi}_c^r \in [0, 2\pi)$ ($\bar{\phi}_c^t \in [0, 2\pi)$) and angular spreads of 10 degrees within each cluster. In simulations for SU-MIMO systems, the average spectral efficiency is plotted versus the number of antenna elements or the signal-to-noise-ratio per subcarrier, defined as $\text{SNR} = \frac{P}{\sigma^2}$, over 500 channel realizations as a performance metric.

3.6.1 Asymptotic Hybrid Beamforming Design Performance Analysis for SU-MIMO systems

The first experiment numerically investigates the performance of asymptotic hybrid beamforming design of Section 3.3 for large antenna arrays in different propagation environments. Here, this simulation considers an $M \times M$ SU-MIMO system with $\text{SNR} = 20\text{dB}$ and $N = 32$ subcarriers in which a transmitter with 4 RF chains sends $N_s = 4$ data streams per subcarrier to a receiver with 4 RF chains. To model the propagation environment, two scenarios are considered, single-scatterer per cluster and multi-scatterers per cluster. In Fig. 3.4(a) and Fig. 3.4(b), the performance of the asymptotic hybrid beamforming design is compared to that of the optimal fully digital beamforming by sweeping the number of antenna elements, M , in environments with $(N_c, N_{sc}) = (15, 1)$ and $(N_c, N_{sc}) = (5, 10)$, respectively. It can be seen in both cases that the achievable rate of asymptotic design converges to that of the fully digital beamforming for sufficiently large number of antennas. However, this convergence is faster in single-scatterer per cluster scenario. This is because in single-scatterer per cluster case the angle of arrivals (departures) are independent and hence the asymptotic orthogonality of the columns of receive (transmit) antenna array response matrix, \mathbf{A}_r (\mathbf{A}_t), is valid for smaller values of M .

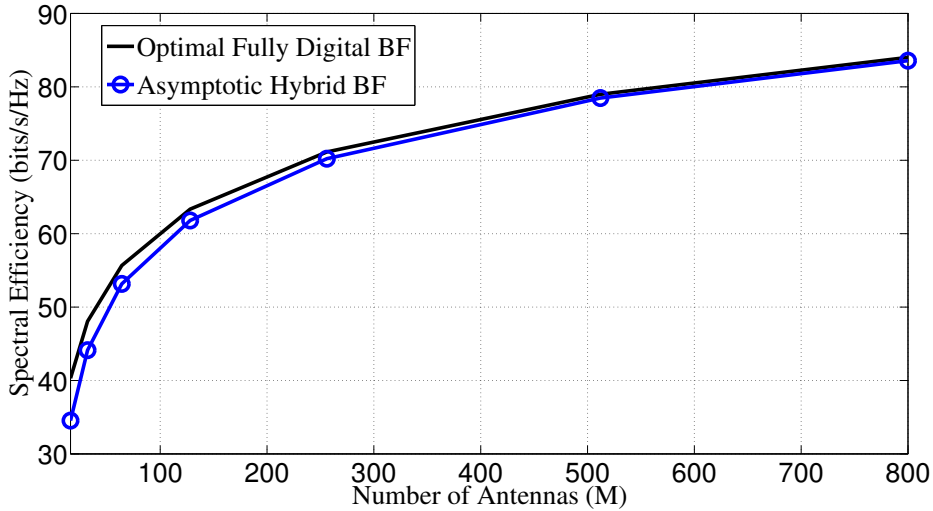
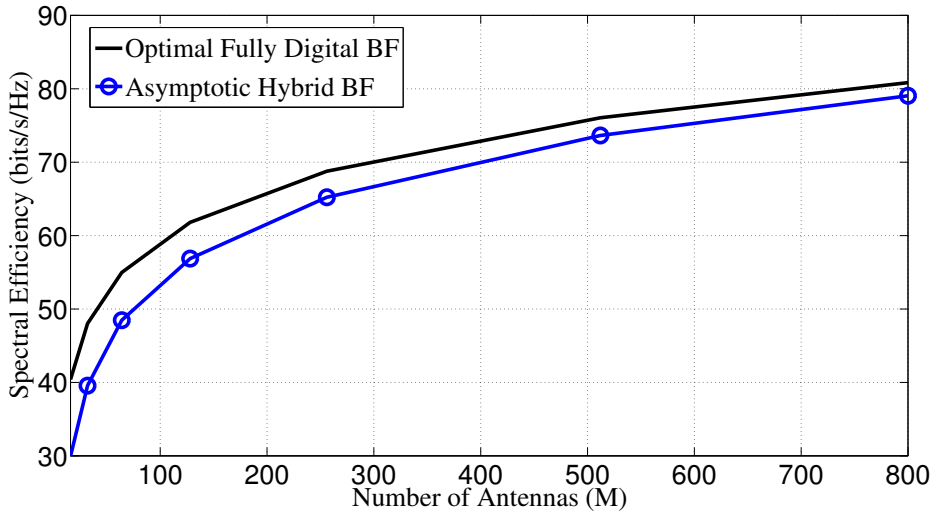
(a) mmWave channel model with $(N_c, N_{sc}) = (15, 1)$.(b) mmWave channel model with $(N_c, N_{sc}) = (5, 10)$.

Fig. 3.4: Comparison between the achievable rates of asymptotic design and the optimal fully digital beamforming for an $M \times M$ SU-MIMO system with $N_s = N_{RF} = 4$, $N = 32$ and SNR = 20dB.

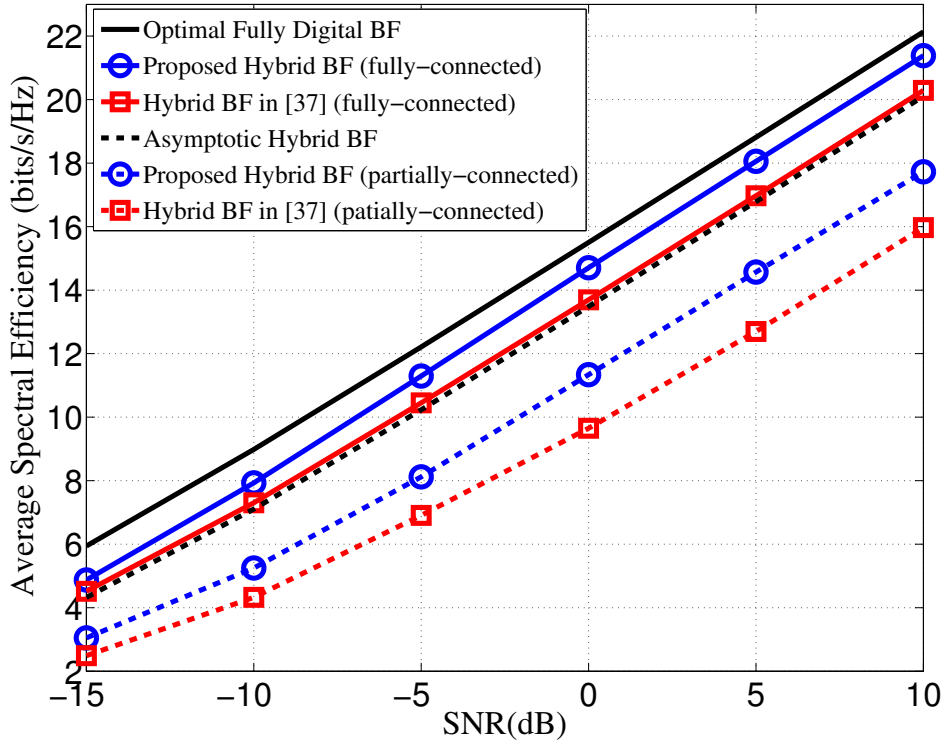


Fig. 3.5: Spectral efficiencies versus SNR of different methods for a 64×32 OFDM-based SU-MIMO system in which hybrid architecture with infinite resolution phase shifters is employed at both transceiver sides and $N_s = 2$, $N_{RF} = 4$, and $N = 64$.

3.6.2 Hybrid Beamforming Performance Analysis in SU-MIMO systems

The next experiment numerically evaluates the performance of the hybrid beamforming design presented in Section 3.4 for OFDM-based SU-MIMO systems in two different system settings:

SU-MIMO system with hybrid beamforming architecture at both transceiver sides

First, consider a 64×32 OFDM-based MIMO system with hybrid beamforming structure at both the transmitter and the receiver where $N_s = 2$, $N_{RF} = 4$ and $N = 64$. Fig. 3.5 shows that the proposed algorithm for both fully-connected and partially-connected structures achieves a higher spectral efficacy as compared to the hybrid beamforming design in [37] which seeks to minimize the distance of the optimal fully digital beamformers and the overall hybrid beamformers instead of tackling the original problem of spectral efficiency maximization directly. Fig. 3.5 also shows that the proposed fully-connected hybrid beamforming design with only

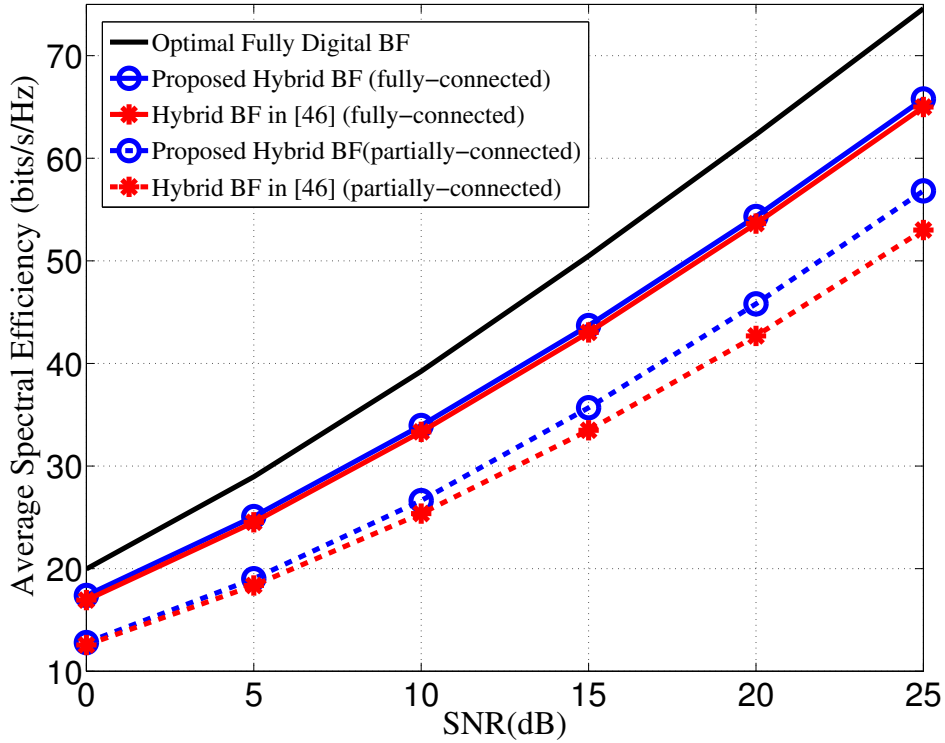


Fig. 3.6: Spectral efficiencies versus SNR of different methods for a 64×8 OFDM-based SU-MIMO system in which hybrid architecture with infinite resolution phase shifters is employed at the transmitter and $N_s = 8$, $N_{RF} = 8$, and $N = 64$.

4 transceiver RF chains can approach the performance of fully digital beamforming which is achieved by the optimal fully digital beamforming utilizing 64 and 32 RF chains at the transmitter and the receiver, respectively. Finally, Fig. 3.5 indicates that for the scenarios in which the number of antenna is not extremely large the proposed algorithm in Section 3.4 can achieve a better performance; about 2dB gain, in comparison with the asymptotic design of Section 3.3.

SU-MIMO system with hybrid beamforming architecture only at the transmitter side

The spectral efficiency maximization problem has been recently considered in [46] for the case that the hybrid beamforming architecture is employed only at the transmitter. In order to compare the performance of the proposed scheme with the algorithm in [46], this experiment considers a 64×8 SU-MIMO system with $N = 64$ subcarriers in which a transmitter with 8 RF

chains sends $N_s = 8$ data symbols per subcarrier to a receiver equipped with 8 RF chains so that the receiver can employ fully digital combining. Fig. 3.6 shows that the proposed algorithm for the partially-connected structure achieves a higher spectral efficiency as compared to the hybrid beamforming design in [46]. However, for the fully-connected case, the achievable rate of the proposed algorithm is very similar to that of the hybrid beamforming design in [46]. This is because [46] already utilizes the fact that for the fully-connected structure, the analog precoder should be designed according to the average of the sample covariance matrices of frequency domain channels, $\mathbf{F}_1 = \frac{1}{N} \sum_{n=1}^N (\mathbf{H}[n]^H \mathbf{H}[n])$. In particular, the algorithm in [46] first finds the set of eigenvectors of \mathbf{F}_1 corresponding to the N_{RF} largest eigenvalues and then sets the columns of analog precoder to the phase of that eigenvectors. It can be seen that without the hybrid constraint, the optimal solution to the proposed analog precoder design problem in (3.23) is also the eigenvectors of \mathbf{F}_1 . Therefore, it is expected that the algorithm in [46] approaches the performance of the proposed algorithm for the cases that fully-connected hybrid architecture with infinite resolution phase shifters is employed at the transmitter.

The next experiment considers the same system parameters as the previous experiment except it is assumed that very low resolution phase shifters are employed at the transmitter, $b = 1$. Fig. 3.7 shows that the proposed algorithm achieves higher performance, i.e., about 1dB, compared to the algorithm in [46] for such a scenario. In overall, the proposed algorithm proposed by this thesis for fully-connected structure has two advantages over the algorithm in [46]: i) The proposed algorithm provides hybrid combining design as well as hybrid precoding design while the algorithm in [46] only considers hybrid precoding design with a fully digital receiver. ii) The performance degradation in hybrid precoding without full degree of freedom, i.e., when the partially-connected structure is used or when low resolution phase shifters are employed, is greater for the algorithm in [46] as compared to the proposed method.

3.6.3 Hybrid Beamforming Performance Analysis in MU-MISO systems

Finally, this part considers a single-cell downlink scenario in which a base station with 64 antennas serves users from 10 different clusters in which the users in the same cluster share the same transmit antenna channel response vectors but have different complex channel gains and pathloss. For the following simulations, it is assumed that many users are randomly and

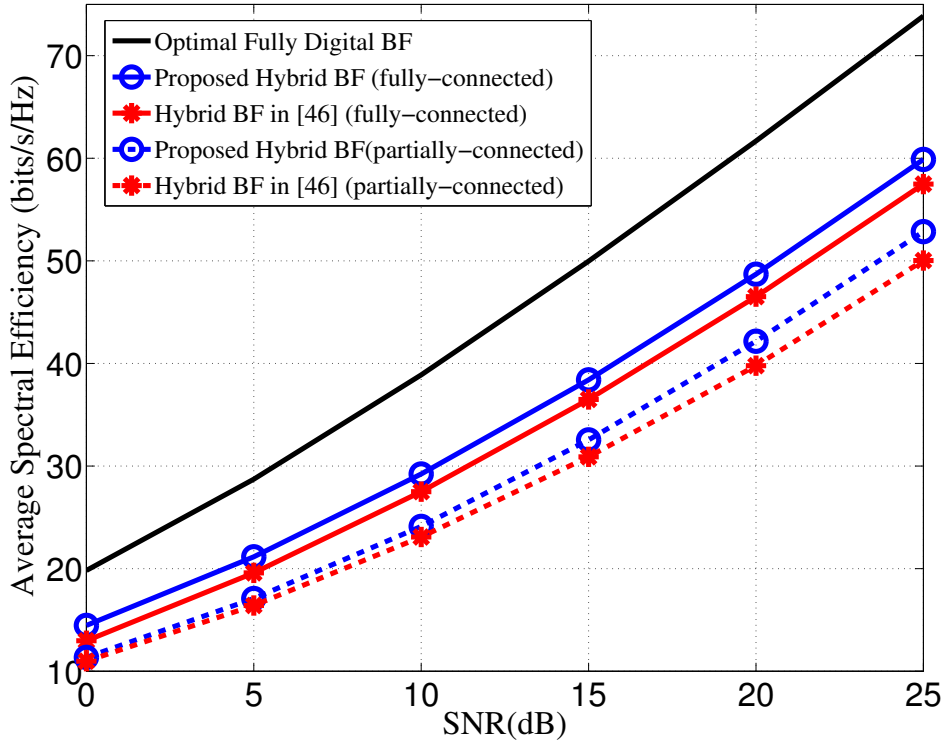


Fig. 3.7: Spectral efficiencies versus SNR of different methods for a 64×8 OFDM-based SU-MIMO system in which hybrid architecture with 1-bit resolution phase shifters is employed at the transmitter and $N_s = 8$, $N_{RF} = 8$, and $N = 64$.

uniformly located in a circular coverage area of radius $R = 0.2\text{km}$. At each time slot, $K = 4$ users are randomly scheduled to be served over the entire band of 32 MHz with 32 subcarriers. Further, it is assumed that the pathloss for a user with distance \bar{d} to the base station is modeled as $128.1 + 37.6 \log_{10}(\bar{d})$. Note that the random scheduling of the users implies that there is a possibility that in each time slot some scheduled users are from the same cluster, or they can be from different clusters. Scheduling users from the same cluster can be useful for increasing the intended signal power since the analog beamformer can be matched to the similar channel response vectors of those users, but this also implies higher inter-user interference. Therefore, it is not straightforward to see whether scheduling users from the same cluster is beneficial for rate maximization or not. This thesis leaves the optimization of user scheduling for the future work and assumes the simple uniformly random scheduling.

The first experiment of this part assumes that the priority weight of each user is set to be

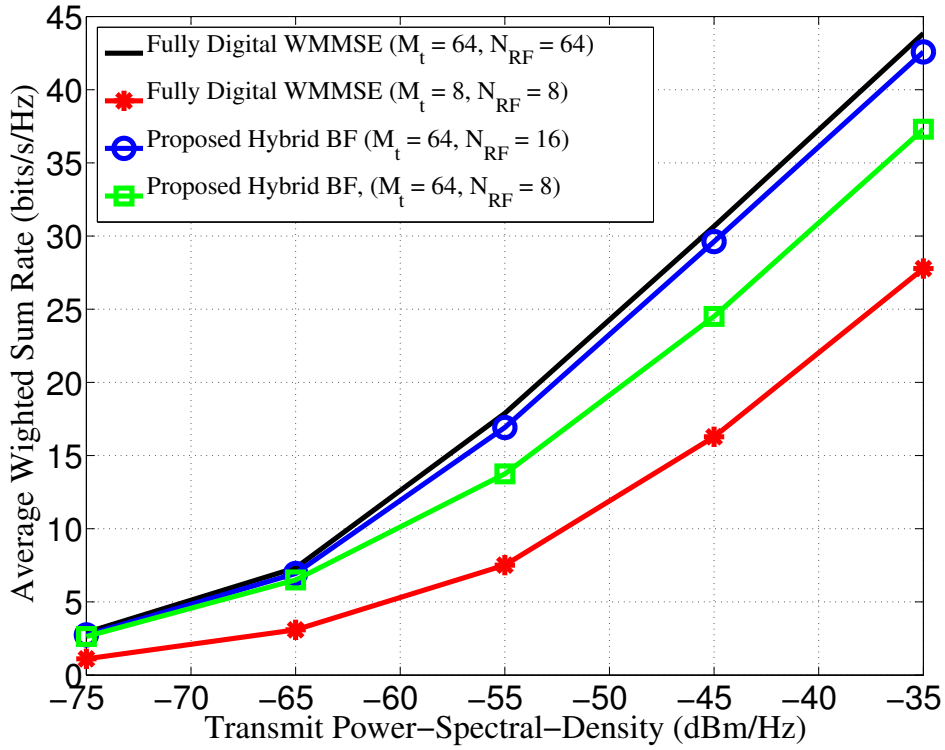


Fig. 3.8: Weighted sum rate versus transmit power spectral density for different methods in an OFDM-based MU-MISO system with $K = 4$, $M_t = 64$, and $N = 32$.

proportional to the inverse of the expected rate of that user when the transmitted power spectral density is -55 dBm/Hz. Further, the power spectral density of the noise is considered to be -139 dBm/Hz. Fig. 3.8 plots the average weighted sum rate for the proposed hybrid beamforming algorithm with different number of RF chains and the fully digital WMMSE algorithm in [5] for different number of antennas. It can be seen that the proposed hybrid beamforming algorithm with 64 antennas and 8 RF chains achieves much higher spectral efficiency as compared to the fully digital WMMSE beamforming utilizing 8 antennas and 8 RF chains. This means that using large-scale antenna arrays can be very beneficial even if the number of available RF chains is limited. Fig. 3.8 also shows that the proposed hybrid beamforming design with 16 RF chains approach the performance of the fully digital WMMSE beamforming with 64 antennas.

The second experiment considers a more practical setup in which the priority weight of each user is adapted over many iterations by setting it to be proportional to the inverse of the experimentally average rate achieved so far. The power spectral densities of the transmitted

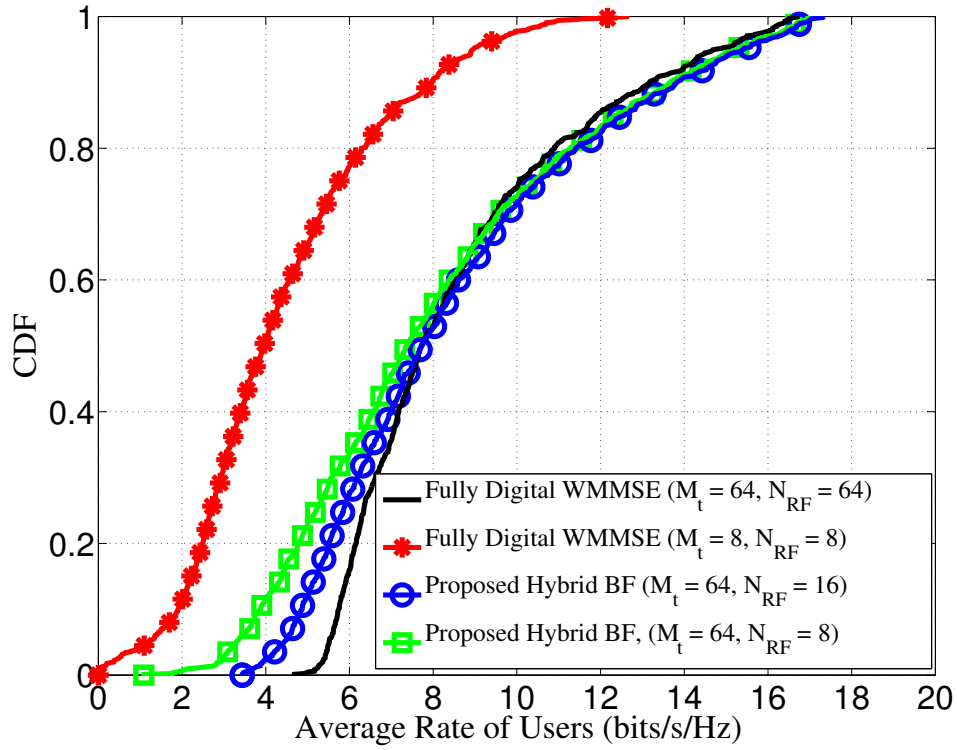


Fig. 3.9: Empirical CDF of the average rate of the users for different methods in an OFDM-based MU-MISO system with $K = 4$ and $N = 32$.

signals and the noise are set to be -45 dBm/Hz and -139 dBm/Hz, respectively. The other parameters are similar to the previous experiment. Fig. 3.9 plots the empirical cumulative distribution function (CDF) of the average rate achieved by the cell users. Fig. 3.9 indicates that the proposed hybrid beamforming strategy with both $N_{\text{RF}} = 8$ and $N_{\text{RF}} = 16$ can approximately achieve the same sum rate as the fully digital WMMSE approach with $M_t = 64$ antennas and $N_{\text{RF}} = 64$ RF chains. However, it can be seen from Fig. 3.9 that the lower 40-percentile users still achieve better rates in fully digital WMMSE beamforming scheme while the other higher 60-percentile users achieve slightly better rates in the proposed hybrid beamforming design. This is because of the fact that the proposed analog precoder is designed for maximizing the sum rate, hence it may favor high rate users at the expense of low rate users.

3.7 Summary

This chapter considers hybrid beamforming design for OFDM-based systems with large-scale antenna arrays. This chapter first shows that the hybrid beamforming architecture is an appropriate scheme for broadband mmWave systems with frequency-selective channels. In particular, for SU-MIMO systems, it is shown that the hybrid structure can asymptotically realize the optimal fully digital beamforming for sufficiently large number of antennas. Then, for practical number of antennas, this chapter proposes a unified heuristic algorithm for designing the hybrid precoders and combiners for two well-known architectures: fully-connected and partially-connected hybrid beamforming. Finally, this chapter generalizes the proposed algorithm for designing the hybrid beamforming in the downlink of a MU-MISO system. The simulation results verify that the proposed algorithms can achieve a better performance as compared to the existing methods for both architectures. Further, it is shown that the proposed designs for the fully-connected architecture can approach the performance of the fully digital beamforming baselines with a reasonable number of RF chains, which is typically much less than the number of antennas.

Chapter 4

One-Bit Precoding for Rich-Scattering Channels

4.1 Chapter Organization

The previous two chapters introduce the hybrid beamforming architecture in which only few high resolution RF chains are employed for reducing the power consumption at the terminals with large antenna arrays. However, in practice, it is possible to find scenarios in which employing many low resolution RF chains leads to less power consumption as compared to employing few high resolution RF chains [90]. Further, the results in Chapter 3 for hybrid beamforming architecture in environments with frequency-selective channels are restricted to the mmWave frequencies in which the channels are sparse; in general the hybrid structure does not provide a good performance in frequency-selective rich-scattering channels [63].

To address the above difficulties of hybrid beamforming architecture, this chapter proposes an alternative 1-bit precoding architecture in which each antenna has one dedicated RF chain but only a 1-bit resolution DAC is employed in each RF chain circuitry. Section 4.2 introduces the architecture of 1-bit precoding in more details. Further, Section 4.2 presents the problem of interest in this thesis for 1-bit precoding, namely, precoder design problem for a downlink MU-MISO system in order to minimize the average SER assuming QAM signalling. For such a system, Section 4.2 recognizes that precoding needs to be performed on a symbol-by-symbol

basis, hence, the 1-bit precoding design problem falls into the symbol-level precoding paradigm. Moreover, Section 4.2 recognizes that it is crucial to design the QAM constellation range for each channel realization in order to perform 1-bit precoding for each symbol of the designed QAM constellation with reasonable accuracy.

Section 4.3 drives a tight expression for the SER of a QAM constellation in symbol-level precoding scheme. This expression shows that for symbol-level precoding in which the noiseless received signal may not line up exactly with the intended constellation symbol, the effective minimum distance for a symbol in the QAM constellation is reduced. This minimum distance reduction is equal to twice the distance between the noiseless received signal and the intended signal of the QAM constellation.

The next parts of this chapter seek to design the QAM constellation range as well as the precoder in 1-bit precoding architecture in order to minimize the SER expression derived in Section 4.3. In order to gain some intuition on how to do so for multi-user scenario, this chapter begins with single-user case. Section 4.4 considers QAM constellation range design problem for single-user scenario. Based on the intuition gained from the case that the infinite resolution DACs are available, Section 4.4 proposes to design the constellation range such that all the points in the QAM constellation can be constructed accurately with the 1-bit precoder. The numerical result of Chapter 4.4 shows that a reasonable choice for the QAM constellation range for 1-bit precoding should be about $\sqrt{2/\pi} \approx 0.8$ times the optimal constellation range in infinite resolution case with instantaneous power constraint.

Section 4.5 considers single-user 1-bit precoder design problem for the already designed QAM constellation range. In order to tackle this combinatorial problem, Section 4.5 proposes a low-complexity two-step algorithm. Inspired by the fact that 1-bit precoder can realize the constellation points closer to the origin of the complex plane more accurately, the first step of the proposed algorithm seeks to iteratively design the transmitted signal at each antenna such that the residual signal to be constructed is as close as possible to the origin. The first step of the algorithm repeats this procedure until the transmitted signal of all the antennas except last few are designed. The second step of the proposed algorithm then performs an exhaustive search in order to determine the best configuration for the transmitted signals of those remaining antennas.

Section 4.6 considers the constellation range and the 1-bit precoding design problem for multi-user case. To design the constellation range, this section first considers the availability of the infinite resolution DACs. Under this assumption, Section 4.6 proposes a QAM constellation range design which suggests that the constellation range for the multi-user case is that of the single-user case multiplied by a factor. Section 4.6 then proposes to further reduce the constellation range in 1-bit precoding by a factor of $\sqrt{2/\pi} \approx 0.8$. Section 4.6 also generalizes the aforementioned two-step algorithm for 1-bit precoding design in Section 4.4 to the multi-user case. Finally, Section 4.6 analytically studies the performance of the proposed design. In particular, it shows that there is about 2dB gap between the performance of the proposed 1-bit precoding design and infinite resolution precoding under the same per-symbol power constraint.

Section 4.7 provides the numerical results to investigate the performance of the proposed designs for single-user and multi-user scenarios. For both scenarios, Section 4.7 first shows that the proposed QAM constellation range design for 1-bit precoding is a reasonable choice. Second, Section 4.7 numerically studies the performance of the proposed design as compared to the infinite resolution precoding and shows that the proposed 1-bit precoding can typically achieve the promised performance with 2dB gap to the infinite resolution precoding scheme.

At the end, Section 4.8 provides the summary of this chapter.

4.2 System Model

Consider the downlink of a MU-MISO system in which a BS with large number of antennas, M , serves K single-antenna users. For such a system, the received signal at user k can be modelled as

$$y_k = \sqrt{\frac{P}{M}} \mathbf{h}_k^H \mathbf{x} + z_k, \quad (4.1)$$

where $\mathbf{h}_k \in \mathbb{C}^{M \times 1}$ is the vector of channel gains to user k , $\mathbf{x} \in \mathbb{C}^{M \times 1}$ is the transmitted signal, $z_k \sim \mathcal{CN}(0, 2\sigma^2)$ is the additive white Gaussian noise, and P is the total transmit power budget.

As discussed earlier in the previous chapters, one dedicated high resolution RF chains per antenna element is required in the conventional fully digital beamforming schemes for constructing the transmitted signal, \mathbf{x} . This potentially leads to high power consumption at the terminals with large-scale antenna arrays. The previous chapters aim to introduce the hybrid

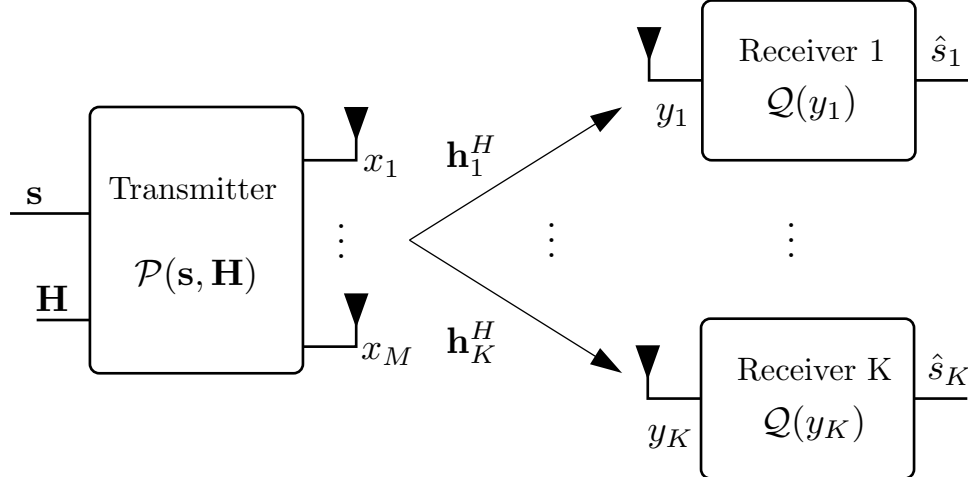


Fig. 4.1: A MU-MISO system with symbol-level precoding.

beamforming scheme in order to reduce the number of RF chains to reduce this high power consumption. Motivated by the fact that the power consumption of DACs employed in the RF chains grows exponentially with the number of quantization bits [21, 22], this chapter considers an alternative architecture with low resolution DACs for the large-scale arrays. In particular, this chapter seeks to design the transmitted signal when one-bit DACs are employed at each antenna element of the BS. This means that the transmitted signal \mathbf{x} must come from a finite alphabet, i.e., $\mathbf{x} \in \mathcal{X}^M$, where

$$\mathcal{X} = \left\{ \frac{1}{\sqrt{2}}(\pm 1 \pm i) \right\}, \quad (4.2)$$

where i is the imaginary unit satisfying $i^2 = -1$. In order to focus on the impact of 1-bit precoding, this chapter assumes that the full CSI is available at the transmitter.

In conventional infinite resolution precoding, the transmitted signal is designed as a product of a beamforming vector and the symbol constellation point. This is not possible to do when the transmitted signal must come from a low resolution alphabet. This chapter considers instead a symbol-level precoding scheme, in which the BS designs the M -dimensional precoded transmitted signal directly on a symbol-by-symbol basis as a function of the instantaneous CSI, $\mathbf{H} = [\mathbf{h}_1, \dots, \mathbf{h}_K]^H$, and the intended constellation point, $\mathbf{s} = [s_1, \dots, s_K]$, as

$$\mathbf{x} = \mathcal{P}(\mathbf{s}, \mathbf{H}), \quad (4.3)$$

where the function $\mathcal{P} : \mathbb{C}^M \times \mathbb{C}^{K \times M} \rightarrow \mathcal{X}^M$ represents the precoder.

At the receiver side, we do not assume the availability of the CSI since obtaining all the channel coefficients at single antenna receivers requires a long training phase which is typically not feasible due to the limited coherence time of the channel. Instead, we assume that in each coherence time of the channel, the constellation range and the constellation size are fed back to the users such that each user seeks to recover its intended symbol, s_k , from its received signal, y_k , by mapping y_k to its nearest constellation point, i.e., $\hat{s}_k = \mathcal{Q}(y_k)$. The overall system model is shown in Fig. 4.1. Note that the concept of symbol-level precoding is considered in the earlier works [24–27] for the infinite-resolution case—it is adopted for the finite-resolution DAC context considered in this paper. We note here that symbol-level precoding requires transmit beamforming adaptation at the symbol rate, rather than at the timescale of channel coherence time as in the case of traditional beamforming. This translates to significantly more demanding transmit processing speed requirement.

This chapter restricts attention to uncoded QAM constellations and also explicitly designs the constellation range for one-bit symbol-level precoding. In particular, this chapter uses N^2 -QAM constellations with the range of c in each dimension and the minimum distance of $d = \frac{c}{N-1}$; an example for $N = 4$ is depicted in Fig. 4.2. In this chapter, a block-fading channel model is assumed in which the channel stays constant for at least hundreds of symbol transmissions so that the constellation range c and the constellation size N only need to be communicated to the receiver as preamble on a per-fading-block basis. It is emphasized that this thesis considers the adaptation of the constellation range to the channel state information only, while the number of constellation points are assumed to be fixed. A complete adaptive modulation scheme in which both the constellation range and the number of constellation points are jointly optimized can be considered as future work. We also emphasize that the techniques presented in this thesis pertain to uncoded transmission only. A complete characterization of the capacity and the optimal transmission strategy for the finite-resolution-input massive MIMO channel is still an open problem.

In general, for the multi-user scenario, different constellations can be designed for different users. However, similar to the references in [69, 70], this chapter considers a simplified problem in which the symbols of all users come from the same constellation. This assumption may

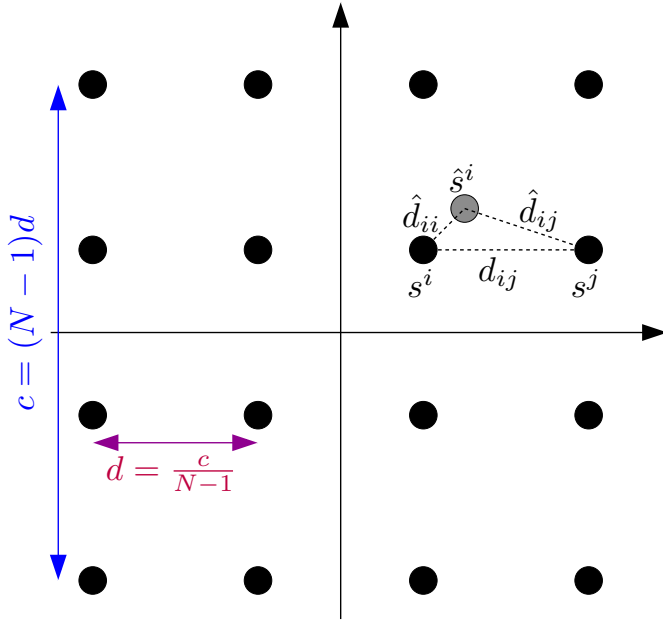


Fig. 4.2: An example of N^2 -QAM constellation for $N = 4$.

force the users with strong channels to operate below their actual capacities, but such fairness concern can be addressed by an intelligent scheduler that groups users with similar channels within each time-frequency slot. For this reason, the rest of this chapter assumes that all users have the same pathloss and shadowing, i.e.,

$$\mathbf{h}_k \sim \mathcal{CN}(\mathbf{0}, \mathbf{I}), \quad \forall k. \quad (4.4)$$

The problem of interest in this chapter is to design the QAM constellation range in each coherence time of the channel, and then design the transmitted signal corresponding to each symbol vector where each element of that symbol vector is chosen from the designed constellation in order to minimize the average symbol error rate. The proposed constellation range design for the multi-user scenario is based on the i.i.d Rayleigh fading channel model in which a similar pathloss and shadowing is assumed for all the users. Generalizing this design for other channel models require further efforts and it can be considered as a future work.

4.3 SER Characterization for Symbol-Level Precoding

This section provides an SER expression of a generic user in a MU-MISO system with symbol-level precoding described in Section 4.2. In order to avoid encumbering the notation, the user index, k is dropped, in the notations throughout this section.

Let this thesis assume that the intended constellation point for the considered receiver is s^i .

Due to the finite resolution DAC constraint in one-bit precoding, the noiseless received signal, i.e.,

$$\hat{s}^i = \sqrt{\frac{P}{M}} \mathbf{h}^H \mathbf{x}_i, \quad (4.5)$$

may not exactly coincide with the intended constellation point. In this case, the received signal is $y = \hat{s}^i + z$ and the pairwise error probability, $\Pr(s^i \rightarrow s^j)$, can be written as

$$\begin{aligned} \Pr(s^i \rightarrow s^j) &\stackrel{\Delta}{=} \Pr(|y - s^i| \geq |y - s^j|) \\ &\stackrel{(a)}{=} \Pr(|\hat{s}^i + z - s^i|^2 \geq |\hat{s}^i + z - s^j|^2) \\ &\stackrel{(b)}{=} \Pr\left(\operatorname{Re}\{\tilde{z}\} \geq \frac{|\hat{s}^i - s^j|^2 - |\hat{s}^i - s^i|^2}{2|s^i - s^j|}\right) \\ &\stackrel{(c)}{=} Q\left(\frac{\hat{d}_{ij}^2 - \hat{d}_{ii}^2}{2d_{ij}\sigma}\right), \end{aligned} \quad (4.6)$$

where $Q(u) = \frac{1}{\sqrt{2\pi}} \int_u^\infty e^{-\frac{v^2}{2}} dv$, $\tilde{z} = ze^{i\angle(s^j - s^i)^\dagger}$ is a Gaussian random variable with the same distribution as z , i.e., $\tilde{z} \sim \mathcal{CN}(0, 2\sigma^2)$, $\hat{d}_{ij} \stackrel{\Delta}{=} |\hat{s}^i - s^j|$, and $d_{ij} \stackrel{\Delta}{=} |s^i - s^j|$. In the above equations, (a) is obtained by substituting $y = \hat{s}^i + z$, (b) is obtained by defining $\tilde{z} = ze^{i\angle(s^j - s^i)^\dagger}$ and rearranging the inequality for \tilde{z} , and (c) is based on the definition of the Q -function.

Similar to the conventional SER analysis for a reasonable SNR range [91], the pairwise probability error of the closest neighbouring constellation points in (4.6) can be used to tightly approximate the overall SER as

$$\text{SER} \approx \frac{1}{N^2} \sum_i \sum_{j \in \bar{\mathcal{N}}_i} Q\left(\frac{\hat{d}_{ij}^2 - \hat{d}_{ii}^2}{2d_{ij}\sigma}\right), \quad (4.7)$$

where $\bar{\mathcal{N}}_i$ is the set of nearest constellation points to s^i .

The expression in (4.7) is complicated and is difficult to use as a metric to design the

constellation range. As a result, this thesis seeks to find an upper-bound for the expression in (4.7). As it can be seen from Fig. 4.2, \hat{d}_{ii} , \hat{d}_{ij} , and d_{ij} can be considered as three edges of a triangular and hence by using the triangular inequality, it is possible to write

$$\frac{\hat{d}_{ij}^2 - \hat{d}_{ii}^2}{2d_{ij}} = \frac{(\hat{d}_{ij} + \hat{d}_{ii})(\hat{d}_{ij} - \hat{d}_{ii})}{2d_{ij}} \quad (4.8a)$$

$$\geq \frac{(d_{ij})(d_{ij} - 2\hat{d}_{ii})}{2d_{ij}} \quad (4.8b)$$

$$= \frac{d_{ij} - 2\hat{d}_{ii}}{2}. \quad (4.8c)$$

Now, using that $Q(\cdot)$ is a decreasing function and $d_{ij} = d$ for all $j \in \bar{\mathcal{N}}_i$ where d denotes the minimum distance in the considered QAM constellation, we can write the following upper-bound on the SER expression in (4.7) as:

$$\text{SER} \lesssim \sum_i \frac{g_i}{N^2} Q\left(\frac{d - 2\hat{d}_{ii}}{2\sigma}\right), \quad (4.9)$$

where g_i is the number of minimum distance neighbours of the symbol s^i .

The rest of this chapter first considers designing the constellation range and the non-linear precoder for the single-user scenario, $K = 1$, by minimizing the expression (4.9), then generalizes the proposed design to the multi-user case.

4.4 Constellation Range Design for Single-User Scenario

This section proposes an appropriate choice of constellation range, c , for 1-bit symbol-level precoding under a fixed MISO channel serving a single user. In order to gain insight on how to design c for 1-bit precoding, this section first considers designing the constellation range of symbol-level precoding with infinite resolution DACs under instantaneous per-symbol total power constraint across the antennas, and also under per-antenna power constraint. The instantaneous per-symbol power constraint refers to that each precoded symbol needs to satisfy a power constraint (instead of the average power across multiple symbols.)

4.4.1 Infinite Resolution Precoding with Total Power Constraint

Under symbol-level precoding, the transmit signal is designed as a function of the constellation point and the instantaneous channel realization. The range of the QAM constellation is an important parameter that needs to be designed to optimize performance. Assuming an N^2 -QAM and using the expression (4.9) as the metric for minimizing the SER with $d = \frac{c}{N-1}$ and $\hat{d}_{ii} = \left| \sqrt{\frac{P}{M}} \mathbf{h}^H \mathbf{x}_i - s^i \right|$, the problem of optimizing the constellation range for symbol-level precoding with infinite resolution precoding and with instantaneous (i.e., per-symbol) total power constraint can be written as

$$\min_{c \geq 0} \sum_{i=1}^{N^2} \frac{g_i}{N^2} \min_{\|\mathbf{x}_i\|_2^2 \leq M} Q \left(\frac{\frac{c}{N-1} - 2 \left| \sqrt{\frac{P}{M}} \mathbf{h}^H \mathbf{x}_i - s^i \right|}{2\sigma} \right). \quad (4.10)$$

With infinite resolution on \mathbf{x}_i , the optimal solution \mathbf{x}_i of the inner minimization problem of (4.10) for any given c is

$$\mathbf{x}_i = \frac{\sqrt{M} \mathbf{h}}{\|\mathbf{h}\|_2} \min \left\{ 1, \frac{|s^i|}{\sqrt{P} \|\mathbf{h}\|_2} \right\} e^{\imath \angle s^i}. \quad (4.11)$$

Intuitively, the optimal \mathbf{x}_i is to match the channel. With infinite resolution on \mathbf{x}_i , the precoded signal can reconstruct s^i perfectly as long as

$$|s^i| \leq \sqrt{P} \|\mathbf{h}\|_2. \quad (4.12)$$

By substituting this solution for all \mathbf{x}_i in (4.10) and taking some simple algebraic steps, the problem (4.10) for designing c can be rewritten as

$$\min_{c \geq 0} \sum_i \frac{g_i}{N^2} Q \left(\frac{\frac{c}{N-1} - 2 \max \left\{ 0, |s^i| - \sqrt{P} \|\mathbf{h}\|_2 \right\}}{2\sigma} \right). \quad (4.13)$$

In (4.13), the Q-function can be accurately approximated by $Q(x) \approx \frac{1}{12} e^{-\frac{x^2}{2}} + \frac{1}{4} e^{-\frac{2}{3}x^2}$, $x > 0$ [92]. This exponential relation between the output of the Q-function and its argument suggests that the value of the objective function in (4.13) is dominated by the error probability of

symbols which result in the smallest argument of the Q -function. Further, since $Q(\cdot)$ is a decreasing function, the smallest argument occurs for the furthest constellation points which have the maximum $|s^i|$, i.e., $\max_i |s^i| = \frac{c}{\sqrt{2}}$. Therefore, it is desirable to consider designing the constellation range such that the argument of the Q -function for those furthest constellation points is maximized, i.e.,

$$\max_{c \geq 0} \left\{ \frac{c}{N-1} - 2 \max \left\{ 0, \frac{c}{\sqrt{2}} - \sqrt{P} \|\mathbf{h}\|_2 \right\} \right\}. \quad (4.14)$$

The objective function of (4.14) is a piecewise linear function of c and the optimal solution of that, $c_{\text{inf},t}^*$, can be calculated as

$$c_{\text{inf},t}^* = \sqrt{2P} \|\mathbf{h}\|_2. \quad (4.15)$$

This result has the following interpretation. As mentioned earlier, with infinite resolution symbol-level precoding under instantaneous total power constraint, it is possible to construct any point in the complex plane inside a circle centered at the origin of the complex plane with radius $\sqrt{P} \|\mathbf{h}\|_2$ exactly as the noiseless received signal. The $\sqrt{2}$ factor comes from the fact that the distance of the furthest constellation point from the origin is $\frac{c}{\sqrt{2}}$. The expression in (4.15) suggests that the range of the constellation, c , should be increased as much as possible subject to the constraint that the furthest constellation point can be constructed by symbol-level precoding. In other words, the furthest constellation points should be designed to be at the distance of $\sqrt{P} \|\mathbf{h}\|_2$ from the origin.

The constellation range in (4.15) is a function of the channel realization, \mathbf{h} . This means that $c_{\text{inf},t}^*$ should adapt to the realization of the channel in each coherence time. However, for large-scale antenna arrays, it is possible to show that $\|\mathbf{h}\|_2$ can be well approximated by a constant \sqrt{M} . This phenomenon, called channel hardening in massive MIMO literature [72], suggests that for large M this thesis can approximate

$$c_{\text{inf},t}^* \xrightarrow{M \rightarrow \infty} \sqrt{2PM}, \quad (4.16)$$

without significant performance degradation. By this design, the constellation range is a func-

tion of the pathloss only and not specific Rayleigh fading component of \mathbf{h} .

4.4.2 Infinite Resolution Precoding with Per-Antenna Power Constraint

This section eventually considers a one-bit precoder for which every antenna has the same transmit power, so as an intermediate step, it is worth considering infinite resolution precoding with per-antenna power constraint rather than total power constraint. In this case, the transmitted signal of each antenna should satisfy $|x_m| \leq 1$ for all m .

Fixing \mathbf{h} , it is possible to show that the complex numbers that can be realized with $\sqrt{\frac{P}{M}}\mathbf{h}^H\mathbf{x}$ under the constraints $|x_m| \leq 1, \forall m$, are exactly all the points inside a circle centered at the origin of the complex plane, but with a reduced radius as compared to the total power constraint case. To show this, let us consider the following optimization problem:

$$\min_{|x_m| \leq 1, \forall m} \left| \sqrt{\frac{P}{M}}\mathbf{h}^H\mathbf{x} - s \right|. \quad (4.17)$$

The optimal solution for \mathbf{x} in (4.17) is given as

$$x_m = \min \left\{ \sqrt{\frac{M}{P\|\mathbf{h}\|_1}}|s|, 1 \right\} e^{i(\angle h_m + \angle s)}, \quad \forall m, \quad (4.18)$$

where h_m is the m^{th} element of the channel vector, \mathbf{h} . Now by substituting (4.18) into the objective function in (4.17), it can be seen that only for complex numbers s inside a circle of $|s| \leq \sqrt{\frac{P}{M}}\|\mathbf{h}\|_1$, it is possible to realize s exactly. The radius of this circle can be denoted by

$$r^* = \sqrt{\frac{P}{M}}\|\mathbf{h}\|_1. \quad (4.19)$$

This thesis remarks that r^* is also the largest range of $\sqrt{\frac{P}{M}}\mathbf{h}^H\mathbf{x}$, i.e.,

$$r^* = \max_{|x_m| \leq 1, \forall m} \left| \sqrt{\frac{P}{M}}\mathbf{h}^H\mathbf{x} \right|. \quad (4.20)$$

This interpretation will be useful in the constellation range design for 1-bit precoding.

Using a similar argument as in Section 4.4.1, it can now be shown that the optimal con-

stellation range for minimizing the SER is the largest constellation range such that all the constellation points can be constructed accurately. Therefore, the furthest constellation point, which is at the distance $\frac{c}{\sqrt{2}}$ for a square constellation, should be at a distance r^* from the origin, yielding that the optimal constellation range is given by

$$c_{\text{inf,p}}^* = \sqrt{\frac{2P}{M}} \|\mathbf{h}\|_1. \quad (4.21)$$

For the considered channel model in which each element of the channel vector has an i.i.d Gaussian distribution, i.e., $h_j \sim \mathcal{CN}(0,1)$, we have $\mathbb{E}\{|h_j|\} = \sqrt{\pi/4}$. Now, using the law of large number in the large-scale antenna array limit when $M \rightarrow \infty$, we can write $\frac{\|\mathbf{h}\|_1}{M} \rightarrow \sqrt{\pi/4}$. Therefore, in systems with massive antenna arrays, it is possible to approximate $\frac{\|\mathbf{h}\|_1}{\sqrt{M}}$ as $\sqrt{(\pi/4)M}$. This result can be used to further simplify the constellation range expression in (4.21) as

$$c_{\text{inf,p}}^* \xrightarrow{M \rightarrow \infty} \sqrt{\pi/4} \sqrt{2PM}. \quad (4.22)$$

Now, it can be seen from (4.16) and (4.22) that the ratio between the constellation ranges in infinite-resolution precoding under total power constraint and under per-antenna power constraint in the massive MIMO limit converges to a constant:

$$\frac{c_{\text{inf,p}}^*}{c_{\text{inf,t}}^*} \rightarrow \sqrt{\pi/4}, \quad \text{as } M \rightarrow \infty, \quad (4.23)$$

i.e., under the per-antenna power constraint, the constellation size should be reduced by about 88% in order for the symbol-level precoder to be able to synthesize the constellation point.

4.4.3 One-Bit Precoding

This part now considers 1-bit symbol-level precoding where $\mathbf{x} \in \mathcal{X}^M$ where

$$\mathcal{X} = \left\{ \frac{1}{\sqrt{2}} (\pm 1 \pm i) \right\}. \quad (4.24)$$

Unlike the infinite resolution case, the realizations of $\sqrt{\frac{P}{M}}\mathbf{h}^H\mathbf{x}$ is no longer a continuum. Thus, it is no longer always true that all constellation points can be constructed exactly at the transmitter. Nevertheless, as long as the reconstruction error is sufficiently small (e.g., below the noise level), one-bit precoding can still provide good performance.

To gain some intuition, Fig. 4.3 is a scatter plot of all 4^M possible realizations of $\mathbf{h}^H\mathbf{x}$ for the case of $M = 8$ antennas. It can be seen that all these points are confined in a circle centered at the origin, yet the radius of the circle in which these points concentrate is further reduced as compared to the infinite resolution cases discussed earlier.

This chapter aims to make a case that similar to the infinite-resolution case, i.e., (4.20), if the constellation range is designed such that the furthest constellation point is located at \bar{r}^* , where

$$\bar{r}^* = \max_{\mathbf{x} \in \mathcal{X}^M} \left| \sqrt{\frac{P}{M}} \mathbf{h}^H \mathbf{x} \right|, \quad (4.25)$$

then all the constellation points can be reconstructed accurately. This is clearly a *necessary* condition for constellation range. But, as shown numerically later in this chapter, when the number of transmit antennas M is large, this is also a *sufficient* condition, i.e., an appropriate 1-bit precoding design can approach any complex number inside the circle with radius \bar{r}^* with negligible error.

Following this design strategy, the constellation range design problem for 1-bit precoding can be written as

$$c_{1\text{-bit}}^* = \sqrt{2} \max_{\mathbf{x} \in \mathcal{X}^M} \left| \sqrt{\frac{P}{M}} \mathbf{h}^H \mathbf{x} \right|. \quad (4.26)$$

The numerical evaluation of the above maximization is, unfortunately, difficult. Instead of solving this problem directly, this thesis proposes to reduce the constellation range for 1-bit precoding (which automatically satisfies per-antenna power constraint) as compared to infinite resolution precoding with per-antenna power constraint by a constant factor. The following result from [93] helps us identify such a factor.

Consider the following optimization problem

$$\max_{\mathbf{x}} \mathbf{x}^H \mathbf{A} \mathbf{x} \quad (4.27a)$$

$$\text{s.t. } x_m \in \mathcal{F}_q, \quad \forall m, \quad (4.27b)$$

where $\mathcal{F}_q = \left\{ 1, e^{i\frac{2\pi}{q}}, \dots, e^{i\frac{2\pi(q-1)}{q}} \right\}$. Further, consider the following semidefinite programming (SDP) relaxation of (4.27) which is now a convex optimization problem,

$$\max_{\mathbf{X} \in \mathbb{C}^{M \times M}} \text{Tr}(\mathbf{AX}) \quad (4.28a)$$

$$\text{s.t.} \quad \mathbf{X} \succeq \mathbf{0}, \quad (4.28b)$$

$$\mathbf{X}(i, i) = 1, \quad \forall i = 1, \dots, M. \quad (4.28c)$$

Suppose \mathbf{X}^* is an optimal solution of problem (4.28). To generate a feasible \mathbf{x} from the solution of problem (4.28), draw a random vector $\zeta \sim \mathcal{CN}(\mathbf{0}, \mathbf{X}^*)$, and then quantize each element of ζ to the nearest point in \mathcal{F}_q . The expectation of the objective function of the solution obtained using the above randomization procedure can be shown to be greater than $\alpha_q \text{Tr}(\mathbf{AX}^*)$ [93], where

$$\alpha_q = \begin{cases} \frac{2}{\pi}, & \text{if } q = 2, \\ \frac{q^2(1 - \cos \frac{2\pi}{q})}{8\pi}, & \text{if } q \geq 3. \end{cases} \quad (4.29)$$

For the given q , let this thesis denote the objective function in (4.27) for the optimal solution as f_q^* when $\mathbf{A} = \frac{P}{M}\mathbf{h}\mathbf{h}^H$. Then, the constellation range for infinite resolution precoding with per-antenna power constraint and 1-bit precoding can be written as $c_{\text{inf,p}}^* = \sqrt{2f_\infty^*}$ and $c_{\text{1-bit}}^* = \sqrt{2f_4^*}$, respectively. Now since it is difficult to exactly characterize f_4^* , we propose to approximate $\frac{f_4^*}{f_\infty^*}$ by the ratio of the SDP approximation bounds $\frac{\alpha_4}{\alpha_\infty} = \frac{2/\pi}{\pi/4} = 8/\pi^2$. This means that

$$c_{\text{1-bit}}^* \approx \sqrt{8/\pi^2} c_{\text{inf,p}}^* \approx \sqrt{2/\pi} c_{\text{inf,t}}^*, \quad (4.30)$$

where the last approximate equality follows from (4.23).

In order to see that the proposed constellation range is an appropriate choice, let this thesis consider as an example of a relatively small system with $M = 8$ antennas and $P = 4$. For a randomly generated channel, Fig. 4.3 plots all 4^M possible realizations of $\mathbf{h}^H \mathbf{x}$. Fig. 4.3 also plots two circles: a dashed black circle with radius of $c_{\text{inf,t}}^* = \sqrt{2P} \|\mathbf{h}\|_2$ and a solid red circle with the radius of $\sqrt{2/\pi} c_{\text{inf,t}}^*$ where the latter is the proposed value for $c_{\text{1-bit}}^*$. It can be seen visually that almost all the realizations of $\mathbf{h}^H \mathbf{x}$ are located inside the solid red circle suggesting

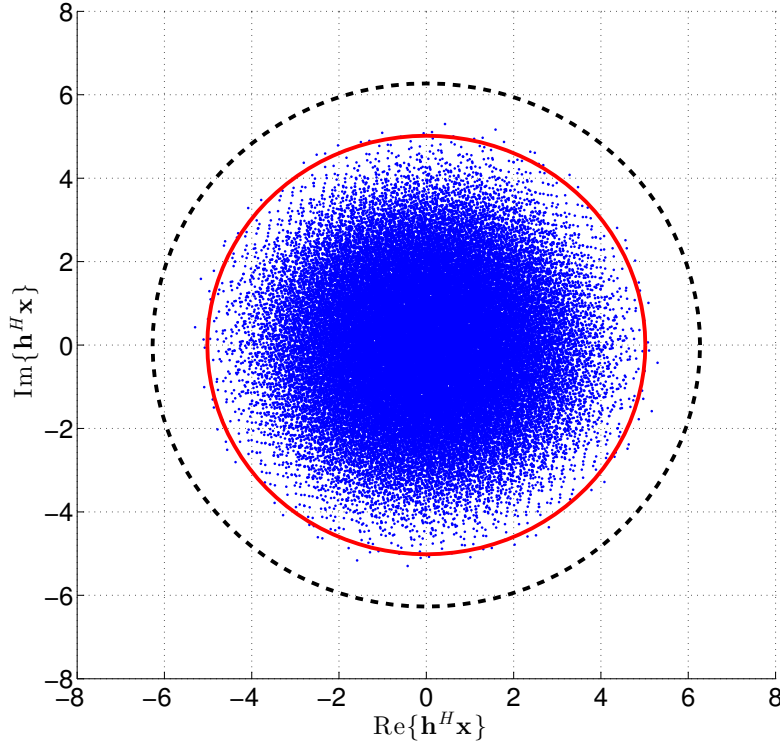


Fig. 4.3: Fix one random channel realization with $M = 8$ and $P = 4$. The data points are the 4^M possible realizations of $\mathbf{h}^H \mathbf{x}$, and the dashed black and solid red lines are circles with radius of $c_{\text{inf},t}^* = \sqrt{2P}\|\mathbf{h}\|_2$ and $\sqrt{2/\pi}c_{\text{inf},t}^*$, respectively. Most data points are confined within the solid red circle.

that the proposed design is a necessary condition for constellation range.

In order to see that the proposed design is also a sufficient condition for constellation range, let define the mean squared error (MSE) as

$$\text{MSE}(s) = \mathbb{E}_{\mathbf{h}} \left\{ \left| \sqrt{\frac{P}{M}} \mathbf{h}^H \mathbf{x} - s \right|^2 \right\}, \quad (4.31)$$

and the parameter

$$\gamma = \frac{|s|}{\sqrt{P}\|\mathbf{h}\|_2}. \quad (4.32)$$

For the same system parameters as in the previous experiment, Fig. 4.4 plots the average MSE against the parameter γ over 10^3 channel realizations. The precoder $\mathbf{x} \in \mathcal{X}^M$ is found by exhaustive search in order to minimize the squared error for given s and \mathbf{h} . It can be seen from

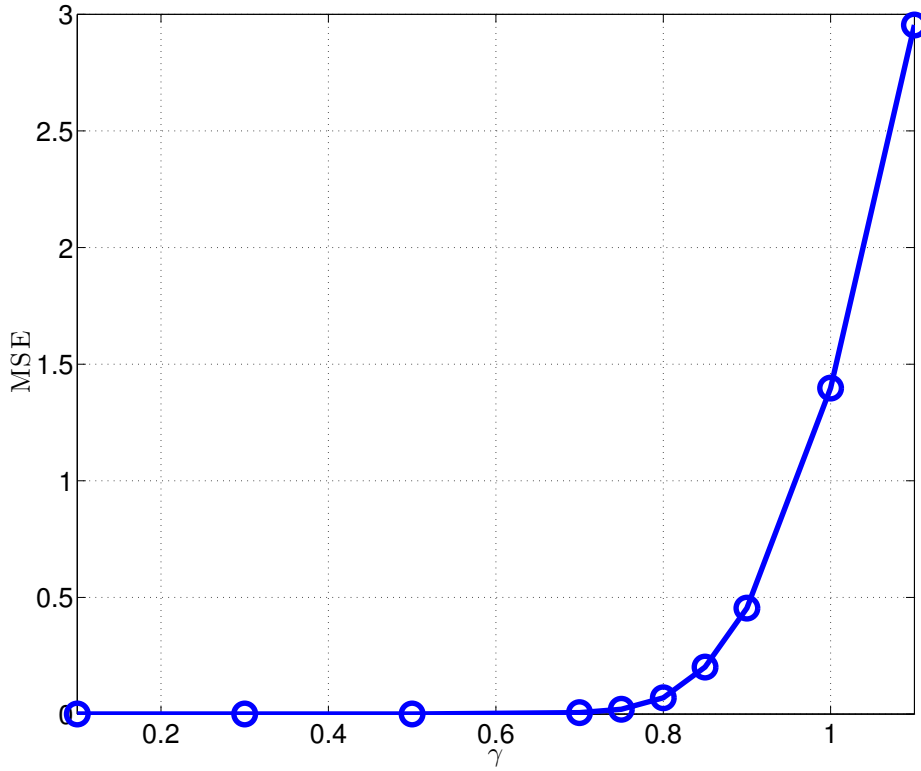


Fig. 4.4: The MSE versus γ for a single-user system with $M = 8$ and $P = 4$. There is a phase transition at $\gamma = \sqrt{2/\pi} \approx 0.8$.

Fig. 4.4 that there is a phase transition around $\gamma_{\text{th}} = \sqrt{2/\pi} \approx 0.8$ before which the MSE is very small while the MSE starts to increase significantly after γ_{th} . This means that any complex number inside the circle with radius $c_{1\text{-bit}}^* = \sqrt{2/\pi}\sqrt{2P}\|\mathbf{h}\|_2$ can be realized accurately while it is infeasible to do so for complex numbers outside of that circle, thereby justifying the choice $c_{1\text{-bit}}^* = \sqrt{2/\pi}c_{\text{inf,t}}^*$. Further numerical evidence is provided in Section 4.7 to support this choice under practical precoding and when M is large.

4.5 One-Bit Precoding Design for Single-User Scenario

This section proposes a practical algorithm for designing the single-user 1-bit symbol-level precoder, or equivalently the transmitting signal, \mathbf{x}_i , corresponding to each symbol, s^i , assuming fixed constellation range c . Using (4.9) as the SER metric, it can be seen that the only term that depends on the precoding for a fixed constellation is $\hat{d}_{ii} = \left| \sqrt{\frac{P}{M}} \mathbf{h}^H \mathbf{x}_i - s^i \right|$. Since the

Q -function is a decreasing function, the transmit signal design problem for the i^{th} symbol can therefore be written as

$$\mathbf{x}_i^* = \underset{\mathbf{x}_i \in \mathcal{X}^M}{\operatorname{argmin}} \left| \sqrt{\frac{P}{M}} \mathbf{h}^H \mathbf{x}_i - s^i \right|. \quad (4.33)$$

Solving this optimization problem is hard due to the combinatorial nature of its constraints. Here, this thesis seeks to find a good solution for (4.33) with low complexity.

Toward this aim, we observe that for a fixed channel \mathbf{h} , the possible realizations of $\mathbf{h}^H \mathbf{x}$, when $\mathbf{x} \in \mathcal{X}^M$, are densely distributed close to the origin; an example for $M = 8$ is depicted in Fig. 4.3. This observation suggests that if we can choose the transmitting signal across a suitably chosen subset of antennas in a greedy fashion so as to bring the residual to be small, then we can use exhaustive search at the remaining (e.g. 8) antennas to drive the residual very close to zero. Based on this, we propose the following two-step algorithm to find a reasonable solution for (4.33):

- **Step 1:** Use an iterative greedy approach to bring the residual close to zero by designing the precoded signal at a suitably chosen subset of $M_1 = M - M_2$ antennas where $M_1 \gg M_2$. In particular, at each iteration, the algorithm selects one antenna and its corresponding transmitting signal to minimize the norm of the residual. This procedure is executed until the transmitting signals for M_1 antennas are all determined.
- **Step 2:** Design the transmitting signals of the other M_2 antennas to further approximate the desired signal by performing an exhaustive search. Note that the exhaustive search is feasible as $M_2 \ll M$.

The mathematical details of the above two-step algorithm are illustrated in Algorithm 5. The overall computational complexity of the algorithm is $O(MM_1) + O(4^{M_2})$, where the first and the second terms correspond to the first and the second steps of the proposed algorithm, respectively. In the numerical results, it is observed that $5 \leq M_2 \leq 10$ is a reasonable range of choices for M_2 which provides good performance with reasonable computational complexity.

Algorithm 5 Single-User Transmitting Signal Design

Inputs: P, M, \mathbf{h}, s^i **Step 1:**Initialize the residual as $s_r = s^i$ and define the set $\mathcal{J} = \{1, \dots, M\}$.**for** $j = 1 \rightarrow M_1$ **do**

$$(j^*, x^*) = \underset{j \in \mathcal{J}, x \in \mathcal{X}}{\operatorname{argmin}} \left| s_r - \sqrt{\frac{P}{M}} h_j^\dagger x \right|,$$

$$x_{j^*} = x^*,$$

$$\mathcal{J} = \mathcal{J} \setminus j^*,$$

$$s_r = s_r - \sqrt{\frac{P}{M}} h_{j^*}^\dagger x_{j^*},$$

end for**Step 2:**Use the exhaustive search method to solve problem $\min_{x_j \in \mathcal{X}, \forall j \in \mathcal{J}} \left| s_r - \sqrt{\frac{P}{M}} \sum_{j \in \mathcal{J}} h_j^\dagger x_j \right|$.

4.6 Constellation Range and One-Bit Precoding Design for Multi-User Scenario

This section generalizes the proposed designs for the QAM constellation range and the transmitting signals in Section 4.4 and Section 4.5 from the single-user scenario to the multi-user scenario.

4.6.1 Constellation Range Design

When a multi-antenna BS serves multiple users at the same time, the constellation range depends not only on the channel, but also on the number of users K being served simultaneously and the constellation size. This section provides an analysis of the constellation range in the massive MIMO regime under multi-user symbol-level precoding. We begin by considering the infinite-resolution ZF scheme with per-symbol total power constraint across the antennas.

Fixing a channel realization \mathbf{H} , the ZF precoding vector can be found by solving the following optimization problem which illustrates the minimum required power so that the noiseless

received signal of each user is exactly equal to its intended signal, namely,

$$\min_{\mathbf{x}} \|\mathbf{x}\|_2^2 \quad (4.34a)$$

$$\text{s.t. } \sqrt{\frac{P}{M}} \mathbf{H} \mathbf{x} = \mathbf{s}. \quad (4.34b)$$

This problem is convex and its optimal solution is given by

$$\mathbf{x}^* = \sqrt{\frac{M}{P}} \mathbf{H}^H (\mathbf{H} \mathbf{H}^H)^{-1} \mathbf{s}. \quad (4.35)$$

The constellation range should be designed such that for a vector of intended constellation points, $\mathbf{s} = [s_1, \dots, s_K]$, the transmitted signal satisfies $\|\mathbf{x}^*\|_2^2 \leq M$. This is equivalent to

$$\mathbf{s}^H (\mathbf{H} \mathbf{H}^H)^{-1} \mathbf{s} \leq P. \quad (4.36)$$

Now using the pseudo-orthogonal property of the channels of different users in the large-scale massive MIMO regime, this thesis can approximate $(\mathbf{H} \mathbf{H}^H)^{-1}$ with a diagonal matrix in which the k^{th} diagonal element is $\frac{1}{\|\mathbf{h}_k\|_2^2}$. By approximating $(\mathbf{H} \mathbf{H}^H)^{-1}$ with that diagonal matrix, the inequality (4.36) can be rewritten as

$$\sum_{k=1}^K \frac{|s_k|^2}{\|\mathbf{h}_k\|_2^2} \leq P. \quad (4.37)$$

This constraint can be further simplified by taking advantage of the channel hardening phenomenon in the massive MIMO regime that allows the approximation $\|\mathbf{h}_k\|_2^2 \approx M$ for all k as

$$\sum_{k=1}^K |s_k|^2 \leq PM. \quad (4.38)$$

The constellation range design problem is then to choose the range c so that the above constraint is satisfied for most realizations of (s_1, s_2, \dots, s_K) if they are within the range.

Consider a particular user k whose intended signal s_k is selected in an independent and identically distributed (i.i.d.) fashion from an N^2 -QAM constellation with range c . A routine

calculation shows that

$$\mu_s = \mathbb{E} \{ |s_k|^2 \} = \frac{N+1}{6(N-1)} c^2, \quad (4.39)$$

and

$$\sigma_s^2 = \mathbb{E} \left\{ (|s_k|^2 - \mu_s)^2 \right\} = \frac{(N+1)(N^2-4)}{90(N-1)^3} c^4. \quad (4.40)$$

When a large number of users are precoded together, by the central limit theorem, it is possible to write

$$\sqrt{K} \left(\frac{1}{K} \sum_{k=1}^K |s_k|^2 - \mu_s \right) \rightarrow \mathcal{N}(0, \sigma_s^2). \quad (4.41)$$

The optimal constellation range for ZF precoding is the maximum range c such that the precoded signal almost always satisfies the per-symbol power constraint, i.e., (4.38). This thesis proposes to design c so that the mean of $\sum_{k=1}^K |s_k|^2$ in (4.38) is within two standard deviation from the constraint PM . This ensures that (4.38) is satisfied with high probability. Using (4.41) and the properties of the Gaussian distribution, this design goal of $K\mu_s + 2\sqrt{K}\sigma_s = PM$ yields that

$$c_{\text{ZF}}^* = \sqrt{\frac{2PM}{f(K, N)}}, \quad (4.42)$$

where

$$f(K, N) = K \frac{N+1}{3(N-1)} + 2 \sqrt{K \frac{(N+1)(N^2-4)}{22.5(N-1)^3}}. \quad (4.43)$$

Comparing the constellation range design of the infinite resolution ZF for the multi-user scenario with that of the single-user case considered in Section 4.4, i.e., (4.42) vs (4.16), it can be seen that there is an extra scaling factor $\sqrt{\frac{1}{f(K, N)}}$ in the constellation range expression when a massive MIMO BS simultaneously serves large number of users.

Finally, this section considers the constellation range design for the 1-bit precoding case. Inspired by the form of (4.42), this thesis proposes to multiply the same scaling factor $\sqrt{\frac{1}{f(K, N)}}$ to the previously proposed single-user constellation range design for 1-bit precoding in (4.30) to account for the effect of serving multiple users, i.e.,

$$c_{1\text{-bit}}^* = \sqrt{2/\pi} \sqrt{\frac{2PM}{f(K, N)}}, \quad (4.44)$$

Numerical results are presented later in this chapter to show that this is an appropriate design.

4.6.2 One-Bit Precoding Design

This part presents a practical algorithm for 1-bit symbol-level ZF precoder design for the multi-user MISO system. In the multi-user scenario where the intended symbol of each user is selected from a N^2 -QAM constellation, the vector of intended symbols has N^{2K} choices. For each choice of \mathbf{s}^i where $i \in \{1, \dots, N^{2K}\}$, this thesis seeks to design the transmitting signal \mathbf{x}_i to minimize the average user SER, mathematically,

$$\min_{\mathbf{x}_i \in \mathcal{X}^M} \sum_k \frac{g_k^i}{N^2} Q \left(\frac{d_{1\text{-bit}} - 2 \left| \sqrt{\frac{P}{M}} \mathbf{h}_k^H \mathbf{x}_i - s_k^i \right|}{2\sigma} \right), \quad (4.45)$$

where

$$d_{1\text{-bit}} = \frac{c_{1\text{-bit}}^*}{N-1}, \quad (4.46)$$

and s_k^i is the k^{th} element of \mathbf{s}^i . Instead of tackling the problem in (4.45), due to the rapidly decreasing shape of the Q -function, this thesis considers the following optimization problem

$$\min_{\mathbf{x}_i \in \mathcal{X}^M} \left\| \sqrt{\frac{P}{M}} \mathbf{H} \mathbf{x}_i - \mathbf{s}^i \right\|_\infty, \quad (4.47)$$

which minimizes the maximum approximation error across all the users. For solving this problem, this thesis uses a generalization of the two-step algorithm proposed in Section 4.5 for the single-user case.

The proposed two-step approach is summarized in Algorithm 6. Specifically, the first step of the proposed algorithm seeks to bring the residual vector close to the origin, i.e., minimize the 2-norm of the residual symbol vector, by choosing the transmit values over a subset of M_1 antennas in a greedy fashion. In the second step of the algorithm, exhaustive search is performed over the remaining $M_2 = M - M_1$ antennas for minimizing the maximum deviation from the residual symbols, i.e., minimizing the ∞ -norm of the residual symbol vector. The rational behind minimizing the 2-norm in the first step is that the realizations of $\sqrt{\frac{P}{M}} \mathbf{H} \mathbf{x}$ for

Algorithm 6 Multi-User Transmitting Signal Design

Inputs: $P, M, \mathbf{H}, \mathbf{s}^i$ **Step 1:**

Initialize the residual symbol vector as $\mathbf{s}_r = \mathbf{s}^i$, define the set $\mathcal{J} = \{1, \dots, M\}$, and denote the j^{th} column of \mathbf{H} by $\tilde{\mathbf{h}}_j$.

for $j = 1 \rightarrow M_1$ **do**

$$(j^*, x^*) = \underset{j \in \mathcal{J}, x \in \mathcal{X}}{\operatorname{argmin}} \left\| \mathbf{s}_r - \sqrt{\frac{P}{M}} \tilde{\mathbf{h}}_j x \right\|_2,$$

$$x_{j^*} = x^*,$$

$$\mathcal{J} = \mathcal{J} \setminus j^*,$$

$$\mathbf{s}_r = \mathbf{s}_r - \sqrt{\frac{P}{M}} \tilde{\mathbf{h}}_{j^*} x_{j^*},$$

end for

Step 2:

Use the exhaustive search method to solve problem $\min_{x_j \in \mathcal{X}, \forall j \in \mathcal{J}} \left\| \mathbf{s}_r - \sqrt{\frac{P}{M}} \sum_{j \in \mathcal{J}} \tilde{\mathbf{h}}_j x_j \right\|_\infty$.

$\mathbf{x} \in \mathcal{X}^M$ are distributed densely close to the origin which means that the vectors with smaller 2-norm are surrounded by more realizations. Therefore, it is expected that the second step of the algorithm achieves a better performance if the residual symbol vector that is passed to it as an input has a smaller 2-norm.

The computational complexity of the first and the second steps of Algorithm 6 are $O(KMM_1)$ and $O(K4^{M_2})$, respectively. Simulation results presented in Section 4.7 show excellent numerical performance of the algorithm with reasonable complexity.

4.6.3 Performance Gap of One-Bit Precoding vs. Conventional ZF

For infinite resolution ZF with the constellation range designed as (4.42), since almost surely the constellation points can be reconstructed exactly, the symbol error rate simply scales with the minimum distance as follows:

$$\text{SER} = \bar{g}_N Q\left(\frac{d}{2\sigma}\right), \quad (4.48)$$

where

$$\bar{g}_N = 4 \left(1 - \frac{1}{N}\right), \quad (4.49)$$

is the average number of nearest neighbours in the symbol constellation, and d is the minimum distance in the constellation, which can be expressed as:

$$d_{\text{ZF}}^* = \frac{c_{\text{ZF}}^*}{N-1} = \sqrt{\frac{2PM}{\tilde{f}(K, N)}}, \quad (4.50)$$

where $\tilde{f}(K, N) = (N-1)^2 f(K, N)$.

In the 1-bit precoding scheme, there is no guarantee that the noiseless received signals can exactly realize the intended symbols. However, since this thesis designs the constellation range carefully so that the 1-bit precoder can approximate the noiseless receive signals to be very close to the intended signals, then the term $2\hat{d}_{ii}$ in (4.9) is negligible as compared to the minimum distance d , and it is possible to tightly approximate the SER of the proposed scheme using the same equation as (4.48) with

$$d_{\text{1-bit}} = \frac{c_{\text{1-bit}}^*}{N-1} = \sqrt{2/\pi} \sqrt{\frac{2PM}{\tilde{f}(K, N)}}. \quad (4.51)$$

This suggests that the amount of required power in 1-bit precoding is about $10 \log_{10} \frac{1}{2/\pi} \approx 2\text{dB}$ more than conventional ZF to achieve the same performance. The simulation results of this chapter indeed show this 2dB gap under the proposed constellation range design, thereby verifying that the proposed design is a reasonable one.

It is also possible to characterize the performance gap of 1-bit precoding and conventional ZF in terms of the number of extra antennas that would need to be added to 1-bit precoding in order to achieve the same performance as conventional ZF. Using (4.48), it can be seen that

$$M_{\text{1-bit}} = \frac{1}{2/\pi} M_{\text{ZF}} \approx 1.56 M_{\text{ZF}}. \quad (4.52)$$

This means that 1-bit precoding with about 50% more number of antennas can achieve the same performance as infinite resolution ZF precoding under the same instantaneous per-symbol power constraint.

It is worth mentioning that although the above discussion pertains to the multi-user case, since the same constellation range design, i.e., $c_{\text{1-bit}}^* = \sqrt{2/\pi} c_{\text{inf,t}}^*$ is used for the single-user case,

the performance gap between the infinite resolution precoding with per-symbol total power constraint and the proposed 1-bit precoding design for the single-user case is also about 2dB, which again translates to requiring about 50% more antennas for 1-bit precoding to achieve the same performance as infinite-resolution precoding.

4.7 Numerical Results

This section presents numerical simulation results to support the proposed design methodology for constellation range and to evaluate the performance of the proposed algorithm for 1-bit symbol-level precoding for both single-user and multi-user scenarios.

4.7.1 MSE Analysis for Choosing M_2

In this part, the performance of the proposed one-bit precoding scheme for different choices of M_2 is studied. Toward this aim, a SU-MISO system in which $M = 128$, $N = 4$, and $P = 1$ is considered. Fig. 4.5 plots the average MSE defined in (4.31) against M_2 . As expected, Fig. 4.5 shows that the performance of the proposed scheme is improved by increasing M_2 . This performance improvement is at the cost of increase in computational complexity. Fig. 4.5 also suggests that the performance improvement in increasing M_2 larger than 6 is negligible for the considered system parameters. For the rest of this section, M_2 is set to 8 in all the simulations in order to achieve a good performance while keeping the complexity manageable.

4.7.2 MSE Analysis for Constellation Range Design

First, this section shows that the constellation range design proposed in Section 4.4.3 for the single-user case, which sets $c_{1\text{-bit}}^* = \sqrt{2/\pi}\sqrt{2P}\|\mathbf{h}\|_2$ is nearly optimal. Consider a BS with M antennas serving one user by transmitting symbols from a 16-QAM constellation with constellation range of c . This part evaluates the average MSE defined in (4.31) against the parameter

$$\lambda = \frac{c}{\sqrt{2P}\|\mathbf{h}\|_2}, \quad (4.53)$$

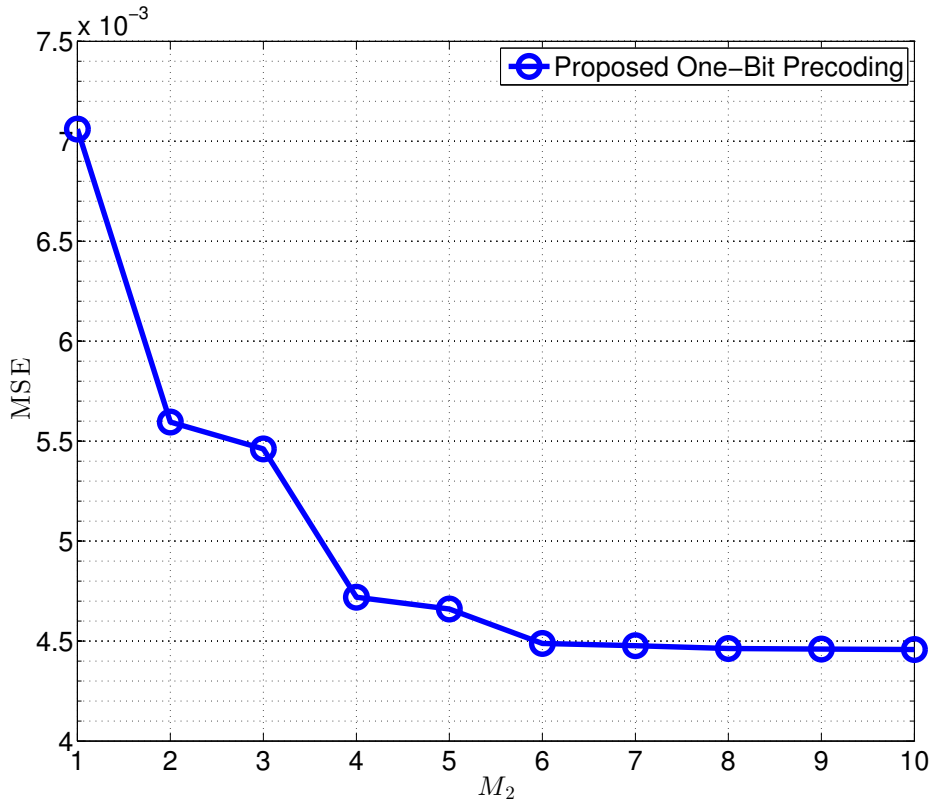


Fig. 4.5: Average MSE versus M_2 in a single-user system where $M = 128$, $N = 4$, and $P = 1$.

where the average is over the channel realizations and 1-bit precoding is performed using Algorithm 5. The transmit power is set to $P = 1$. The number of antennas M ranges from 128 to 1024.

Fig. 4.6 shows that there is a sharp phase transition in MSE for both infinite resolution and 1-bit precoding. The phase transition occurs at $\lambda = 1$ for infinite resolution precoding with instantaneous per-symbol total power constraint, thus verifying the constellation range design (4.15), i.e., $c_{\text{inf},t}^* = \sqrt{2P}\|\mathbf{h}\|_2$. For 1-bit precoding, the phase transition occurs at about $\lambda = \sqrt{2/\pi} \approx 0.8$, thus verifying the constellation range design (4.30), i.e., $c_{\text{1-bit}}^* = \sqrt{2/\pi}\sqrt{2P}\|\mathbf{h}\|_2$ even with the proposed low-complexity practical 1-bit precoding algorithm.

In Fig. 4.6, the MSE for the values of λ smaller than the phase transition point indicates the quality of the 1-bit precoder design. One may ask whether the MSE achieved by the proposed 1-bit precoding is sufficiently small so that it does not significantly degrade the SER performance. The answer is affirmative under typical system parameter ranges. Fig. 4.6 suggests that for the

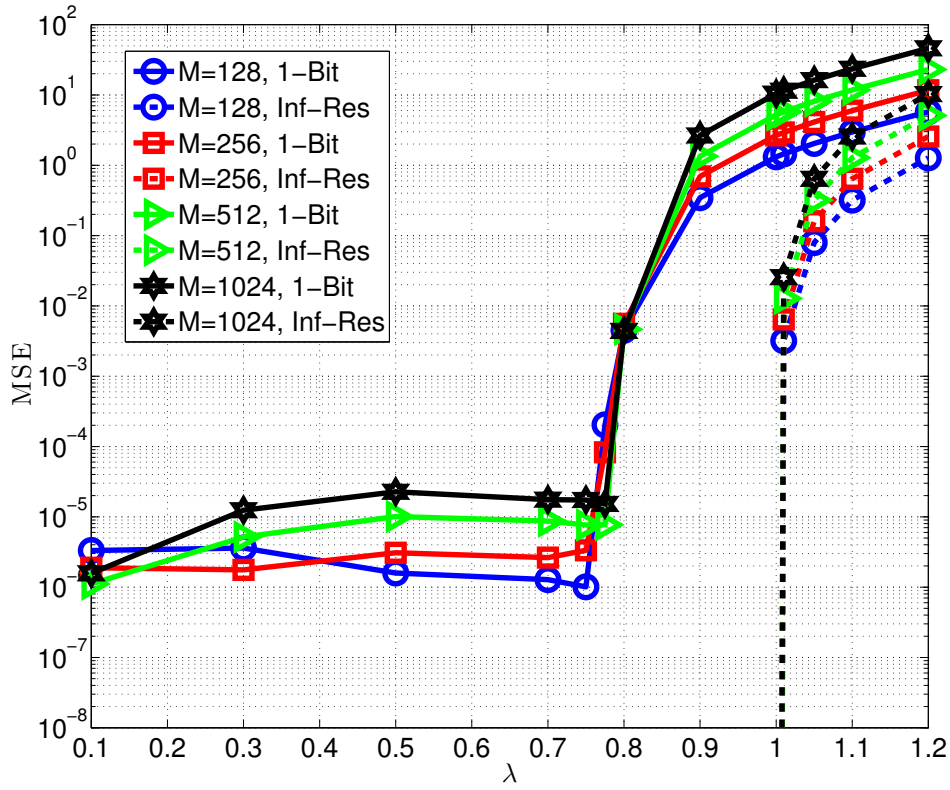


Fig. 4.6: Average MSE versus λ in a single-user system for different numbers of antennas, M , when $P = 1$ and $M_2 = 8$.

transmit power budget $P = 1$ the MSE about 10^{-5} can be achieved by the proposed algorithm. Since the MSE scales with the power budget, the MSE of the proposed algorithm with the power budget P is about $10^{-5}P$. Using the SER expression in (4.9) and observing that the MSE is nearly uniform for all symbols before the phase transition, it can be shown that

$$\text{SER} \approx \bar{g}_N Q \left(\frac{c_{1\text{-bit}}^*}{2\sigma(N-1)} - \frac{\sqrt{\text{MSE}}}{\sigma} \right), \quad (4.54)$$

where $\bar{g}_N = 4(1 - 1/N)$ is the average number of nearest neighbours in the symbol constellation. For the typical operating regime of SER (e.g. $10^{-3} - 10^{-6}$), the contribution of the second term in the Q -function can be ignored if it is at least one order of magnitude smaller than the first term, i.e.,

$$0.1 \frac{c_{1\text{-bit}}^*}{2\sigma(N-1)} \leq \frac{\sqrt{\text{MSE}}}{\sigma}. \quad (4.55)$$

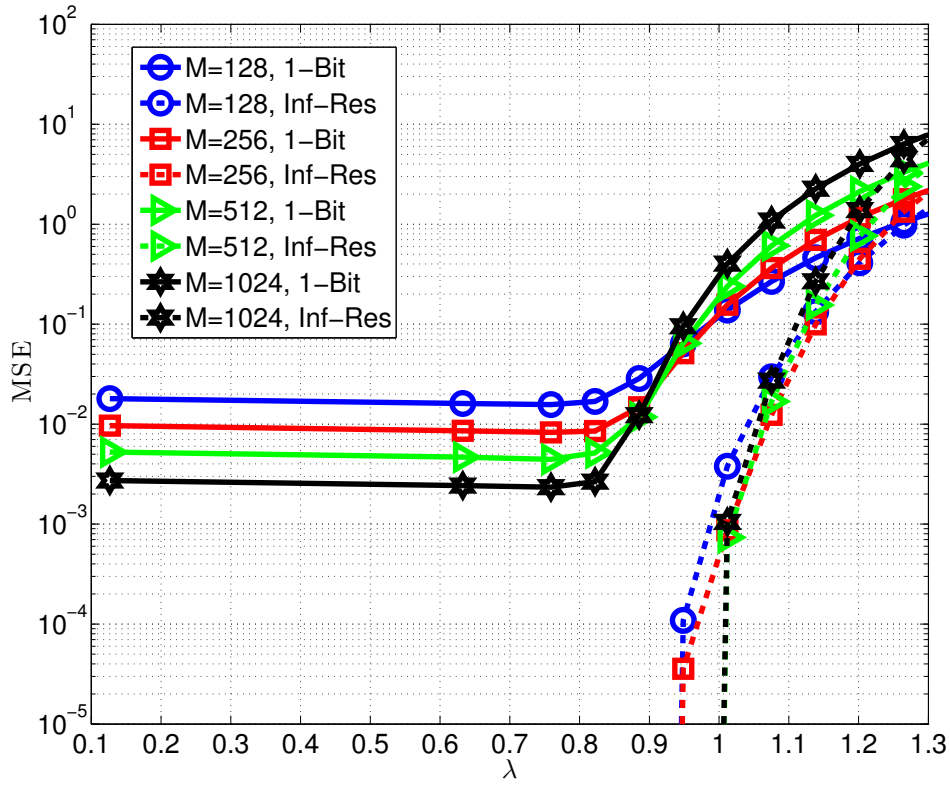


Fig. 4.7: Average MSE versus λ in a 8-user system for different numbers of antennas, M , when $P = 1$ and $M_2 = 8$.

For $\text{MSE} = 10^{-5}P$ and $c_{1\text{-bit}}^* = \sqrt{2/\pi}\sqrt{2P}\|\mathbf{h}\|_2 \approx 0.8\sqrt{2PM}$, this condition translates to an upper-bound on the number of constellation points as:

$$N \leq 17.9\sqrt{M} + 1. \quad (4.56)$$

This condition is clearly satisfied in a typical single-user MISO system, with for example 128 antennas and with constellation size at most $N^2 = 2^{12}$. Therefore, the MSE of the proposed 1-bit precoding has negligible influence on the SER in such a system.

Next, this section shows that the constellation range design for the multi-user case proposed in Section 4.6.1, which sets $c_{1\text{-bit}}^* = \sqrt{2/\pi}\sqrt{\frac{2PM}{f(K,N)}}$ is also nearly optimal. Toward this aim, the next experiment considers a 8-user system with transmit power $P = 1$ and 16-QAM signalling, i.e., $N = 4$. This experiment then varies the constellation range of 16-QAM constellation and

plots the average MSE, which for the multi-user setup is defined as

$$\text{MSE}(\mathbf{s}) = \mathbb{E}_{\mathbf{H}} \left\{ \left| \sqrt{\frac{P}{M}} \mathbf{Hx} - \mathbf{s} \right|^2 \right\}, \quad (4.57)$$

against the parameter λ defined as

$$\lambda = \frac{c}{\sqrt{\frac{2PM}{f(K,N)}}}. \quad (4.58)$$

Fig. 4.7 shows that for the multi-user scenario, there is a phase transition at λ very close to 1 for infinite resolution ZF precoding, and $\sqrt{2/\pi} \approx 0.8$ for 1-bit precoding, respectively. This verifies the proposed design choices (4.42) and (4.44), i.e., $c_{\text{ZF}}^* = \sqrt{\frac{2PM}{f(K,N)}}$ and $c_{\text{1-bit}}^* = \sqrt{2/\pi} \sqrt{\frac{2PM}{f(K,N)}}$.

4.7.3 SER of One-Bit Precoding

This part evaluates the SER performance of the proposed one-bit precoding scheme. In the following simulations, the performance of different methods are evaluated using the empirical average SER of the users that is calculated by averaging the SER over 10^3 channel realizations and in each of realizations 200 symbols are transmitted. This means that the coherence time of the channel is considered to be able to allocate 200 symbol transmissions. Further, the signal-to-noise ratio is defined as $\text{SNR} = 10 \log_{10} \left(\frac{P}{2\sigma^2} \right)$.

The first experiment of this part evaluates a single-user communication setup with 256-QAM, i.e., $N = 16$. In this experiment, the parameter M_2 is set to be 8 in the proposed 1-bit precoding algorithm. The BS is assumed to be equipped with $M = 256$ antennas. In Fig. 4.8, the performance of the proposed 1-bit precoding method with different constellation range designs is compared to the infinite resolution precoding benchmark with per-symbol power constraint and constellation range of $c = \sqrt{2P} \|\mathbf{h}\|_2$. It can be seen from Fig. 4.8 that the constellation range of $\sqrt{2/\pi}c \approx 0.8c$ achieves the overall best performance, justifying the proposed design (4.30) for 1-bit precoding.

Fig. 4.8 shows that for the 1-bit precoding methods with constellation range of larger than

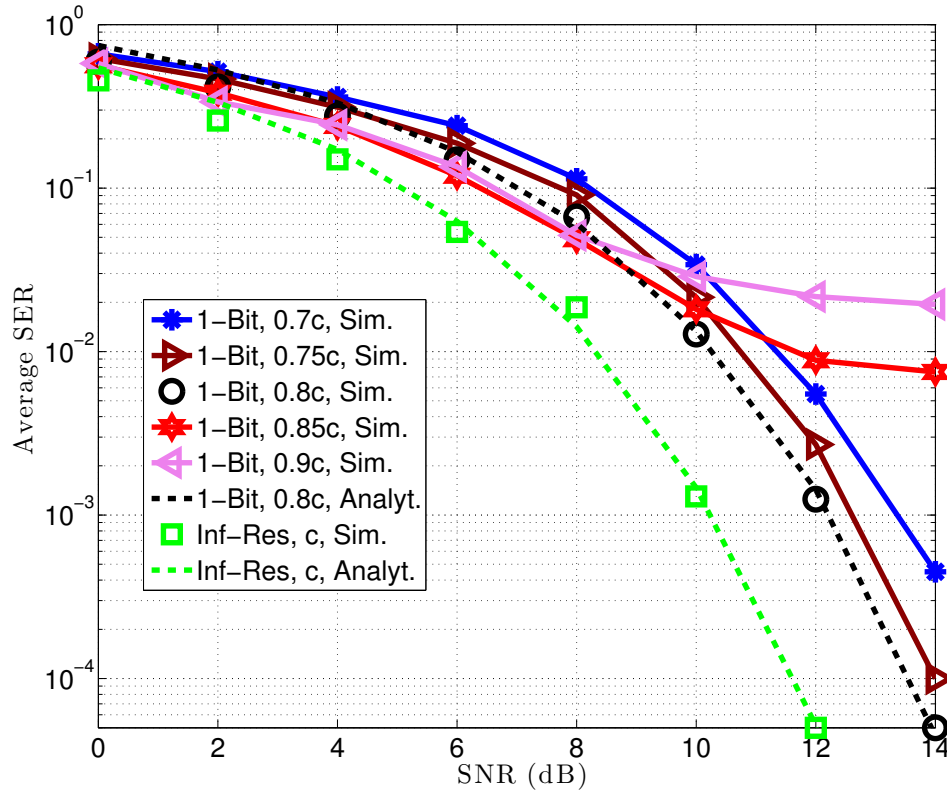


Fig. 4.8: Average SER versus SNR for different methods in a SU-MISO system with $M = 256$ and $N = 16$.

$0.8c$, there is an error floor in the large SNR regime. This is because in the large SNR regime, the average SER is dominated by the worst-case symbols, which are the corner constellation points. One-bit precoding with constellation range larger than $\sqrt{2/\pi}c \approx 0.8c$ leads to high reconstruction MSE for the corner points.

Moreover, Fig. 4.8 shows that the analytic SER expressions provided in Section 4.6.3 for the infinite resolution precoding and the proposed 1-bit precoding with constellation range of $0.8c$ perfectly match the numerical simulation results and the performance gap between the proposed method and the infinite resolution case is about 2dB, as predicted by the SER analysis.

The next experiment considers a single-user setup in which 16-QAM constellation is employed and the SNR is set to be -4dB . For such a system, Fig. 4.9 plots the average SER against the number of antennas at the BS for the proposed 1-bit precoding method as well as the infinite resolution precoding method. It can be observed from Fig. 4.9 that the proposed

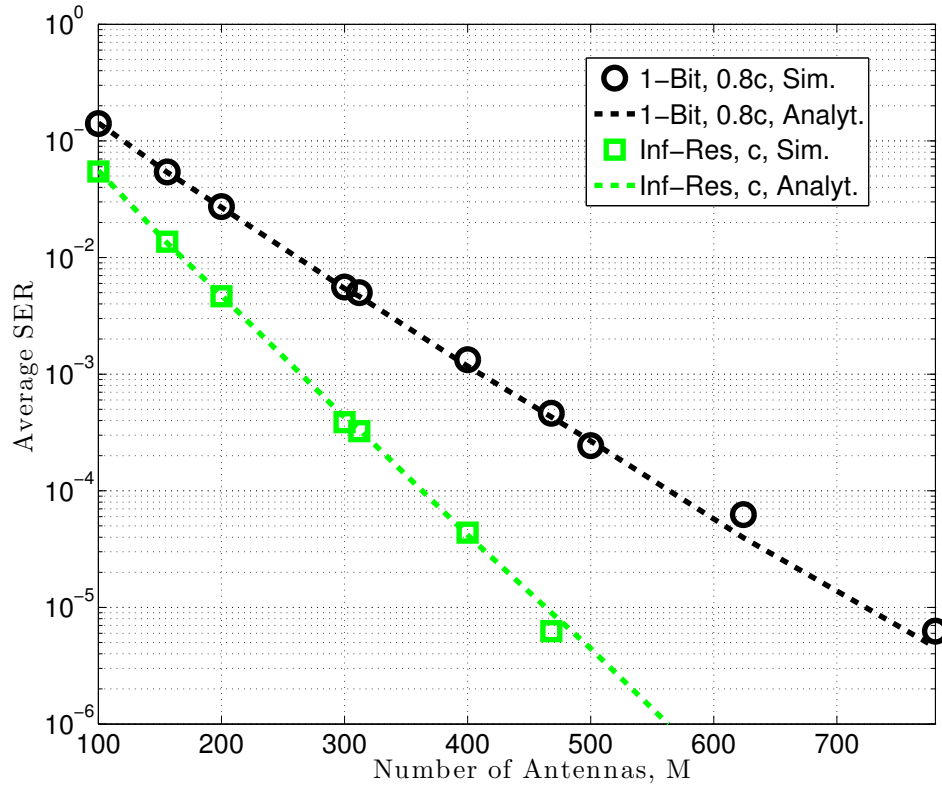


Fig. 4.9: Average SER versus the number of antennas, M , for different methods in a SU-MISO system with $\text{SNR} = -4\text{dB}$ and $N = 4$.

1-bit precoding design can achieve the same performance as the infinite resolution precoding if the BS in the 1-bit precoding architecture is equipped with about 50% more number of antennas as compared to the infinite resolution case, as predicated by the SER analysis in Section 4.6.3.

The final experiment considers a multi-user scenario in which $K = 8$ users are served with a BS equipped with 512 antennas using 16-QAM, i.e., $N = 4$. The performance of the proposed one-bit precoding method with $M_2 = 8$ and different design choices for constellation range is evaluated as compared to the infinite resolution ZF benchmark with constellation range of $c = \sqrt{\frac{2PM}{f(K,N)}}$ described in Section 4.6. Fig. 4.10 plots the average SER against the SNR.

It can be observed from Fig. 4.10 that the analytic SER expression presented in Section 4.6.3 accurately characterizes the average SER in the simulation for the infinite resolution ZF precoding as well as the proposed 1-bit precoding with $\sqrt{2/\pi}c \approx 0.8c$.

Further, similar to the single-user case, a performance gap of 2dB between the proposed

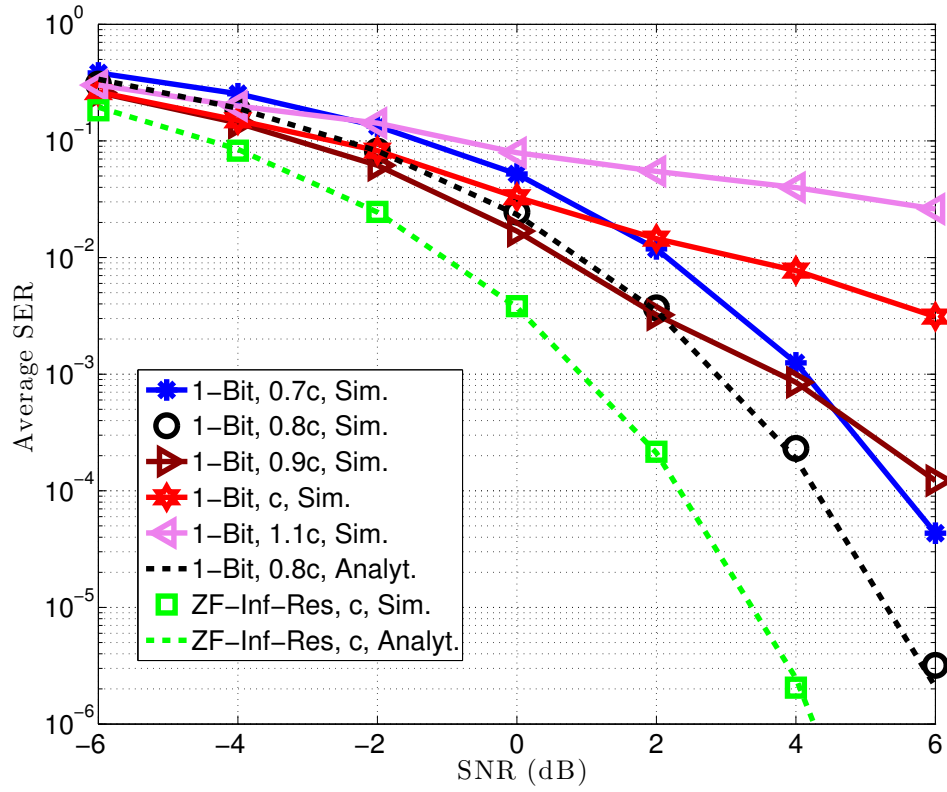


Fig. 4.10: Average SER versus SNR for different methods in a 8-user MISO system with $M = 512$ and $N = 4$.

method with constellation range $0.8c$ and conventional ZF is observed in Fig. 4.10. Finally, the 1-bit precoding schemes with constellation range larger than the proposed design of $0.8c$ all suffer from an error floor in the high SNR regime, leading to the conclusion that $0.8c$ is an appropriate design for the constellation range.

4.8 Summary

This chapter considers the 1-bit symbol-level precoding architecture for a downlink massive MIMO system. First, this chapter considers the problem of designing the QAM constellation range and the precoder for the single-user scenario in order to minimize the SER. This chapter proposes to set the QAM constellation range of 1-bit precoding as the optimal constellation range of infinite resolution precoding reduced by the factor of $\sqrt{2/\pi}$ or about 0.8. This chapter then proposes a two-step heuristic algorithm to design the precoder, which enjoys a low

complexity and exhibits excellent numerical performance. This chapter also generalizes the proposed designs for the multi-user scenario and proposes constellation range design for the infinite resolution ZF case then further scales it by $\sqrt{2/\pi}$ for the 1-bit precoding case. Finally, this chapter analytically studies the performance of the proposed scheme and shows that for large-scale antenna arrays, there is a constant 2dB gap between the proposed design and the conventional ZF scheme with per-symbol power constraint. The simulation results verify that the proposed design can achieve a promising performance for large-scale antenna arrays with low resolution DACs.

Chapter 5

Conclusion and Future Work

This thesis considers hybrid beamforming and one-bit precoding architectures as two power-efficient candidates for large antenna array systems which can significantly reduce the power consumption of the conventional fully digital beamforming schemes.

The first part of this thesis studies the performance of the hybrid beamforming architecture in the narrowband flat-fading channels. On the theoretical front, bounds on the minimum number of RF chains that are required to realize the fully digital beamforming are presented. It is shown that the hybrid structure can achieve the same performance as a fully digital beamforming scheme if the number of RF chains is greater than or equal to twice the number of data streams. This result suggests that in scenarios that the number of data streams is much smaller than the number of antennas, hybrid beamforming architecture can theoretically achieve the performance of fully digital beamforming while it significantly reduces the number of RF chains and the corresponding power consumption.

On the practical design front, heuristic hybrid beamforming design strategies are proposed for maximizing the spectral efficiency of SU-MIMO and MU-MISO systems for the cases that the number of RF chains is less than twice the number of data streams. The proposed design strategies involve decoupling the design of analog beamformers from the design of digital beamformers. Loosely speaking, it is proposed to design the analog beamformers such that the quality of the effective channel seen from the digital part is improved. For fixed analog beamforming, it is then proposed to use the conventional digital beamforming techniques such as eigen beamforming and ZF beamforming in SU-MIMO and MU-MISO scenarios, respectively.

The numerical results verify the effectiveness of the proposed designs.

Considering the mmWave systems as one of the main applications of the hybrid beamforming architecture, the second part of this thesis studies the performance of the hybrid structure in the mmWave wideband channels. From a theoretical perspective, it is shown that the hybrid beamforming can achieve the performance of the fully digital beamforming in the asymptotic regime where the number of antennas goes to infinity. This asymptotic result, which is based on the intrinsic low-rank structure of mmWave channels, provides an intuition as to why hybrid beamforming with much simpler architecture can approach the performance of the fully digital beamforming in mmWave wideband channels.

For systems with a practical number of antennas, the second part of this thesis then proposes heuristic hybrid beamforming designs for SU-MIMO as well as MU-MISO and further numerically shows the effectiveness of those designs. In the proposed designs, the analog precoder is designed based on the average of the sample covariance matrices of frequency domain channels while the digital part is designed using the conventional digital beamforming techniques. By simultaneously considering the proposed analog beamforming design strategy for wideband systems in this thesis and the two-time-scale hybrid beamforming designs for narrowband systems in [19, 53, 54], it can be seen that for a wideband system with large number of subcarriers and with pedestrians mobility where the average of sample covariance of frequency domain channels converges to the time domain second order channel statistics, designing the analog beamformers according to the second order channel statistics is an appropriate choice.

It should be mentioned that all the aforementioned proposed algorithms for hybrid beamforming architecture are based on the assumption of the perfect and instantaneous CSI. However, obtaining accurate CSI is very challenging in practice, especially for systems with large-scale antenna arrays. One of the possible directions for the future work is to device a scheme to efficiently estimate the channel of a large-scale MIMO system with hybrid beamforming architecture. It would also be desirable to characterize the CSI error of that scheme and to design the hybrid beamformers that are robust to that CSI error.

The problem of channel estimation and beamforming is even more challenging for multi-cell large-scale MIMO systems due to the existence of pilot contamination; i.e., the interference between the pilot sequences transmitted by the users during the channel estimation phase.

Therefore, studying the effect of pilot contamination on the performance of the channel estimation and beamforming schemes for hybrid architecture would be the other interesting direction for the future research.

The good performance of the hybrid structure in mmWave wideband channels is mainly due to the sparse nature of the channels in mmWave frequencies and therefore hybrid structure is not an appropriate choice for rich-scattering environments. To address that, the last part of this thesis considers an alternative one-bit precoding architecture for rich-scattering environments. For such a system, this thesis first considers designing the QAM constellation range adaptive to the CSI of each fading block. In particular, this thesis shows that a reasonable choice for the QAM constellation range in one-bit precoding is that of the infinite-resolution precoding scaled by a factor of $\sqrt{2/\pi} \approx 0.8$. Further, a low-complexity symbol-level one-bit precoding design for the fixed constellation range is proposed. Finally, it is both analytically and numerically shown that the performance of the proposed one-bit precoding scheme for systems with sufficiently large antenna arrays is within 2dB gap of the performance of infinite resolution ZF precoding.

It should be mentioned that this thesis considers some simplifying assumptions in the system model to study the performance of the one-bit precoding architecture which is recently proposed for massive MIMO systems. This thesis assumes the availability of perfect CSI at the BS with one-bit precoding architecture. However, a BS with one-bit DACs (and ADCs) may not be able to acquire such an accurate CSI. Therefore, modeling the practical imperfect CSI at the BS and designing the one-bit precoder to deal with that imperfect CSI is the first direction for the future research. This thesis also considers i.i.d Rayleigh fading with similar pathloss and shadowing for all the users and consequently design one common constellation range for all the users. Extending the results of this thesis for more complicated channel model and possibly designing different constellation ranges for different users can be considered as another direction for the future work. Finally, this thesis considers minimizing the average uncoded SER as a utility metric rather than maximizing the capacity because of the difficulties in characterizing the capacity for a system with one-bit precoding architecture. Therefore, it is absolutely desirable to characterize the capacity of the one-bit precoding architecture and then to design the constellation parameters as well as the precoder to optimize that capacity.

In summary, this thesis provides a comprehensive study of the hybrid beamforming and one-

bit precoding architectures for large-scale antenna arrays. In particular, this thesis proposes different beamforming algorithms for different transmission setups. Although the proposed algorithms developed in this thesis all require perfect CSI, they nevertheless serve as benchmark for the ultimate performance of hybrid beamforming and one-bit precoding architectures.

Bibliography

- [1] J. G. Andrews, S. Buzzi, W. Choi, S. V. Hanly, A. Lozano, A. C. Soong, and J. C. Zhang, “What will 5G be?” *IEEE J. Sel. Areas Commun.*, vol. 32, no. 6, pp. 1065–1082, June 2014.
- [2] T. L. Marzetta, E. G. Larsson, H. Yang, and H. Q. Ngo, *Fundamentals of Massive MIMO*. Cambridge University Press, 2016.
- [3] F. Rusek, D. Persson, B. K. Lau, E. G. Larsson, T. L. Marzetta, O. Edfors, and F. Tufvesson, “Scaling up MIMO: Opportunities and challenges with very large arrays,” *IEEE Signal Process. Mag.*, vol. 30, no. 1, pp. 40–60, Jan. 2013.
- [4] E. Telatar, “Capacity of multi-antenna Gaussian channels,” *Eur. Trans. Telecommun.*, vol. 10, no. 6, pp. 585–595, 1999.
- [5] Q. Shi, M. Razaviyayn, Z.-Q. Luo, and C. He, “An iteratively weighted MMSE approach to distributed sum-utility maximization for a MIMO interfering broadcast channel,” *IEEE Trans. Signal Process.*, vol. 59, no. 9, pp. 4331–4340, Sept. 2011.
- [6] A. Wiesel, Y. C. Eldar, and S. Shamai, “Zero-forcing precoding and generalized inverses,” *IEEE Trans. Signal Process.*, vol. 56, no. 9, pp. 4409–4418, Sept. 2008.
- [7] V. Venkateswaran and A. J. van der Veen, “Analog beamforming in MIMO communications with phase shift networks and online channel estimation,” *IEEE Trans. Signal Process.*, vol. 58, no. 8, pp. 4131–4143, Aug. 2010.

- [8] L. Chen, Y. Yang, X. Chen, and W. Wang, "Multi-stage beamforming codebook for 60GHz WPAN," in *Proc. 6th Int. ICST Conf. Commun. Network.*, Harbin, China, Aug. 2011, pp. 361–365.
- [9] Y. M. Tsang, A. S. Poon, and S. Addepalli, "Coding the beams: Improving beamforming training in mmWave communication system," in *IEEE Global Commun. Conf. (GLOBECOM)*, Houston, TX, USA, Dec. 2011, pp. 1–6.
- [10] S. Hur, T. Kim, D. Love, J. Krogmeier, T. Thomas, and A. Ghosh, "Millimeter wave beamforming for wireless backhaul and access in small cell networks," *IEEE Trans. Commun.*, vol. 61, no. 10, pp. 4391–4403, Oct. 2013.
- [11] S. Sanayei and A. Nosratinia, "Antenna selection in MIMO systems," *IEEE Commun. Mag.*, vol. 42, no. 10, pp. 68–73, Oct. 2004.
- [12] A. F. Molisch, M. Z. Win, Y.-S. Choi, and J. H. Winters, "Capacity of MIMO systems with antenna selection," *IEEE Trans. Wireless Commun.*, vol. 4, no. 4, pp. 1759–1772, July 2005.
- [13] A. F. Molisch, M. Z. Win, and J. H. Winters, "Reduced-complexity transmit/receive-diversity systems," *IEEE Trans. Signal Process.*, vol. 51, no. 11, pp. 2729–2738, Nov. 2003.
- [14] A. F. Molisch and X. Zhang, "FFT-based hybrid antenna selection schemes for spatially correlated MIMO channels," *IEEE Commun. Lett.*, vol. 8, no. 1, pp. 36–38, Jan. 2004.
- [15] R. R. Müller, M. A. Sedaghat, and G. Fischer, "Load modulated massive MIMO," in *IEEE Global Conf. Signal Inf. Process. (GlobalSIP)*, Dec. 2014, pp. 622–626.
- [16] M. A. Sedaghat, V. I. Barousis, R. R. Müller, and C. B. Papadias, "Load modulated arrays: A low-complexity antenna," *IEEE Commun. Mag.*, vol. 54, no. 3, pp. 46–52, Mar. 2016.
- [17] A. Kalis, A. G. Kanatas, and C. B. Papadias, *Parasitic Antenna Arrays for Wireless MIMO Systems*. Springer, 2014.

- [18] X. Zhang, A. F. Molisch, and S.-Y. Kung, “Variable-phase-shift-based RF-baseband code-sign for MIMO antenna selection,” *IEEE Trans. Signal Process.*, vol. 53, no. 11, pp. 4091–4103, Nov. 2005.
- [19] P. Sudarshan, N. B. Mehta, A. F. Molisch, and J. Zhang, “Channel statistics-based RF pre-processing with antenna selection,” *IEEE Trans. Wireless Commun.*, vol. 5, no. 12, pp. 3501–3511, Dec. 2006.
- [20] A. F. Molisch, V. V. Ratnam, S. Han, Z. Li, S. L. H. Nguyen, L. Li, and K. Haneda, “Hybrid beamforming for massive MIMO: A survey,” *IEEE Commun. Mag.*, vol. 55, no. 9, pp. 134–141, 2017.
- [21] R. H. Walden, “Analog-to-digital converter survey and analysis,” *IEEE J. Sel. Areas Commun.*, vol. 17, no. 4, pp. 539–550, Apr. 1999.
- [22] C. Svensson, S. Andersson, and P. Bogner, “On the power consumption of analog to digital converters,” in *Proc. IEEE Norchip Conf.*, Linköping, Sweden, Nov. 2006, pp. 49–52.
- [23] S. K. Mohammed and E. G. Larsson, “Per-antenna constant envelope precoding for large multi-user MIMO systems,” *IEEE Trans. Commun.*, vol. 61, no. 3, pp. 1059–1071, Mar. 2013.
- [24] M. Joham and W. Utschick, “Symbol rate processing for the downlink of DS-CDMA systems,” *IEEE J. Sel. Areas Commun.*, vol. 19, no. 1, pp. 61–68, Jan. 2001.
- [25] C. Masouros and E. Alsusa, “Dynamic linear precoding for the exploitation of known interference in MIMO broadcast systems,” *IEEE Trans. Wireless Commun.*, vol. 8, no. 3, pp. 1396–1404, Mar. 2009.
- [26] M. Alodeh, S. Chatzinotas, and B. Ottersten, “Constructive multiuser interference in symbol level precoding for the MISO downlink channel,” *IEEE Trans. Signal Process.*, vol. 63, no. 9, pp. 2239–2252, May 2015.
- [27] ——, “Symbol-level multiuser MISO precoding for multi-level adaptive modulation,” *IEEE Trans. Wireless Commun.*, vol. 16, no. 8, pp. 5511–5524, Aug. 2017.

- [28] R. W. Heath, N. Gonzalez-Prelcic, S. Rangan, W. Roh, and A. M. Sayeed, "An overview of signal processing techniques for millimeter wave MIMO systems," *IEEE J. Sel. Topics Signal Process.*, vol. 10, no. 3, pp. 436–453, 2016.
- [29] J. Ahmadi-Shokouh, S. H. Jamali, and S. Safavi-Naeini, "Optimal receive soft antenna selection for MIMO interference channels," *IEEE Trans. Wireless Commun.*, vol. 8, no. 12, pp. 5893–5903, Dec. 2009.
- [30] T. E. Bogale, L. B. Le, A. Haghigat, and L. Vandendorpe, "On the number of RF chains and phase shifters, and scheduling design with hybrid analog-digital beamforming," *IEEE Trans. Wireless Commun.*, vol. 15, no. 5, pp. 3311–3326, May 2016.
- [31] O. El Ayach, S. Rajagopal, S. Abu-Surra, Z. Pi, and R. Heath, "Spatially sparse precoding in millimeter wave MIMO systems," *IEEE Trans. Wireless Commun.*, vol. 13, no. 3, pp. 1499–1513, Mar. 2014.
- [32] A. Alkhateeb, O. El Ayach, G. Leus, and R. W. Heath, "Hybrid precoding for millimeter wave cellular systems with partial channel knowledge," in *Proc. Inf. Theory Appl. Workshop (ITA)*, San Diego, CA, USA, Feb. 2013, pp. 1–5.
- [33] A. Alkhateeb, O. El Ayach, G. Leus, and R. Heath, "Channel estimation and hybrid precoding for millimeter wave cellular systems," *IEEE J. Sel. Topics Signal Process.*, vol. 8, no. 5, pp. 831–846, Oct 2014.
- [34] T. E. Bogale and L. B. Le, "Beamforming for multiuser massive MIMO systems: Digital versus hybrid analog-digital," in *IEEE Global Commun. Conf. (GLOBECOM)*, Austin, TX, USA, Dec. 2014, pp. 4066–4071.
- [35] L. Liang, Y. Dai, W. Xu, and X. Dong, "How to approach zero-forcing under RF chain limitations in large mmwave multiuser systems?" in *IEEE/CIC Int. Conf. Commun. in China*, Shanghai, Oct. 2014, pp. 518–522.
- [36] L. Liang, W. Xu, and X. Dong, "Low-complexity hybrid precoding in massive multiuser MIMO systems," *IEEE Wireless Commun. Lett.*, vol. 3, no. 6, pp. 653–656, Dec. 2014.

- [37] X. Yu, J.-C. Shen, J. Zhang, and K. Letaief, “Alternating minimization algorithms for hybrid precoding in millimeter wave MIMO Systems,” *IEEE J. Sel. Topics Signal Process.*, vol. 10, no. 3, pp. 485–500, Apr. 2016.
- [38] A. Alkhateeb, G. Leus, and R. W. Heath, “Limited feedback hybrid precoding for multi-user millimeter wave systems,” *IEEE Trans. Wireless Commun.*, vol. 14, no. 11, pp. 6481–6494, Nov. 2015.
- [39] W. Ni and X. Dong, “Hybrid block diagonalization for massive multiuser MIMO systems,” *IEEE Trans. Commun.*, vol. 64, no. 1, pp. 201–211, Jan. 2016.
- [40] R. Rajashekhar and L. Hanzo, “Iterative matrix decomposition aided block diagonalization for mm-Wave multiuser MIMO systems,” *IEEE Trans. Wireless Commun.*, vol. 16, no. 3, pp. 1372–1384, Mar. 2017.
- [41] S. Montori, C. Fritzsch, L. Marcaccioli, R. V. Gatti, R. Jakoby, and R. Sorrentino, “Design and measurements of a 1-bit reconfigurable elementary cell for large electronic steerable reflectarrays,” in *Eur. Microw. Conf. (EuMC)*, Paris, France, Sept. 2010, pp. 918–921.
- [42] J. D. Krieger, C.-P. Yeang, and G. W. Wornell, “Dense delta-sigma phased arrays,” *IEEE Trans. Antennas Propag.*, vol. 61, no. 4, pp. 1825–1837, Apr. 2013.
- [43] W. Zhao, S. H. Lee, and A. Khisti, “Phase-only zero forcing for secure communication with multiple antennas,” *IEEE J. Sel. Topics Signal Process.*, vol. 10, no. 8, pp. 1334–1345, Dec 2016.
- [44] Ö. T. Demir and T. E. Tuncer, “Antenna selection and hybrid beamforming for simultaneous wireless information and power transfer in multi-group multicasting systems,” *IEEE Trans. Wireless Commun.*, vol. 15, no. 10, pp. 6948–6962, Oct 2016.
- [45] A. Alkhateeb and R. W. Heath, “Frequency selective hybrid precoding for limited feedback millimeter wave systems,” *IEEE Trans. Commun.*, vol. 64, no. 5, pp. 1801–1818, May 2016.
- [46] S. Park, A. Alkhateeb, and R. W. Heath, “Dynamic subarrays for hybrid precoding in wideband mmWave MIMO systems,” *IEEE Trans. Wireless Commun.*, vol. 16, no. 5, pp. 2907–2920, May 2017.

- [47] L. Kong, S. Han, and C. Yang, "Wideband hybrid precoder for massive MIMO systems," in *Proc. IEEE Global Conf. Signal Inf. Process. (GlobalSIP)*, Orlando, USA, Dec. 2015, pp. 305–309.
- [48] Z. Zhou, J. Fang, L. Yang, H. Li, Z. Chen, and R. S. Blum, "Low-rank tensor decomposition-aided channel estimation for millimeter wave MIMO-OFDM systems," *IEEE J. Sel. Areas Commun.*, vol. 35, no. 7, pp. 1524–1538, July 2017.
- [49] C. Cheung and R. S. Cheng, "Adaptive modulation in frequency spreading OFDM system with low transmit power spectral density constraint," in *Proc. IEEE Wireless Commun. Netw. Conf. (WCNC)*, Hong Kong, Mar. 2007, pp. 1433–1438.
- [50] E. Guéguen, M. Crussiere, and J.-F. Hélard, "An OFDM-CDMA scheme for high data rate UWB applications," in *Proc. IEEE Veh. Technol. Conf. (VTC)*, Dublin, Ireland, Apr. 2007, pp. 2905–2909.
- [51] T. P. Lewis and R. A. Scholtz, "An ultrawideband signal design with power spectral density constraints," in *Asilomar Conf. Signals, Syst., Comput.*, vol. 2, Nov. 2004, pp. 1521–1525.
- [52] Y. F. Liu and Y. H. Dai, "On the complexity of joint subcarrier and power allocation for multi-user OFDMA systems," *IEEE Trans. Signal Process.*, vol. 62, no. 3, pp. 583–596, Feb. 2014.
- [53] A. Adhikary, J. Nam, J. Y. Ahn, and G. Caire, "Joint spatial division and multiplexing—The large-scale array regime," *IEEE Trans. Inf. Theory*, vol. 59, no. 10, pp. 6441–6463, Oct. 2013.
- [54] Z. Li, S. Han, and A. F. Molisch, "Optimizing channel-statistics-based analog beamforming for millimeter-wave multi-user massive MIMO downlink," *IEEE Trans. Wireless Commun.*, vol. 16, no. 7, pp. 4288–4303, July 2017.
- [55] S. Blandino, C. Desset, C.-M. Chen, A. Bourdoux, and S. Pollin, "Multi-user frequency-selective hybrid MIMO demonstrated using 60 GHz RF modules," [Online] available: <https://arxiv.org/abs/1711.02968>, 2017.

- [56] C. Risi, D. Persson, and E. G. Larsson, “Massive MIMO with 1-bit ADC,” [*Online*] Available: <http://arxiv.org/abs/1404.7736>, Apr. 2014.
- [57] J. Mo and R. W. Heath, “Capacity analysis of one-bit quantized MIMO systems with transmitter channel state information,” *IEEE Trans. Signal Process.*, vol. 63, no. 20, pp. 5498–5512, Oct. 2015.
- [58] Y. Li, C. Tao, G. Seco-Granados, A. Mezghani, A. L. Swindlehurst, and L. Liu, “Channel estimation and performance analysis of one-bit massive MIMO systems,” *IEEE Trans. Signal Process.*, vol. 65, no. 15, pp. 4075–4089, Aug. 2017.
- [59] S. Jacobsson, G. Durisi, M. Coldrey, U. Gustavsson, and C. Studer, “Throughput analysis of massive MIMO uplink with low-resolution ADCs,” *IEEE Trans. Wireless Commun.*, vol. 16, no. 6, pp. 4038–4051, June 2017.
- [60] C. Mollén, J. Choi, E. G. Larsson, and R. W. Heath, “Uplink performance of wideband massive MIMO with one-bit ADCs,” *IEEE Trans. Wireless Commun.*, vol. 16, no. 1, pp. 87–100, Jan. 2017.
- [61] C. Studer and G. Durisi, “Quantized massive MU-MIMO-OFDM uplink,” *IEEE Trans. Commun.*, vol. 64, no. 6, pp. 2387–2399, June 2016.
- [62] A. K. Saxena, I. Fijalkow, and A. L. Swindlehurst, “On one-bit quantized ZF precoding for the multiuser massive MIMO downlink,” in *Proc. IEEE Sensor Array Multichannel Signal Process. Workshop (SAM)*, Rio de Janeiro, Brazil, July 2016, pp. 1–5.
- [63] ——, “Analysis of one-bit quantized precoding for the multiuser massive MIMO downlink,” *IEEE Trans. Signal Process.*, vol. 65, no. 17, pp. 4624–4634, Sept. 2017.
- [64] A. Swindlehurst, A. Saxena, A. Mezghani, and I. Fijalkow, “Minimum probability-of-error perturbation precoding for the one-bit massive MIMO downlink,” in *Proc. IEEE Int. Conf. Acoust., Speech, Signal Process. (ICASSP)*, Mar. 2017, pp. 6483–6487.
- [65] H. Jedda, J. A. Nossek, and A. Mezghani, “Minimum BER precoding in 1-bit massive MIMO systems,” in *Proc. IEEE Sensor Array Multichannel Signal Process. Workshop (SAM)*, Rio de Janeiro, Brazil, July 2016.

- [66] O. B. Usman, H. Jedda, A. Mezghani, and J. A. Nossek, “MMSE precoder for massive MIMO using 1-bit quantization,” in *Proc. IEEE Int. Conf. Acoust., Speech, Signal Process. (ICASSP)*, Shanghai, China, Mar. 2016, pp. 3381–3385.
- [67] O. B. Usman, J. A. Nossek, C. A. Hofmann, and A. Knopp, “Joint MMSE precoder and equalizer for massive MIMO using 1-bit quantization,” in *Proc. IEEE Int. Conf. on Commun. (ICC)*, Paris, France, May 2017.
- [68] D. B. Amor, H. Jedda, and J. Nossek, “16 QAM communication with 1-bit transmitters,” in *Proc. IEEE Int. ITG Workshop Smart Antennas (WSA)*, Berlin, Germany, Mar. 2017.
- [69] O. Castañeda, T. Goldstein, and C. Studer, “POKEMON: A non-linear beamforming algorithm for 1-bit massive MIMO,” in *Proc. Int. Conf. Acoust., Speech, Signal Process. (ICASSP)*, New Orleans, USA, Mar. 2017, pp. 3464–3468.
- [70] S. Jacobsson, G. Durisi, M. Coldrey, T. Goldstein, and C. Studer, “Quantized precoding for massive MU-MIMO,” *to appear in IEEE Trans. Commun.*, 2017.
- [71] ———, “Nonlinear 1-bit precoding for massive MU-MIMO with higher-order modulation,” in *Proc. Asilomar Conf. Signals, Syst., Comput.*, Nov. 2016, pp. 763–767.
- [72] B. M. Hochwald, T. L. Marzetta, and V. Tarokh, “Multiple-antenna channel hardening and its implications for rate feedback and scheduling,” *IEEE Trans. Inf. Theory*, vol. 50, no. 9, pp. 1893–1909, Sept. 2004.
- [73] H. Jedda, A. Noll, and J. Nossek, “PSK precoding in multi-user MISO systems,” in *Proc. IEEE Int. ITG Workshop Smart Antennas (WSA)*, Berlin, Germany, Mar. 2017.
- [74] H. Jedda, A. Mezghani, J. A. Nossek, and A. L. Swindlehurst, “Massive MIMO downlink 1-bit precoding with linear programming for PSK signaling,” in *Proc. IEEE Workshop Signal Process. Adv. Wireless Commun. (SPAWC)*, Sapporo, Japan, Jul. 2017.
- [75] M. B. Shenouda and T. N. Davidson, “Convex conic formulations of robust downlink precoder design with quality of service constraints,” *IEEE J. Sel. Topics Signal Process.*, vol. 1, no. 4, pp. 714–724, Dec. 2007.

- [76] B. Chalise, S. Shahbazpanahi, A. Czylwik, and A. B. Gershman, "Robust downlink beamforming based on outage probability specifications," *IEEE Trans. Wireless Commun.*, vol. 6, no. 10, pp. 3498–3503, Oct. 2007.
- [77] G. Caire, N. Jindal, M. Kobayashi, and N. Ravindran, "Multiuser MIMO achievable rates with downlink training and channel state feedback," *IEEE Trans. Inf. Theory*, vol. 56, no. 6, pp. 2845–2866, June 2010.
- [78] F. Sohrabi and T. N. Davidson, "Coordinate update algorithms for robust power loading for the MU-MISO downlink with outage constraints," *IEEE Trans. Signal Process.*, vol. 64, no. 11, pp. 2761–2773, June 2016.
- [79] K.-Y. Wang, A. M.-C. So, T.-H. Chang, W.-K. Ma, and C.-Y. Chi, "Outage constrained robust transmit optimization for multiuser MISO downlinks: Tractable approximations by conic optimization," *IEEE Trans. Signal Process.*, vol. 62, no. 21, pp. 5690–5705, Nov. 2014.
- [80] A. Goldsmith, S. A. Jafar, N. Jindal, and S. Vishwanath, "Capacity limits of MIMO channels," *IEEE J. Sel. Areas Commun.*, vol. 21, no. 5, pp. 684–702, June 2003.
- [81] C. B. Peel, B. M. Hochwald, and A. L. Swindlehurst, "A vector-perturbation technique for near-capacity multiantenna multiuser communication-Part I: Channel inversion and regularization," *IEEE Trans. Commun.*, vol. 53, no. 1, pp. 195–202, Jan. 2005.
- [82] H. Dahrouj and W. Yu, "Coordinated beamforming for the multicell multi-antenna wireless system," *IEEE Trans. Wireless Commun.*, vol. 9, no. 5, pp. 1748–1759, May 2010.
- [83] D. P. Palomar, J. M. Cioffi, and M. A. Lagunas, "Joint Tx-Rx beamforming design for multicarrier MIMO channels: A unified framework for convex optimization," *IEEE Trans. Signal Process.*, vol. 51, no. 9, pp. 2381–2401, Sept. 2003.
- [84] Z. Pi, "Optimal transmitter beamforming with per-antenna power constraints," in *IEEE Int. Conf. Commun. (ICC)*, Ottawa, Canada, June 2012, pp. 3779–3784.
- [85] M. S. Bartlett, "An inverse matrix adjustment arising in discriminant analysis," *Ann. Math. Stat.*, pp. 107–111, 1951.

- [86] P. Sudarshan, N. B. Mehta, A. F. Molisch, and J. Zhang, “Antenna selection with RF pre-processing: Robustness to RF and selection non-idealities,” in *IEEE Radio Wireless Conf.*, Atlanta, GA, USA, 2004, pp. 391–394.
- [87] Z. Pi and F. Khan, “An introduction to millimeter-wave mobile broadband systems,” *IEEE Commun. Mag.*, vol. 49, no. 6, pp. 101–107, June 2011.
- [88] O. El Ayach, R. W. Heath, S. Abu-Surra, S. Rajagopal, and Z. Pi, “The capacity optimality of beam steering in large millimeter wave MIMO systems,” in *Proc. IEEE Workshop Signal Process. Adv. Wireless Commun. (SPAWC)*, Cesme, Turkey, June 2012, pp. 100–104.
- [89] M. R. Akdeniz, Y. Liu, M. K. Samimi, S. Sun, S. Rangan, T. S. Rappaport, and E. Erkip, “Millimeter wave channel modeling and cellular capacity evaluation,” *IEEE J. Sel. Areas Commun.*, vol. 32, no. 6, pp. 1164–1179, June 2014.
- [90] A. Swindlehurst, A. Saxena, A. Mezghani, and I. Fijalkow, “Minimum probability-of-error perturbation precoding for the one-bit massive MIMO downlink,” in *Proc. Int. Conf. Acoust., Speech, Signal Process. (ICASSP)*, Mar. 2017, pp. 6483–6487.
- [91] J. G. Proakis and M. Salehi, *Digital communications*, 5th ed. McGraw-Hill, 2008.
- [92] M. Chiani, D. Dardari, and M. K. Simon, “New exponential bounds and approximations for the computation of error probability in fading channels,” *IEEE Trans. Wireless Commun.*, vol. 2, no. 4, pp. 840–845, July 2003.
- [93] S. Zhang and Y. Huang, “Complex quadratic optimization and semidefinite programming,” *SIAM Journal on Optimization*, vol. 16, no. 3, pp. 871–890, 2006.